

# Coupling of different length scales in molecular dynamics simulations

Anja Streit

Dissertation

D368

Vom Fachbereich Mathematik der Universität Kaiserslautern  
zur Verleihung des akademischen Grades Doktor der  
Naturwissenschaften (Doctor rerum naturalium, Dr. rer. nat.)  
genehmigte Dissertation

Gutachter:  
Prof. Dr. Axel Klar  
Prof. Dr. Karsten Albe

Datum der Disputation: 21.12.2006



I would like to thank all the people who supported the work on this thesis in various ways.

First of all, I thank Prof. Michael Junk for the supervision during the first one and a half years of my work on this thesis, Prof. Axel Klar for his supervision afterwards and Prof. Karsten Albe for being the co-referee.

I thank Prof. Achi Brandt and Dr. Sc. Valery Ilyin for interesting and helpful discussions and comments and a very interesting visit at the Weizmann Institute of Science.

Special thanks to Dr. Peter Klein for suggesting this interesting problem, for explaining me the important aspects in this field from the point of view of a physicist, many interesting discussions and his help with various problems.

This work was done with the financial support of Fraunhofer ITWM Kaiserslautern. I thank Dr. Franz-Josef Pfreundt for giving me the opportunity to work in the Competence Center High Performance Computing and Visualization and all colleagues from the department. Especially Dr. Susanne Hahn and Dr. Robert Zillich for the good cooperation and help in theoretical physics.

I thank Dr. Joachim Wipper for carefully reading the manuscript.

Special thanks to my family and friends for their continuous support.

# Contents

<b>Symbols</b>	<b>5</b>
<b>Introduction</b>	<b>7</b>
<b>1 Molecular dynamics simulations of a sputtering process</b>	<b>9</b>
1.1 Sputtering process . . . . .	9
1.2 Hamiltonian systems . . . . .	10
1.3 Statistical mechanics . . . . .	12
1.4 Molecular dynamics . . . . .	14
<b>2 Approximations in molecular dynamics simulations</b>	<b>17</b>
2.1 Approximations in the simulation of the sputtering process . . . . .	17
2.2 Definition of microscopic stress tensor . . . . .	19
2.3 Comparing the solutions . . . . .	22
2.4 Concurrent coupling of length scales method . . . . .	24
2.5 Bridging scales approximation . . . . .	27
<b>3 One dimensional analysis and extension of existing methods</b>	<b>33</b>
3.1 Harmonic chain of atoms . . . . .	33
3.1.1 Concurrent coupling of length scales method . . . . .	37
3.1.2 Bridging scales approximation . . . . .	43
3.2 Longer ranging harmonic and anharmonic potentials . . . . .	50
3.2.1 Concurrent coupling of length scales . . . . .	52
3.2.2 Bridging scales approximation . . . . .	55
<b>4 Hamiltonian formulation, boundary conditions and interpolation functions</b>	<b>61</b>
4.1 Bridging scales approximation not energy conserving . . . . .	62
4.2 Orthogonal displacement splitting . . . . .	63
4.3 Coupling of atomistic and coarse scale region . . . . .	66
4.4 Calculation of the random force . . . . .	71
4.5 Mori-Zwanzig projection operator formalism . . . . .	75
4.6 Choosing the interpolation functions . . . . .	79

<b>5</b>	<b>Approximations and numerical results for one dimensional harmonic potentials</b>	<b>83</b>
5.1	Computation of better interpolation weights . . . . .	83
5.2	Approximations in the Lagrangian for harmonic potential . . . . .	90
5.3	Numerical integration and other numerical errors . . . . .	95
<b>6</b>	<b>Two dimensional examples</b>	<b>103</b>
6.1	Two dimensional simulations . . . . .	103
6.2	New interpolation functions in two dimensions . . . . .	105
6.3	Reflectionless boundary condition in two dimensions . . . . .	110
6.3.1	Small atomistic system . . . . .	111
6.3.2	Coupling of atomistic and coarse scale . . . . .	112
6.4	Test cases, comparison of interpolation functions . . . . .	115
	<b>Summary</b>	<b>125</b>

# Symbols

$a_0$	equilibrium distance of atoms
$a$	atomistic accelerations
$b$	fine scale displacements
$B$	matrix of interpolation weights from fine scale values to the equilibrium positions of the atoms
$c(\kappa)$	wave speed
$C$	elasticity constant
$C^l(\Omega_1, \Omega_2)$	$l$ -times continuous differentiable mapping from $\Omega_1$ to $\Omega_2$
$d$	displacements of coarse scale nodes
$E$	energy
$E_{\text{kin}}$	instantaneous kinetic energy
$E_{\text{pot}}$	instantaneous potential energy
$f, F$	forces
$\bar{F}_\alpha$	coarse scale deformation gradient
$g(x)$	weight function
$H$	Hessian
$I$	identity matrix
$k$	spring constant
$k_B$	Boltzmann's constant
$L$	Laplace transformation
$\hat{L}$	Liouville operator
$m$	atomic mass
$\tilde{m}$	space dimension
$\hat{m}$	number of extra weights for new interpolation
$M$	atomic mass matrix
$n$	number of atoms
$\tilde{n}$	ratio of the distance of coarse scale nodes, compared to equilibrium distance of atoms
$N$	matrix of interpolation weights from coarse scale values to the equilibrium positions of the atoms
$p$	atomistic momenta
$P$	projection operator
$q$	atomic positions
$q^0$	atomistic equilibrium positions
$Q$	orthogonal projection operator

$r_{0,\alpha\beta}$	interatomic distance in undeformed state
$r_{\alpha\beta}$	interatomic distance in deformed state
$R(t)$	random force
$T$	temperature
$u$	atomic displacements
$u_c$	coarse scale part of atomistic displacements
$u_f$	fine scale part of atomistic displacements
$w$	interpolation weight
$W_\alpha$	energy density
$x$	positions of coarse scale nodes
$\delta(x)$	delta function
$\delta_{j,k}$	Kronecker symbol
$\Delta t$	time discretization
$\Delta T$	coarse scale time step
$\Delta x, \Delta y$	atomic discretisation
$\Delta X, \Delta Y$	coarse scale discretisation
$\epsilon_r$	relative error in the energy
$\kappa$	wave vector
$\rho$	phase space density
$\Sigma$	stress tensor
$\Sigma_C$	configurational part of the stress tensor
$\Sigma_K$	kinetic part of the stress tensor
$\Theta(t)$	memory kernel
$\Phi$	potential energy
$\omega$	wave frequency
$\mathcal{B}$	fine scale momenta
$\mathcal{H}$	Hamiltonian function
$\mathcal{L}$	Lagrangian function
$\mathcal{O}$	Landau symbol
$\mathcal{P}$	coarse scale momenta

# Introduction

Molecular dynamics, the numerical solution of the Newtonian evolution equations for particles, first came up in the 1950th when the first computer simulations of liquids were carried out [5]. It is constantly developed further and is nowadays a widely used method to study diverse effects in material science of liquids and solids.

A problem of such simulations is, that the system under consideration often consists of a huge number of particles with complicated interaction and requires a very small time step for the numerical solution of the system of ordinary differential equations. The simulation of a huge system with molecular dynamics is therefore often not directly possible. In many cases, periodic boundary conditions [5] can be used to avoid this problem, but it depends on the effects of interest if such an approximation is applicable. E.g. for the simulation of surface coating by sputtering, we cannot use periodic boundary conditions, at least not in growth direction, since a free surface is necessary there. A possible solution is to describe the surface effects with an atomistic model and to use a coarser model several atomic layers away from the boundary.

Such problems do not only occur in molecular dynamics simulations but in different areas in the computer simulation of real materials. To describe an effective material behaviour often requires to take into account different physical effects. The characteristic length and time scales of these can be very different. Therefore, a simulation of all relevant effects on the finest scale is often impossible. The different effects can thereby be important in different parts of the domain or in the whole domain, and they usually influence each other. Different mathematical models, valid on different length and time scales or in different parts of the domain, are then necessary to describe the complex behaviour. These models can be e.g. quantum-mechanical, atomistic or continuum descriptions.

The coupling of different models, the transition between them and the effective numerical solution are therefore a basic requirement for the study of material behaviour by computer simulation. Dependent on the type of interaction between the different scales, several coupling or approximation methods have been developed.

The first class are the hierarchical methods. The computations on each scale are performed separately, and the results determine the parameters or the constitutive equations on the next coarser scale (e.g. [24, 25, 26, 6]). The fine scale computations in this upscaling approaches are often performed on a small representative volume element, to compute the effective properties for the model on the next coarser level. An example is the computation of macroscopic properties like the diffusion coefficient or the viscosity from microscopic simulations. They are then used in macroscopic



simulations on the level of continuum mechanics.

Another possibility, especially for different models in different parts of the domain, is the coupling by multi-scale boundary conditions. The results in one part of the domain are used as boundary conditions for another part. They can be updated in every time step for dynamic and in every iteration step for static simulations, or they can be prescribed for the whole simulation. An example for the latter one are the extended system methods in molecular dynamics simulations, where the atomistic evolution equations are changed to guarantee e.g. a constant temperature in the whole domain or at the boundary (cf. [11, 33, 43, 44]).

The third class are the concurrent coupling approaches, where the results on the different scales are computed simultaneously. In contrast to the hierarchical methods, not only the information of the fine scale is used on the coarse scale but also vice versa.

The focus of this thesis are concurrent coupling methods in molecular dynamics simulations for the coupling of an atomistic and a coarse scale region. Different methods for such a coupling are constructed in the literature. An example for the case of a static problem is the quasi-continuum method [46, 64, 65, 68], for dynamic problems there are many approaches like the concurrent coupling of length scales method [1, 16, 69], the bridging scales method [53, 55, 55, 71], the coarse grained molecular dynamics [58, 60] and many others [10, 17, 21, 23, 27, 28, 32, 47, 50, 62, 63, 72, 73]. For an overview of different methods see e.g. [22, 49, 56, 59].

**Outline** In the first chapter, we explain the physical effects in a sputtering process and present the basic ideas of molecular dynamics simulations. In chapter 2, the special requirements in the approximation of the simulation of surface coating by sputtering are explained, local observables to compare the results are defined and the concurrent coupling of length scales and the bridging scales method are presented. In chapter 3, we investigate both methods with regard to their applicability in the simulation of surface coating. We show that the first one leads to the reflection of fine scale waves at the interface between atomistic and coarse scale region, the second one gives an approximation that is not energy conserving. Therefore, we present in chapter 4 a new method, based on the displacement splitting of the bridging scales method and motivated by a projection operator approach, to derive the coupling of an atomistic and a coarse scale region, together with a reflectionless boundary condition at the interface, directly from the Lagrangian function of the system. Possible approximations in the Lagrangian that lead to energy conserving approximations for the coupling are discussed in chapter 5, as well as numerical aspects of this approximations. Additionally, we show how to choose the interpolation from coarse to fine scale in such a way that the dispersion relation in the coarse scale region is correct for the approximations. Examples for one dimensional simulations are given. In chapter 6, the use of this orthogonal displacement splitting for two dimensional simulations is explained and examples and comparisons with the bridging scales method and for different interpolation functions are given.

# Chapter 1

## Molecular dynamics simulations of a sputtering process

In this chapter, the basic ideas of molecular dynamics simulation as a numerical method to solve Hamiltonian systems are presented. In section 1.1, we explain the physical effects in a sputtering process that is one example of a system, where a simulation on different scales can be necessary. Then we state some basic principles of Hamiltonian systems in section 1.2 and of statistical mechanics in section 1.3, to provide the necessary fundamental concepts for a classical mechanics model of the sputtering process. In section 1.4, the numerical solution of the model with molecular dynamics is explained.

### 1.1 Sputtering process

Sputtering processes are used e.g. in the production of semiconductors. Single copper atoms are sputtered there on a silicon crystal, in such a way that after a while a thin layer of copper builds out on top of the crystal. This layer typically consists of several mono-layers of copper atoms.

The atoms hitting the crystal usually have a high kinetic energy, which leads to several effects. First of all, the crystal heats up due to the extra kinetic and binding energy. Therefore, in the real production process, some cooling is necessary, to avoid this increase in temperature. Later on we will see, that one of the most important problems in numerical simulations of a sputtering process is to model this energy transfer. In addition to this heating up, an excitation is imported, leading to waves travelling through the crystal. When an atom hits the crystal, it does not necessarily remain on top of the other atoms, but, due to its high kinetic energy, it can penetrate into the already sputtered layers or even into the crystal, producing again travelling waves. Altogether, this leads to the development of stresses. This should usually be controlled in the production process.

Since it is very difficult in the real process to detect the influence of the process parameters on this stress development, the aim of a DFG project at the Fraunhofer ITWM is to simulate the sputtering process with molecular dynamics, which will be

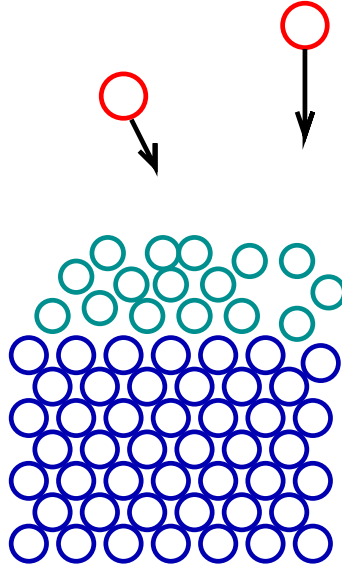


Figure 1.1: schematic illustration of the sputtering process

explained in the following.

## 1.2 Hamiltonian systems

We give an overview of some basic concepts of classical mechanics. The notation follows [2], a more detailed derivation of the equations can be found there or in other textbooks of classical mechanics.

To simulate the sputtering process numerically, we first need a mathematical model to describe the atomic motion. In classical mechanics, this is given by Newton's second law,

$$m_j a_j(t) = F_j(t), \quad j \in \{1, \dots, n\}$$

where  $a_j$  and  $m_j$  denote the acceleration and the mass of atom  $j$ ,  $F_j$  the force acting on this atom and  $n$  the number of atoms.

The second possibility to get the system of equations, is to derive them from the Lagrangian formulation. The Lagrangian function  $\mathcal{L}$  is defined as

$$\mathcal{L}(q, \dot{q}, t) := \frac{1}{2} \sum_{j=1}^n m_j \dot{q}_j^2(t) - \Phi(q_1(t), \dots, q_n(t)),$$

where the first term on the right is the kinetic energy,  $\Phi(q)$  is the potential energy and  $q_j$  and  $\dot{q}_j$  denote the position and velocity of atom  $j$ . We concentrate in the following only on pair potentials. If  $\mathcal{L}$  is a smooth function, the variational principle of Hamilton states, that the atoms move in such a way that the first variation of the integral over the Lagrangian function vanishes, i.e.

$$\delta \int_a^b \mathcal{L}(q, \dot{q}, t) = 0.$$

From this principle, the equations of motions can be derived as

$$\nabla_q \mathcal{L}(q, \dot{q}, t) - \frac{d}{dt} \nabla_{\dot{q}} \mathcal{L}(q, \dot{q}, t) = 0,$$

with  $\nabla_x = (\frac{\partial}{\partial x_1}, \dots, \frac{\partial}{\partial x_n})$  [2]. Introducing the conjugate momenta,

$$p_j(t) := \frac{\partial \mathcal{L}}{\partial \dot{q}_j},$$

we can change from Lagrangian to Hamiltonian description via Legendre transformation,

$$\begin{aligned} (q, \dot{q}, t) &\mapsto (q, p, t) \\ \mathcal{H}(q, p, t) &:= \sum_{j=1}^n \frac{p_j^2}{m_j} - \mathcal{L}(q, \dot{q}(p), t) = \frac{1}{2} \sum_{j=1}^n \frac{p_j^2}{m_j} + \Phi(q). \end{aligned}$$

Now, the Hamiltonian system can be derived as partial derivatives of this Hamiltonian  $\mathcal{H}$ ,

$$\begin{aligned} \dot{q}_j &= \frac{\partial \mathcal{H}}{\partial p_j} = \frac{p_j}{m_j}, \\ \dot{p}_j &= -\frac{\partial \mathcal{H}}{\partial q_j} = -\frac{\partial \Phi}{\partial q_j} = F_j. \end{aligned} \tag{1.1}$$

We end up with a system of first order differential equations, where the right hand side can be highly nonlinear, since the potential energy can be rather complicated.

Since

$$\begin{aligned} \frac{d}{dt} \mathcal{H}(q, p, t) &= \sum_{j=1}^n \left( \frac{\partial \mathcal{H}(q, p, t)}{\partial q_j} \dot{q}_j + \frac{\partial \mathcal{H}(q, p, t)}{\partial p_j} \dot{p}_j \right) \\ &= \sum_{j=1}^n \left( \frac{\partial \mathcal{H}(q, p, t)}{\partial q_j} \frac{\partial \mathcal{H}(q, p, t)}{\partial p_j} - \frac{\partial \mathcal{H}(q, p, t)}{\partial p_j} \frac{\partial \mathcal{H}(q, p, t)}{\partial q_j} \right) \\ &= 0 \end{aligned} \tag{1.2}$$

holds, the Hamiltonian is a first integral, called the energy [37, 2].

If we define the Liouville operator  $\hat{L}$  in the following way,

$$i\hat{L} := \sum_{j=1}^n \dot{q}_j \frac{\partial}{\partial p_j} + \dot{p}_j \frac{\partial}{\partial q_j} = \sum_{j=1}^n \frac{\partial \mathcal{H}}{\partial p_j} \frac{\partial}{\partial q_j} - \frac{\partial \mathcal{H}}{\partial q_j} \frac{\partial}{\partial p_j},$$

the energy conservation (1.2) can be rewritten as

$$i\hat{L}\mathcal{H} = 0.$$

If we have a mechanical system, consisting of many atoms and a Hamiltonian formulation, describing its time evolution, we can try to solve the Hamiltonian system of equations, to get the positions and momenta at every arbitrary point in time. However, in most of the simulations, we are not interested in this huge amount of data, but only in the time evolution of so called observables, which are functions that depend on the actual positions and momenta of the atoms,

$$\mathcal{A}(t) = \mathcal{A}(q(t), p(t)).$$

This are e.g. autocorrelation functions or transport coefficients that can be calculated from ensemble averages of autocorrelation functions. An example is the diffusion coefficient  $D$ , which can be calculated from the autocorrelation of the velocity  $v$ ,

$$D = \frac{1}{3} \int_0^\infty \langle v(t)v(0) \rangle dt,$$

with  $\langle \cdot \rangle$  the ensemble average, which is explained in the next section.

The observables are usually quantities that are available from measurements. Therefore, they can be used to validate theoretical models of real life systems or to compute this quantities in case that measurements are very difficult. In terms of the Liouville operator, their evolution is given as

$$\dot{\mathcal{A}}(q(t), p(t)) = i\hat{L}\mathcal{A}(q(t), p(t)),$$

with the formal solution

$$\mathcal{A}(q(t), p(t)) = \exp(i\hat{L}t)\mathcal{A}(q(0), p(0)).$$

### 1.3 Statistical mechanics

If we can solve the Hamiltonian equations, we can compute the values of the observables from the positions and momenta of the atoms. Since real physical systems often consist of millions of atoms, in many cases statistical methods can be used to calculate averages and fluctuations of certain observables. Some of the basic ideas of statistical mechanics are outlined in the following. A more detailed description can be found e.g. in [40, 70, 35].

If we have a mechanical system, consisting of  $n$  atoms in a  $d$  dimensional space, the system is well defined by its  $2nd$  degrees of freedom, the position and momentum of each atom in each coordinate direction. Every configuration of the coordinates of the system can be considered as a point in a  $2nd$ -dimensional space, the so called phase space. By  $\Gamma = (q, p)$  we denote a point in this phase space and a collection of points is called an ensemble. Since a Hamiltonian system is energy conserving, the total energy is given by its initial conditions. If the system is evolving in time, the trajectory can only reach points on the surface of a sphere in phase space that conserves this energy.

If we are not especially interested in the positions and momenta of the atoms, but only in macroscopic quantities, like temperature, pressure, etc. that are calculated

from the microscopic configuration, it is sufficient to consider the phase space density  $\rho(\Gamma)$ . This function is a probability density that gives the probability of finding a system of  $n$  atoms in a given region in phase space. Therefore, we get

$$\int \rho(\Gamma) dp dq = 1$$

if we integrate over the whole phase space. This density can change in time. But since systems can neither be destroyed nor created, the total derivative of the density is zero. This fact is stated by the Liouville theorem,

$$\frac{d\rho}{dt} = \frac{\partial \rho}{\partial t} + \sum_{i=1}^n \dot{q}_i \frac{\partial \rho}{\partial q_i} + \dot{p}_i \frac{\partial \rho}{\partial p_i} = \frac{\partial \rho}{\partial t} + i\hat{L}\rho = 0$$

or

$$\frac{\partial \rho}{\partial t} = -i\hat{L}\rho,$$

which can be considered as the foundation of statistical mechanics.

If the density  $\rho$  in every point in phase space does not change in time,  $\partial \rho / \partial t = 0$ , the corresponding ensemble is ergodic and is called an equilibrium ensemble. For an ergodic system the ergodic hypothesis

$$\lim_{t \rightarrow \infty} \int_0^t \mathcal{A}(\Gamma(t)) dt = \langle \mathcal{A}(t) \rangle_t = \langle \mathcal{A}(\Gamma) \rangle_{\text{ens}} = \int \mathcal{A}(\Gamma) \rho(\Gamma) d\Gamma \quad (1.3)$$

holds, which states that the time average is equal to the ensemble average. The symbol  $\langle \cdot \rangle$  will be used in the following for expectations. According to the ergodic theorem, we can compute them from time average or from phase space average, as long as the system is in equilibrium. In molecular dynamics simulations (cf. section 1.4), the averages are computed from the time average over a long time interval, in Monte Carlo simulations from ensemble averaging.

As mentioned above, the phase space density depends on the macroscopic properties of the system. If we consider a closed system, the invariants are the energy  $E$ , the volume  $V$  and the number of particles  $N$ . The corresponding ensemble is called the microcanonical ensemble or  $NVE$  ensemble, with a density distribution proportional to the delta-function

$$\rho(E) \sim \delta(E - \mathcal{H}).$$

If the system under consideration is a subsystem of a larger system with energy exchange but without particle exchange, the invariants are the temperature  $T$ , again the number of particles  $N$  and the volume  $V$ . Therefore, it is called  $NVT$  ensemble and the phase space density is given by

$$\rho \sim \exp(-\mathcal{H}/k_B T).$$

Furthermore, for a Hamiltonian system the equipartition theorem holds, i.e.

$$\left\langle p_i \frac{\partial \mathcal{H}}{\partial p_j} \right\rangle = \delta_{i,j} k_B T, \quad \left\langle q_i \frac{\partial \mathcal{H}}{\partial q_j} \right\rangle = \delta_{i,j} k_B T, \quad (1.4)$$

where  $k_B$  is Boltzmann's constant and  $\delta_{i,j}$  the Kronecker symbol. It states that, on average, we get the same energy for each degree of freedom in the system. The temperature  $T$  is the average over the instantaneous temperature  $\mathcal{T}$  defined as

$$\mathcal{T} = \frac{2E_{\text{kin}}}{dnk_B} = \frac{1}{dnk_B} \sum_{i=1}^n \frac{p_i^2}{m_i},$$

with  $E_{\text{kin}}$  the instantaneous kinetic energy [5]. We need this definition of temperature later on for the constant temperature simulation in our approximation.

The concepts of statistical mechanics, presented above, are of course not only valid for systems of atoms but for all kinds of systems of particles with an analogous Hamiltonian formulation.

## 1.4 Molecular dynamics

With (1.3) we can compute averages over observables in general with the distribution function  $\rho$ , without solving the system of ordinary differential equations (1.1). However, evaluation of the integral is not possible in most of the cases, especially if the Hamiltonian is very complicated. Additionally, in our example of the surface sputtering process, the system is out of equilibrium if an atom hits the surface of the crystal. Therefore, even with statistical methods, there is a need to solve the Hamiltonian system of equations numerically. This is done in molecular dynamics simulations. We present the basic concepts and refer to some textbooks, e.g. [38] or [5], for more details.

Since the Hamiltonian system (1.1) is energy conserving, we should discretise the system in time and choose a symplectic numerical integrator, i.e. one that conserves the energy of the system. Widely used is the Verlet algorithm or one of its several modifications. In the following, we use the velocity Verlet algorithm that gives the positions and velocities  $v(t) = \dot{q}(t)$  to second order accuracy. The position update is obtained from the Taylor expansion

$$q(t + \Delta t) = q(t) + \Delta t v(t) + \frac{1}{2}\Delta t^2 a(t) + \mathcal{O}(\Delta t^3),$$

with the accelerations  $a(t) = \ddot{q}(t)$ . To derive the velocity update, we need the Taylor expansion of the velocity and the acceleration update,

$$v(t + \Delta t) = v(t) + \Delta t a(t) + \frac{1}{2}\Delta t^2 \dot{a}(t) + \mathcal{O}(\Delta t^3), \quad (1.5)$$

$$a(t + \Delta t) = a(t) + \Delta t \dot{a}(t) + \mathcal{O}(\Delta t^2). \quad (1.6)$$

We insert  $\dot{a}(t)$  from (1.6) in (1.5) to obtain

$$v(t + \Delta t) = v(t) + \frac{1}{2}\Delta t(a(t) + a(t + \Delta t)) + \mathcal{O}(\Delta t^3).$$

We use this update algorithm, since it gives the positions and velocities in the same time step. Other algorithms use staggered time steps for the computation of

positions and velocities, e.g.  $q(t + \Delta t)$  and  $v(t + \Delta t/2)$ , and interpolate the velocities in between, to compute the kinetic and potential energy at the same time.

In a simulation, the update of the velocity Verlet algorithm is usually performed in three steps,

$$\begin{aligned} q(t + \Delta t) &= q(t) + \Delta t v(t) + \frac{1}{2} \Delta t^2 a(t), \\ v\left(t + \frac{\Delta t}{2}\right) &= v(t) + \frac{1}{2} \Delta t a(t), \\ v(t + \Delta t) &= v\left(t + \frac{\Delta t}{2}\right) + \frac{1}{2} \Delta t a(t + \Delta t), \end{aligned}$$

to avoid the necessity of storing the acceleration of the old and new time step simultaneously.

Since the computation of the atomic forces is usually the most time consuming part of a molecular dynamics simulation, implicit integration schemes, that require additionally the calculation of the Hessian of the potential, can typically not be used. It is less costly to take an explicit integration scheme with a smaller time step.

As important as the choice of the numerical integrator, is the sampling of initial conditions for molecular dynamics simulations. From the equipartition theorem (1.4), it is known, that the average kinetic energy per degree of freedom is proportional to the temperature in an equilibrium system. For the momenta, we get directly the variance of the distribution  $\langle p_i \frac{\partial \mathcal{H}}{\partial p_i} \rangle = \langle p_i^2 / m_i \rangle = 1/m_i \sigma(p_i) = k_B T$ . We can choose them e.g. from a Gaussian ( $N$ ) distribution or a uniform ( $\mathcal{U}$ ) distribution,

$$p_i \sim N(0, k_B T m_i) \quad \text{or} \quad p_i \sim \mathcal{U}\left(-\sqrt{3k_B T m_i}, \sqrt{3k_B T m_i}\right).$$

The situation is different for the positions, since  $\langle q_i \frac{\partial \mathcal{H}}{\partial q_i} \rangle$  gives not their variance, i.e. we cannot sample them directly from a given distribution. A possibility to circumvent this problem is to choose all positions at the equilibrium values  $q^0$ , which are the positions of minimal potential energy, and to sample the momenta with twice the temperature. The system will reach the equilibrium after some time, i.e. the energy will be distributed equally to all degrees of freedom according to the equipartition theorem. However, the number of time steps necessary for this equilibration depends strongly on the system.





# Chapter 2

## Approximations in molecular dynamics simulations

Since in many molecular dynamics simulations a huge system of ordinary differential equations has to be solved, some efforts have been made to develop methods that reduce the complexity of the system. They range from the use of periodic simulation boxes [5] to the upscaling of atomistic equations, e.g. [6, 25, 26]. All these methods have in common, that their applicability depends strongly on the underlying atomistic model and on the effects that we want to study. In section 2.1, we explain the advantages of using a coupled system as an approximation in the molecular dynamics simulation of the sputtering process. Then, we define a local stress tensor for the atomistic model in section 2.2, and we explain in section 2.3 how we want to compare fully atomistic and approximated solutions with respect to this local stress tensor and the energy in the system. In sections 2.4 and 2.5 two methods to derive such a coupled system are presented. We will analyse and compare them for model problems in the next chapter.

### 2.1 Approximations in the simulation of the sputtering process

The basic problems in molecular dynamics simulations are often very time consuming force calculations and the requirement of very small time steps in the simulation. The tabular gives an overview of the different time scales for the sputtering process.

time scale [s]	process
$10^{-15}$	time step of the integrator
$10^{-5}$ - $10^{-4}$	time between two copper atoms hitting a typical simulated crystal slap
$10^{-1}$	time for a complete copper layer to grow

The number of atoms for which the Hamiltonian system of equations can be solved, is therefore strongly limited, as is the total simulation time. One possibility to circumvent this problems, is to use a small simulation box with periodic boundary

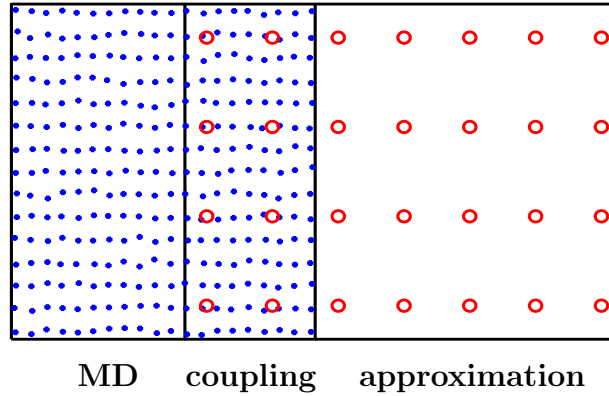


Figure 2.1: different regions of the crystal

conditions. However, this method cannot be used in the simulation of the sputtering process, at least not in all coordinate directions, since we need a free boundary at the surface of the crystal, where the layer of copper develops. Additionally, periodic boundary conditions are mainly used for the simulation of equilibrium situations. In contrast to this, our system is not in equilibrium anymore, after a copper atom hits the surface.

Using only a small system without periodic boundary conditions is also not possible. This would lead to a heating up of the system, since the high energy of the sputtered atoms cannot leave the system. Each atom hitting the crystal generates a perturbation, travelling through the crystal, that would be reflected at the boundary of our simulation box, causing another non physical effect in the system.

On the other hand, we do not want to use an upscaling approach, in the sense of deriving evolution equations on a larger scale and solving them numerically on a coarser grid. The effects near the surface, like atomic hopping [63] or the penetration of atoms into the crystal, occur on the atomic level and cannot be covered by a model valid on a larger scale. However, such effects are very improbable several layers of atoms away from the surface. We can assume that the important effects there, like travelling waves, are of such kind that we do not need the whole atomistic information anymore, but can describe them on a coarser scale. Like this, we get a division of our crystal in two parts, one with an atomistic description, one with a description on a coarse level and a transition region in between, see figure 2.1.

On the coarse level, we want to use again a system of ordinary differential equations, but with less degrees of freedom due to a larger space discretisation. For such an approximation we have to face two problems. First, we need good evolution equations on the coarse scale, i.e. the information that we compute on this scale should be the equivalent information that we would get from an atomistic simulation. Second, we have to couple the coarse scale equations to the atomistic ones. In our simulations, the information that we want to keep on the coarse scale is the velocity of propagation of coarse scale waves. How we can verify that this quantity is correct, is explained in section 2.3.

## 2.2 Definition of microscopic stress tensor

In section 1.1, the development of stresses in the crystal during the sputtering process was explained. Naturally, the stress is a quantity measured on a macroscopic scale, defined for a continuum model of a system. If we want to calculate something like a stress in atomistic simulations, we first need the connection of this quantity to the microscopic scale. The derivation, used in the following, was carried out in [36]. We summarize shortly the derivation of the microscopic stress tensor, which will be used here for the one and two dimensional case ( $d = 1, 2$ ), using the notation of [45].

The basic idea is to define mesoscopic quantities as local averages of microscopic values. The derivation of a local stress tensor starts with the definition of a local continuous mass density function,

$$\rho(x, t) := \sum_{i=1}^n m_i g(q_i(t) - x), \quad (2.1)$$

which is a weighted average of the mass of the particles in the neighbourhood of the continuum point  $x$ . The weight function  $g(x)$  should fulfil the following conditions:

- $g(x)$  is a non-negative local function in space, i.e. the function is non-zero only in a small neighbourhood of  $x$ ,
- $g(x) \in C^1(\mathbb{R}^d, \mathbb{R})$ , i.e.  $g(x)$  is a differentiable mapping from  $\mathbb{R}^d$  to  $\mathbb{R}$ ,
- $g(x)$  is normalized:

$$\int_{\mathbb{R}^d} g(x) dx = 1.$$

The third condition is necessary to obtain spatial averages for the mesoscopic functions, which are consistent with the microscopic quantities. These quantities are defined like the mesoscopic ones, with a delta-function instead of  $g(x)$ . For the mass density we get the equality

$$\int_{\mathbb{R}^d} \sum_{i=1}^n m_i \delta(q_i(t) - x) dx = \int_{\mathbb{R}^d} \sum_{i=1}^n m_i g(q_i(t) - x) dx.$$

Taking the time derivative of (2.1) and using the Hamilton equations (1.1), we can derive from the macroscopic equation of continuity,

$$\frac{\partial \rho(x, t)}{\partial t} = - \operatorname{div} p(x, t),$$

a continuum expression for the momentum  $p(x, t)$ ,

$$p(x, t) = \sum_{i=1}^n p_i(t) g(q_i(t) - x).$$

The spatial divergence is defined as

$$\operatorname{div} f := \sum_{k=1}^d \frac{\partial}{\partial x_k} f_k.$$

With the momentum conservation equation, a similar expression for the microscopic stress tensor  $\sigma$  can be derived,

$$\frac{\partial p(x, t)}{\partial t} = \operatorname{div} \sigma(x, t).$$

Since the component of the time derivative of the continuous momentum in coordinate direction  $\alpha$ ,

$$\dot{p}^\alpha(t) = - \sum_{i=1}^n \frac{\partial \Phi}{\partial q_i^\alpha} g(q_i(t) - x) + \sum_{i=1}^n \sum_{\beta=1}^d \frac{p_i^\alpha p_i^\beta}{m_i} \frac{\partial}{\partial q_i^\beta} g(q_i(t) - x), \quad (2.2)$$

consists of two parts, we split the stress tensor  $\sigma$  accordingly into a configurational and a kinetic part, i.e.

$$\sigma = \sigma_C + \sigma_K. \quad (2.3)$$

If the kinetic part is defined as

$$\sigma_K^{\alpha\beta}(t) := - \sum_{i=1}^n \frac{p_i^\alpha p_i^\beta}{m_i} g(q_i(t) - x), \quad (2.4)$$

its divergence gives directly the second part of (2.2).

To find  $\sigma_C$  in such a way that its divergence is the first part of (2.2), this part is rewritten as

$$\begin{aligned} - \sum_{i=1}^n \frac{\partial \Phi}{\partial q_i^\alpha} g(q_i(t) - x) &= - \frac{1}{2} \sum_{i=1}^n \sum_{\substack{j=1 \\ i \neq j}}^n \frac{\partial \Phi}{\partial q_i^\alpha} [g(q_i(t) - x) - g(q_j(t) - x)] \\ &= - \sum_{i=1}^n \sum_{j>i}^n \frac{\partial \Phi}{\partial q_i^\alpha} \int_{\mathcal{C}_{ij}} \nabla_q g(q(t) - x) dq. \end{aligned} \quad (2.5)$$

In (2.5)  $\mathcal{C}_{ij}$  denotes a curve from  $q_i$  to  $q_j$ . If the gradient is taken with respect to  $x$  instead of  $q$  and  $\mathcal{C}_{ij}$  is the straight line connecting  $q_i$  and  $q_j$ , one obtains

$$\begin{aligned} - \sum_{i=1}^n \frac{\partial \Phi}{\partial q_i^\alpha} g(q_i(t) - x) &= \nabla_x \sum_{i=1}^n \sum_{j>i}^n \frac{\partial \Phi}{\partial q_i^\alpha} \int_{\mathcal{C}_{ij}} g(q(t) - x) dq \\ &= \nabla_x \sum_{i=1}^n \sum_{j>i}^n \frac{\partial \Phi}{\partial q_i^\alpha} (q_i(t) - q_j(t)) \int_0^1 g(q_i(t) - q_{ij}s - x) ds, \end{aligned}$$

with  $q_{ij} := q_i(t) - q_j(t)$ . The derivative of a pair potential can be rewritten as

$$\frac{\partial \Phi}{\partial q_i^\alpha} = \Phi'(|q_{ij}|) \frac{q_{ij}^\alpha}{|q_{ij}|},$$

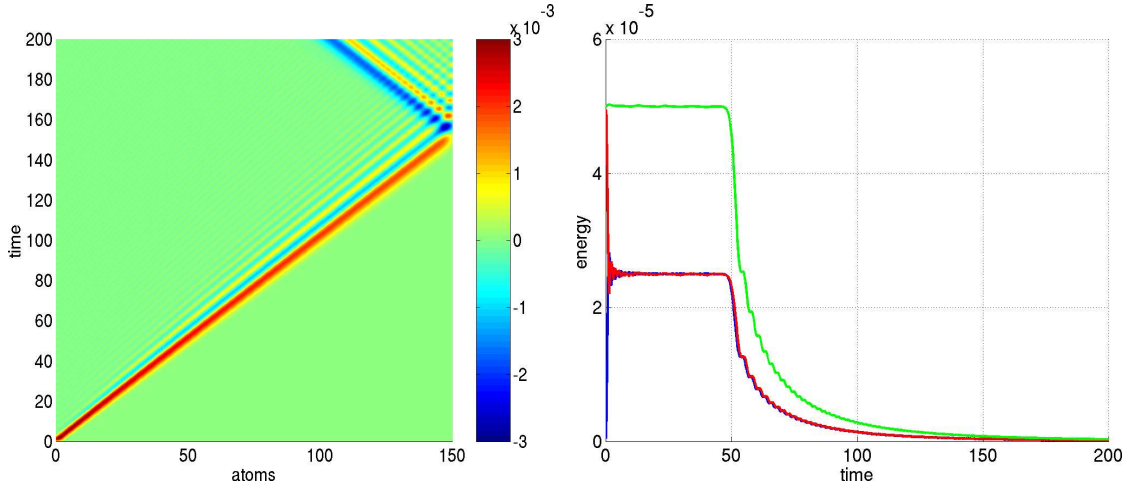


Figure 2.2: one dimensional example for stress tensor (left) and atomistic energy (right)

to get finally

$$\sigma_C^{\alpha\beta}(t) = \sum_{i=1}^n \sum_{j=i+1}^n \Phi'(|q_{ij}|) \frac{q_{ij}^\alpha q_{ij}^\beta}{|q_{ij}|} \int_0^1 g(q_i(t) - q_{ij}s - x) ds.$$

For the evaluation of the continuum stress, the weight function is not considered in every continuum point  $x$  but only at points on a regular coarse grid. A possible choice of the function  $g(x)$ , which will be used in the following, is

$$g(x) := \prod_{\alpha=1}^d \frac{1}{\delta^\alpha} \cos^2 \left( \frac{\pi x^\alpha}{2 \delta^\alpha} \right) \Theta \left( (\delta^\alpha)^2 - (x^\alpha)^2 \right),$$

where  $\Theta(x)$  denotes the characteristic function,

$$\Theta(x) = \begin{cases} 1, & x \geq 0 \\ 0, & x < 0 \end{cases},$$

and  $\delta^\alpha$  gives the width of the support of the weight function in every coordinate direction  $\alpha$ .

Figure 2.2 shows on the left panel a one dimensional example of this stress tensor, for a chain of 151 atoms and a harmonic potential with nearest neighbour interaction. All stress and energy plots for the one dimensional examples are made with Matlab 6.5. Initial displacements and momenta are zero for all atoms, only the first atom gets a non-zero initial momentum to produce a perturbation in the chain. In chapter 3, this model problem will be explained in more detail. On one axis we mark the equilibrium positions of the atoms, on the other the simulation time ( $\Delta t = 0.1$ ,  $k = m = a_0 = 1$ ). The colour corresponds to the value of the stress tensor that has only one entry for the one dimensional case. The perturbation is travelling from the left end of the chain to the right, where it is reflected. It

produces a stress in the chain at the atoms that are moved due to the perturbation. Therefore, the local stress tensor can be used to visualize the time evolution of such a perturbation. The support of the weight function  $g(x)$  in figure 2.2 is  $\delta = 3a_0$ . If the spatial coarse graining of the stress tensor is increased, by increasing  $\delta$ , the resolution of the stress tensor decreases, since very small local effects get lost in the averaging.

### 2.3 Comparing the solutions

Our main goal is to find an approximation for the huge system of ordinary differential equations, which describes the sputtering process. According to section 2.1, this should be done in such a way that the atomistic information is kept in one part of the domain and a coarse scale approximation is used in the remaining part, to reduce the overall system size.

If this reduced system is solved numerically, of course, some information contained in the original system gets lost. Therefore, it is not possible to compare positions and momenta of the two systems one by one, but it has to be defined with respect to which quantities the solutions should be identical.

The transport of energy in the system is of special importance for the sputtering process. Therefore, the first quantity for the comparison of fully atomistic and approximated solution is the time evolution of the energy in the atomistic region. On the right panel of figure 2.2, the energy of the first 51 atoms of the example considered in section 2.2,

$$E_{\text{at}} = \frac{1}{2} \sum_{i=1}^{51} \frac{p_i^2}{m_i} + \frac{1}{2} \sum_{i=2}^{51} k(q_i - q_{i-1} - a_0)^2, \quad (2.6)$$

is given over time. The red line is the kinetic, the blue one the potential and the green line the total energy. When the perturbation is travelling through the chain and leaves the region of the first 51 atoms, the energy of this atoms decreases. We will show later that one of the basic problems in the coupling of atomistic and coarse scale equations is the reflection of waves in the transition region from atomistic to pure coarse scale description. If parts of the waves are reflected, the energy decrease in the atomistic region is changed, since the perturbation cannot leave this region completely.

The second quantity, to compare the solution of fully atomistic and approximated system, is the microscopic stress tensor, defined in the previous section. If we have spurious reflections in the transition region, they can be observed as deviations from the fully atomistic stress in 2.2.

With the atomistic energy and the local microscopic stress tensor, two criteria are defined, to check for reflections of waves and other influences of an approximation on the solution in the atomistic region.

Additional to the requirement that this influences should be as small as possible, the information computed on the coarse scale should be the corresponding information of the atomistic solution. If some perturbation is travelling through the crystal,

the velocity of this perturbation in the coarse scale region should be conserved. We will explain now how this velocity is computed for the one dimensional case.

A perturbation consists of different harmonic waves with different wave vectors  $\kappa$ , and each wave vector has a different velocity in an atomistic system. If the harmonic solution of atom  $i$  for given  $\kappa$ ,

$$u_j(t) = \exp(i(\omega t + j\kappa\Delta x)),$$

is plugged into the system of differential equations, we can solve for the frequency  $\omega(\kappa)$ . The dependence of the frequency on the wave vector is called the dispersion relation, and  $\Delta x$  denotes here the space discretisation parameter. With this information, the velocity of propagation of the harmonic wave can be computed as

$$c(\kappa) = \frac{\omega(\kappa)}{\kappa}.$$

To resolve a wave on a grid, we need at least two discretisation points per wave length  $\lambda = 2\pi/\kappa$ . This is the spatial analogon to the Nyquist sampling theorem, which states, that a signal has to be sampled with twice its frequency that it can be reconstructed from the sampling information. Therefore, the maximum wave vector is given by the space discretisation,

$$\kappa \in \left(0, \frac{\pi}{\Delta x}\right].$$

Since the number of harmonic solutions of the system corresponds to the number of atoms, the different wave vectors are

$$\kappa_j = \frac{\pi}{j\Delta x}, \quad j \in \{1, \dots, n-1\}.$$

As an example, we compute the wave speed for the chain of 151 atoms with harmonic nearest neighbour interaction from section 2.2. Each inner atom has the evolution equation

$$m\ddot{u}_l(t) = k(u_{l-1} - 2u_l + u_{l+1}),$$

with  $l$  the index of the atom. The resulting dispersion relation is

$$\omega^2 = 4\frac{k}{m} \sin^2\left(\frac{\kappa a_0}{2}\right).$$

The limit of the velocity,

$$c(0) := \lim_{\kappa \rightarrow 0} \frac{\omega(\kappa)}{\kappa} = \frac{d\omega(\kappa)}{d\kappa} \Big|_{\kappa=0} = \sqrt{\frac{k}{m}} a_0,$$

depends only on the parameters  $m$ ,  $k$  and  $a_0$ . If the velocity is scaled with the inverse of this factor,

$$\tilde{c}(\kappa) := \frac{\omega(\kappa)}{\kappa} \frac{1}{a_0} \sqrt{\frac{m}{k}}, \quad (2.7)$$

the result is a function with limit 1, independent of parameters. Figure 2.3 shows this scaled dispersion relation for the example.

The quantities presented here for the comparison of atomistic and approximated solutions will be used in the next chapters for the evaluation of several approximations of some model problems.



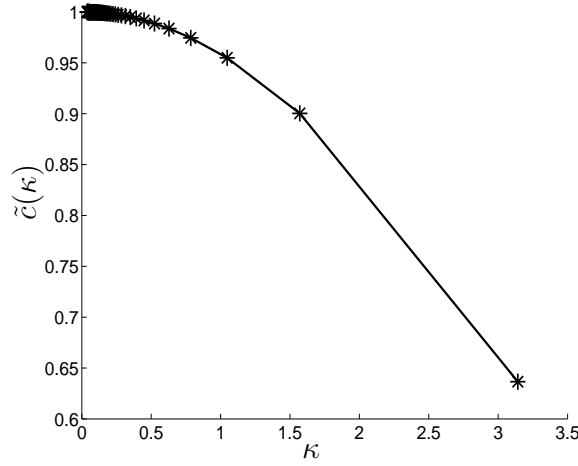


Figure 2.3: example of dispersion relation

## 2.4 Concurrent coupling of length scales method

This method to approximate a large molecular dynamics system by the coupling with a finite element approximation of partial differential equations was developed in 1998 [1], as a dynamic extension of the quasicontinuum method [68, 64, 65], used to approximate quasi-static atomistic problems, e.g. nano-indentation in a crystal. It includes also a coupling with a quantum mechanical tight-binding scheme for more exact interatomic force calculations, which will not be considered here. In the following, we give a short outline of the coupling of molecular dynamics with the finite element method. The method is described in detail in [1, 69], the atomistic calculation of the finite element elasticity constants in [68, 16]. The finite element method as an approximation for the solution of partial differential equations will not be explained here, since it can be found in many textbooks (e.g. [74, 12, 9]). We mention here only the important aspects for the coupling.

The main idea is to divide the domain into a molecular dynamics and a finite element region, depending on the required accuracy of the solution. Then, an overall Hamiltonian is defined, depending on the atomistic positions  $q$  and velocities  $\dot{q}$  in the molecular dynamics part  $\mathcal{H}_{\text{MD}}$ , on the displacements  $u$  and velocities  $\dot{u}$  in the finite element part  $\mathcal{H}_{\text{FE}}$ , and on both in the transition region  $\mathcal{H}_{\text{MD/FE}}$ :

$$\mathcal{H}(q, \dot{q}, u, \dot{u}) := \mathcal{H}_{\text{MD}}(q, \dot{q}) + \mathcal{H}_{\text{MD/FE}}(q, \dot{q}, u, \dot{u}) + \mathcal{H}_{\text{FE}}(u, \dot{u}).$$

The molecular dynamics Hamiltonian is defined in the usual way,

$$\mathcal{H}_{\text{MD}}(q, \dot{q}) := \frac{1}{2} \sum_{i \in I} m_i \dot{q}_i^2 + \frac{1}{2} \sum_{i, j \in I} \Phi(|q_i - q_j|),$$

and the finite element Hamiltonian is defined as the variational integral of linear elasticity [61],

$$\mathcal{H}_{\text{FE}}(u, \dot{u}) := \frac{1}{2} \int \sum_{\mu, \nu, \lambda, \sigma} \epsilon_{\mu\nu}(x) C_{\mu\nu\lambda\sigma} \epsilon_{\lambda\sigma}(x) d\Omega + \frac{1}{2} \int \rho(x) \dot{u}^2(x) d\Omega,$$

with the linearised strain tensor

$$\epsilon_{\mu\nu} := \frac{1}{2} \left[ \frac{\partial u_\mu}{\partial x_\nu} + \frac{\partial u_\nu}{\partial x_\mu} \right].$$

Stress and strain are linearly related by the fourth order elasticity tensor  $C$  that can be determined from the underlying atomistic model [68, 16]. In chapter 3, we will give an example for the computation of  $C$ . It is however not necessary to assume linear elasticity in the finite element region [69].

The finite element Hamiltonian is continuous, therefore we have to discretise it to find a numerical solution and to define the coupling in the transition region. As usual in solving partial differential equations with the finite element method, the domain is discretised in so called finite elements, e.g. triangles in two or tetrahedra in three dimensions, and local interpolation functions  $\varphi(x)$ , e.g. linear hat functions, are defined on this discretisation.

If the displacements and velocities on the finite elements are approximated with this local functions,

$$u(x) = \sum_j u_j \varphi_j(x), \quad \dot{u}(x) = \sum_j \dot{u}_j \varphi_j(x),$$

we get again a discrete Hamiltonian

$$\mathcal{H}_{\text{FE}} = \frac{1}{2} \sum_k \sum_{i,j} (u_i K_{ij}^k u_j + \dot{u}_i M_{ij}^k \dot{u}_j).$$

The coefficients  $K_{ij}^k$  and  $M_{ij}^k$  are computed from the finite element interpolation functions,

$$M_{ij}^k = \int_{\Omega^k} \rho \varphi_i(x) (\varphi_j(x))^T dx, \quad K_{ij}^k = \int_{\Omega^k} \nabla \varphi_i(x) C (\nabla \varphi_j(x))^T dx,$$

where  $\Omega^k$  denotes the finite element  $k$ . We assume that the mass density  $\rho$  is constant in the whole domain. The coefficients are computed separately for each element, to be able to compute also the forces for each element separately in the transition region. For the finite element masses, we can use a so called lumped mass approximation, i.e. the mass of every node is defined as the sum of all corresponding coefficients  $M_{ij}^k$ ,

$$M_{ii} = \sum_k \sum_j M_{ij}^k, \quad M_{ij} = 0, \text{ for } j \neq i.$$

Then, the finite element Hamiltonian has the same structure as the atomistic Hamiltonian,

$$\mathcal{H}_{\text{FE}} = \frac{1}{2} \sum_{k \in K} \sum_{i,j \in I} u_i K_{ij}^k u_j + \frac{1}{2} \sum_{i \in I} M_{ii} \dot{u}_i^2. \quad (2.8)$$

This has the advantage, that we can use the same update algorithm as in the atomistic region. Since we want to use this finite element Hamiltonian only for the

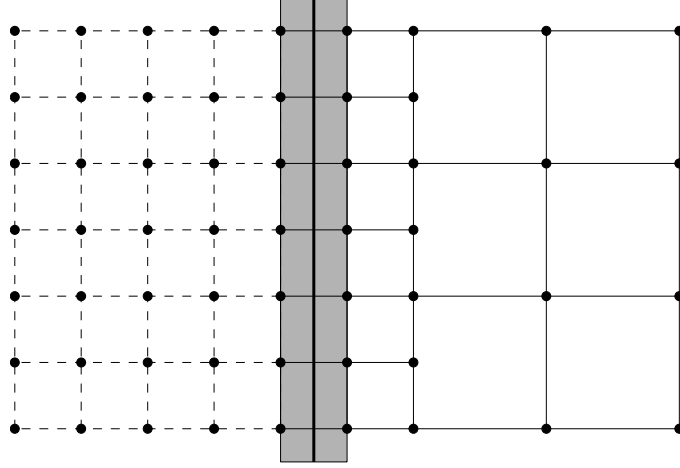


Figure 2.4: transition region between atoms (left) and finite elements (right)

elements in the pure coarse scale region, the set  $K$  denotes the elements and  $I$  the nodes in this region.

Finally, we need a Hamiltonian for the transition region between atoms and finite elements, which is marked grey in figure 2.4. By starting with a continuous formulation in the finite element region, the information of the transition from atomistic to approximated equations is lost, and it has to be reproduced now artificially. Therefore, the finite element nodes in this region are chosen as the equilibrium positions of the atoms, i.e. every displacement of an atom from its equilibrium position can be considered as a nodal displacement and vice versa. Forces due to interaction over the interface are computed with respect to both the atomistic and the finite element description and contribute both with half of their weight to the resulting force in the transition region. That is

$$\begin{aligned} \mathcal{H}_{\text{MD/FE}} &:= \frac{1}{4} \sum_{i \in \tilde{I}} m_i \dot{q}_i^2 + \frac{1}{4} \sum_{i,j \in \tilde{I}} \Phi(|q_i - q_j|) \\ &+ \frac{1}{4} \sum_{k \in \tilde{K}} \sum_{i,j \in \tilde{I}} u_i K_{ij}^k u_j + \frac{1}{4} \sum_{i \in \tilde{I}} M_{ii} \dot{u}_i^2, \\ \text{with} \quad &\dot{u}_i = \dot{q}_i, \quad u_i = q_i - q_{\text{eq},i}, \quad \forall i \in \tilde{I}, \end{aligned}$$

where the set  $\tilde{I}$  denotes atoms and the set  $\tilde{K}$  elements in the transition region, and  $q_{\text{eq},i}$  is the equilibrium position of atom  $i$ , i.e. the position of minimal potential energy. This choice of the Hamiltonian in the transition region is somehow artificial, since it is not motivated by transition from atomistic to coarse scale.

In [65] a three dimensional example of crack propagation was computed with this coupling scheme, with an atomistic region and two neighbouring finite element regions in one direction. In the orthogonal direction periodic boundary conditions were used, for both the atoms and the finite element nodes, and in the finite element region a two dimensional solution was computed under the assumption of a plane strain situation. For a constant strain rate at the finite element boundaries and a

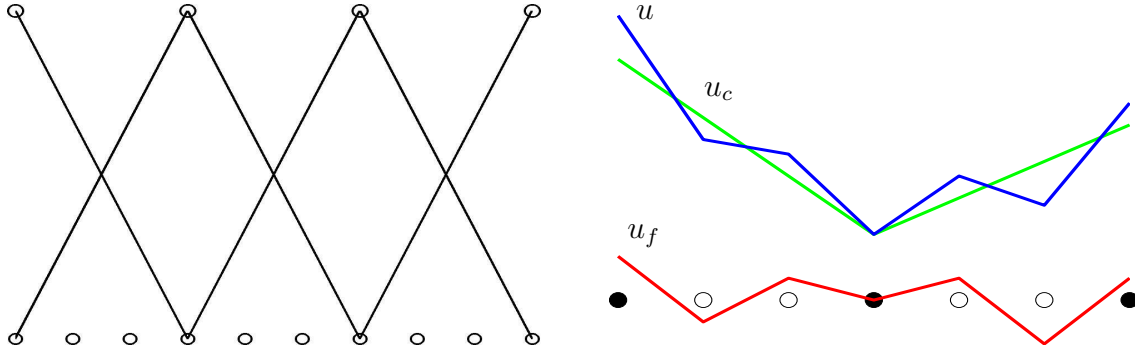


Figure 2.5: linear interpolation from coarse scale nodes to atoms (left) and displacement splitting (right)

constant velocity gradient within the slab, no reflection of waves at the interface between atomistic and finite element region was observed. However, for waves with small wave length in the atomistic region, this cannot be expected. The influence of this reflections in the situation of the sputtering process and the dependence on the coupling scheme will be investigated in chapter 3.

The coupling of length scales scheme was also used for other applications, like dislocation emission at the silicon/silicon-nitride interface [7], a projectile impact on a 3D block of crystalline silicon [52], and induced stress distributions in silicon/silicon-nitride nano-pixels [48].

## 2.5 Bridging scales approximation

Another approach, for approximating the huge system of ordinary differential equations in molecular dynamics simulations, was developed in 2003 by G. Wagner and W. K. Liu [71]. The main difference to the coupling of length scales approach is, that a coarse scale description is not derived as an approximation of a continuum formulation. Instead, a coarse scale grid is defined, and evolution equations are derived for the coarse scale nodes. We summarize the main ideas and refer to the original publication for a more detailed description.

**Coarse and fine scale Lagrangian** The starting point is the choice of the coarser grid. We choose the equilibrium position of every  $\tilde{n}$ th atom as a coarse scale node. On this grid, we define an interpolation from the coarse scale nodes back to the atomic scale. With  $N_j$  we denote the interpolation function of node  $j$ , with  $N_{ij}$  its evaluation at the equilibrium position of atom  $i$ ,

$$N_{ij} = N_j(q_{\text{eq},i}), \quad i \in \{1, \dots, n\}, \quad j \in \{1, \dots, n_c\},$$

where  $n_c$  denotes the number of coarse scale nodes. We can choose e.g. linear finite element hat functions as interpolation functions. Figure 2.5 shows on the left panel an example for  $\tilde{n} = 3$ . The advantage of evaluating the interpolation functions at

the equilibrium positions, instead of the time dependent atomic positions is, that the interpolation matrix is constant in time.

The displacements of the atoms from their equilibrium positions,

$$u = (u_i(t))_{i \in \{1, \dots, n\}} = (q_i(t) - q_{eq,i})_{i \in \{1, \dots, n\}},$$

are split into the contribution from the coarse scale  $u_c$ , and from the fine scale  $u_f$ ,

$$u = u_c + u_f.$$

The coarse scale contribution is given by the interpolation from the coarse scale node displacements, denoted by  $d = (d_i)_{i \in \{1, \dots, n_c\}}$ ,

$$u_c := Nd. \quad (2.9)$$

While the interpolation defines the transition from coarse to fine scale, we need also a projection as transition from fine to coarse scale. It is defined as the least square approximation of the atomistic displacements with respect to the atomic mass matrix  $M$ , which is a diagonal matrix with the atomic masses  $m_i$ . Hence

$$(u - Nd)^T M (u - Nd) \mapsto \min \quad \Rightarrow \quad d = (N^T M N)^{-1} N^T M u. \quad (2.10)$$

This definition assures that the projection of interpolated displacements reproduces the original values:

$$d = (N^T M N)^{-1} N^T M N d.$$

With (2.9) and (2.10), we can define the projection operator  $P$ ,

$$Pu := u_c = Nd = N(N^T M N)^{-1} N^T M u,$$

and, with the orthogonal operator  $Q := I - P$ , the fine scale part of the displacements is defined as

$$u_f = u - u_c = (I - P)u = Qu,$$

with the identity matrix  $I$ . Finally, the atomistic displacements can be written as

$$u = Pu + Qu = Nd + Qu, \quad (2.11)$$

with the singular matrix  $Q$ .

On the right panel of figure 2.5, we show an example for the displacement splitting. The coarse scale part (green) is linear between two coarse scale nodes, the fine scale part (red) is the difference to the whole atomistic displacements (blue).

If we put (2.11) into the molecular dynamics Lagrangian, we get

$$\begin{aligned} \mathcal{L} &= \frac{1}{2} \sum_{i=1}^n m_i \dot{u}_i^2 - \Phi(u) = \frac{1}{2} \dot{u}^T M \dot{u} - \Phi(u) \\ &= \frac{1}{2} \dot{u}^T Q^T M Q \dot{u} + \frac{1}{2} \dot{d}^T N^T M N \dot{d} - \Phi(Nd + Qu), \end{aligned} \quad (2.12)$$

where, due to

$$N^T M Q = N^T M (I - N(N^T M N)^{-1} N^T M) = 0,$$

the kinetic energy terms decouple.

From the Lagrangian, we can derive the equations of motion

$$\frac{d}{dt} \left( \frac{\partial \mathcal{L}}{\partial \dot{d}} \right) - \frac{\partial \mathcal{L}}{\partial d} = 0 \Rightarrow N^T M N \ddot{d} = -\frac{\partial \Phi}{\partial d} = -N^T \Phi'(Nd + Qu), \quad (2.13)$$

$$\frac{d}{dt} \left( \frac{\partial \mathcal{L}}{\partial \dot{u}} \right) - \frac{\partial \mathcal{L}}{\partial u} = 0 \Rightarrow Q^T M Q \ddot{u} = -\frac{\partial \Phi}{\partial u} = -Q^T \Phi'(Nd + Qu), \quad (2.14)$$

where  $\Phi'$  denotes the derivative of  $\Phi$  with respect to the whole argument. Since the matrix  $Q$  is a projection, i.e.  $QQ = Q$ , and commutes with the mass matrix  $M$ ,  $MQ = Q^T M$ , even if not all atomic masses are identical,  $Q^T M Q = Q^T M$  holds. In equation (2.14) we get

$$Q^T M \ddot{u} = -Q^T \Phi'(Nd + Qu).$$

Since  $Q$  is singular, this system of equations has no unique solution, but a particular solution is given by the solution of the original molecular dynamics system,

$$M \ddot{u} = -\Phi'(u), \quad (2.15)$$

and its projection.

In this case, the information of the first system of equations (2.13) is completely redundant. But since we want to calculate the total displacement only in one part of the domain and neglect the fine scale information in the rest, we need in particular the derived coarse scale equations. Since the equations for the fine scale and the coarse scale displacements do not decouple, some approximation is necessary to get pure coarse scale equations.

**Domain decomposition: coupling of coarse and full dynamics** We divide the atoms into the real ones, denoted in the following with subscript 1, and those for which we want to neglect the fine scale part of the displacement, marked with subscript 2. Omitting this fine scale displacements leads to wave reflections at the interface and wrong dispersion relation in the pure coarse scale region. Therefore, Wagner and Liu proposed to use a reflectionless boundary condition at the interface and the computation of coarse scale internal forces  $-N^T \Phi'(u)$  with the so called Cauchy-Born rule, see below.

**Reflectionless boundary condition** To derive the reflectionless boundary condition, the force is first linearised with respect to the fine scale displacements which we want to neglect.

$$-\Phi'(u) = f(u) = f(u_c, u_{1,f}, u_{2,f}) \approx f(u_c, u_{1,f}, 0) - K_2 u_{2,f},$$

with  $K_2$  denoting the coefficients of the linear terms of  $u_{2,f}$  of the Taylor expansion of  $f$  around  $u_{2,f} = 0$ . With this approximation, we get the evolution equations:

$$\begin{aligned} M_1 \ddot{u}_1 &\approx f_1(u_c, u_{1,f}, 0) - K_{12} u_{2,f}, \\ M_2 \ddot{u}_2 = M_2(\ddot{u}_{2,c} + \ddot{u}_{2,f}) &\approx f_2(u_c, u_{1,f}, 0) - K_{22} u_{2,f}, \end{aligned} \quad (2.16)$$

where  $M_1$ ,  $M_2$  and  $K_{12}$ ,  $K_{22}$  denote the parts of the matrices  $M$  and  $K_2$  for the two kinds of atoms. Next, the force  $f_2$  is linearised with respect to  $u_{1,f}$ , and it is assumed that  $\ddot{u}_{2,c}$  depends only on  $u_c$ :

$$M_2 \ddot{u}_{2,c} \approx f_2(u_c, 0, 0) \Rightarrow M_2 \ddot{u}_{2,f} \approx -K_{21} u_{1,f} - K_{22} u_{2,f}, \quad (2.17)$$

where  $K_{21}$  denotes the coefficients of the linear terms of the expansion of  $f_2$  around  $u_{1,f} = 0$ .

Laplace transformation of the second equation, with  $U(s) := L\{u(t)\}$ , yields

$$[s^2 I + M_2^{-1} K_{22}] U_{2,f}(s) = -M_2^{-1} K_{21} U_{1,f}(s) + s u_{2,f}(0) + \dot{u}_{2,f}(0).$$

If we solve for  $U_{2,f}$  and make an inverse Laplace transformation, we obtain an expression for  $u_{2,f}$  and with (2.16) new approximate evolution equations for the real atoms,

$$M_1 \ddot{u}_1 = f_1(u_c, u_{1,f}, 0) - \int_0^t \theta(t - \tau) \tilde{a}_2(\tau) d\tau + R(t),$$

with

$$\theta(t) = K_{12} L^{-1} \{ [s^2 I + M_2^{-1} K_{22}]^{-1} \}, \quad (2.18)$$

$$\begin{aligned} \tilde{a}_2(t) &= -M_2^{-1} K_{21} u_{1,f}(t), \\ R(t) &= \dot{\theta}(t) u_{2,f}(0) + \theta(t) \dot{u}_{2,f}(0). \end{aligned} \quad (2.19)$$

The term  $R(t)$  represents the influence of the initial fine scale displacements and velocities which we want to neglect on the force calculation of the real atoms. The memory integral, with the memory kernel  $\theta(t)$ , gives the influence of this fine scale displacements due to the interaction of the corresponding atoms with the real atoms.

Boundary conditions to avoid reflections of waves are also used e.g. in [29, 30] for the wave equation.

**Coarse scale forces** The other problem is the coarse scale force calculation in (2.13), in the region where we want to neglect the fine scale displacements. The approach used here to calculate this forces is similar to that in the quasi-continuum method and in the concurrent coupling of length scales method.

The derivation of the coarse scale forces is based on two assumptions. The first one is to assume that the potential energy can be written in terms of an energy density  $W_\alpha$ , that is

$$\Phi(u) = \sum_{\alpha} W_{\alpha}(u) \Delta V_{\alpha},$$

with  $\Delta V_\alpha$  the volume per atom. The second assumption is, that this energy density depends on the coarse scale displacements only through the coarse scale deformation gradient  $\bar{F}_\alpha$ , defined as

$$\bar{F}_\alpha := I + \sum_j \frac{\partial N_j}{\partial x}(q_{\text{eq},\alpha}) d_j.$$

The force at a coarse scale node can be written as

$$\begin{aligned} -(N^T \Phi'(u))_j &= -\frac{\partial \Phi(u)}{\partial d_j} = -\sum_\alpha \frac{\partial W_\alpha(u)}{\partial d_j} \Delta V_\alpha = -\sum_\alpha \frac{\partial W_\alpha}{\partial \bar{F}_\alpha} \frac{\partial \bar{F}_\alpha}{\partial d_j} \Delta V_\alpha \\ &= -\sum_\alpha \frac{\partial N_j}{\partial x}(q_{\text{eq},\alpha}) \frac{\partial W_\alpha}{\partial \bar{F}_\alpha} \Delta V_\alpha. \end{aligned} \quad (2.20)$$

We can calculate the change in the energy density according to the deformation gradient, under the assumption that the interatomic distances  $r_{\alpha\beta}$  in the deformed state depend on the initial ones  $r_{0,\alpha\beta}$  through the deformation gradient  $\bar{F}_\alpha$ , as

$$r_{\alpha\beta} = (\bar{F}_\alpha - 1)r_{0,\alpha\beta}. \quad (2.21)$$

This connection is known as Cauchy-Born rule [68]. If we determine the potential energy from the atomistic distances (2.21), we can compute the energy density and the force for every node just from the coarse scale displacements. In chapter 3, we will give an example of such a computation of the coarse scale force.

**Remarks** The first example problem, considered in [71], was a one dimensional chain of atoms with harmonic potential and an initial perturbation given by the superposition of a coarse and a fine scale initial displacement, with good results for the reflectionless boundary condition.

The method was extended and applied for the two and three dimensional case [55, 53], using a Green's function approach for the numerical computation of the reflectionless boundary condition [42], and to a continuum temperature equation [54].

An advantage of the bridging scales algorithm is, that we have two systems of equations, one for the coarse and one for the fine scale degrees of freedom. Therefore, the coupling scheme allows easily to use a larger time step for the update of the coarse scale equations. The only thing we have to do, is to interpolate the coarse scale displacements in time, to get the necessary values for the atomistic force calculation (2.14) [71].

A disadvantage is, that due to the approximation in equation (2.17), the boundary condition cannot be derived from the Lagrangian of the system and that due to the splitting of the fine scale displacements into two parts, according to the atoms on both sides of the interface, the approximation is not energy conserving. This will be discussed in detail in section 4.1.





# Chapter 3

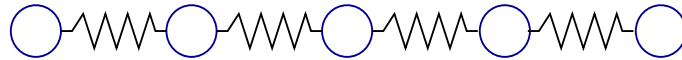
## One dimensional analysis and extension of existing methods

x To find out how applicable the methods presented in the previous chapter are in the numerical simulation of the sputtering process, we consider now some model problems. Starting with the easiest interatomic interaction, a one dimensional harmonic potential with nearest neighbour interaction, we analyse in section 3.1 the concurrent coupling of length scales and the bridging scales method for this problems. Continuing with more complicated potentials, still harmonic ones with more than nearest neighbour interaction and anharmonic ones in section 3.2, we study the additional problems. Extensions of the bridging scales method that solve some of the remaining problems are given.

In the following, we consider always the case of an atom at the boundary of the domain with high initial momentum, instead of a sputtered atom. This is reasonable, since it is difficult to model the sputtering with a harmonic potential and we are only interested in the coupling of atomistic and coarse grained description, some atomistic layers away from the surface.

### 3.1 Harmonic chain of atoms

As a first example, we consider the easiest one dimensional model problem, a chain of  $n$  atoms connected with springs.



The Hamiltonian for the harmonic potential with nearest neighbour interaction is

$$\mathcal{H} = \frac{1}{2} \sum_{i=1}^n \frac{p_i^2}{m} + \frac{1}{2} \sum_{i=2}^n k(q_i - q_{i-1} - a_0)^2, \quad (3.1)$$

with  $k$  the spring constant,  $m$  the atomic mass and  $a_0$  the equilibrium distance of the atoms. The Hamilton equations of motion for each atom  $i$  are

$$\begin{aligned}\dot{q}_i &= \frac{\partial \mathcal{H}}{\partial p_i} = \frac{p_i}{m}, \\ \dot{p}_i &= -\frac{\partial \mathcal{H}}{\partial q_i} = k(q_{i-1} - 2q_i + q_{i+1}).\end{aligned}$$

For this model problem, the transition from the atomistic system of ordinary differential equations to the corresponding continuum partial differential equation, the linear wave equation, can be derived by taking the limit  $a_0 \rightarrow 0$  while keeping  $m/(ka_0^2)$  constant [34]. But even if we know the correct continuum description, the problem of the discretisation of the continuum equation and the coupling to the molecular dynamics equations remains.

In the following, we want to analyse the two coupling schemes, presented in the previous chapter, for this model problem. We consider two numerical examples and compare and discuss the results for the two different approximations.

**Numerical example 1** For the first numerical example, we consider a chain with  $n = 151$  atoms. Initially, all atoms are in their equilibrium position. To find out how the approximations deal with an atomistic perturbation travelling through the chain, the first atom gets a high initial momentum, while the momenta of the other atoms are zero,

$$q_i(0) = q_{\text{eq},i}, \quad i \in \{1, \dots, n\}, \quad p_1(0) = 0.01, \quad p_i(0) = 0, \quad i \in \{2, \dots, n\}.$$

The atomic parameters are set to  $m = k = a_0 = 1$ , and we solve the molecular dynamics system with a velocity Verlet algorithm with time step  $\Delta t = 0.1$ . For the different approximations, we consider the first 51 atoms as real atoms, i.e. their evolution is computed according to the original Hamilton equations, while the solution of the remaining 100 atoms is approximated. In figure 3.1, we compare the stress over time of the fully atomistic system (left) with a very rough approximation, where we just omit the equations for the right 100 atoms (right). In both cases, the stress is evaluated according to equation (2.3), with the width of the support of the weight function  $\delta = 3a_0$ , at the equilibrium positions of all 151 atoms. We run the computation over 2400 time steps.

In the left panel of the figure, we see that the perturbation travels from left to right and is only reflected at the end of the chain. We see also dispersion of the different wave lengths contained in the perturbation that have different wave speeds. In the right panel, we can see, that the perturbation is again reflected at the last moving atom, i.e. the system behaves like a chain of only 51 atoms. There is no possibility for the perturbation to leave the region of the real atoms, and the resulting stress differs significantly from that of the solution for the whole chain.

Beside the stress, we want to compare the approximations with respect to the energy  $E_{\text{at}}$  of the first 51 atoms, given by equation (2.6), and the displacement of a

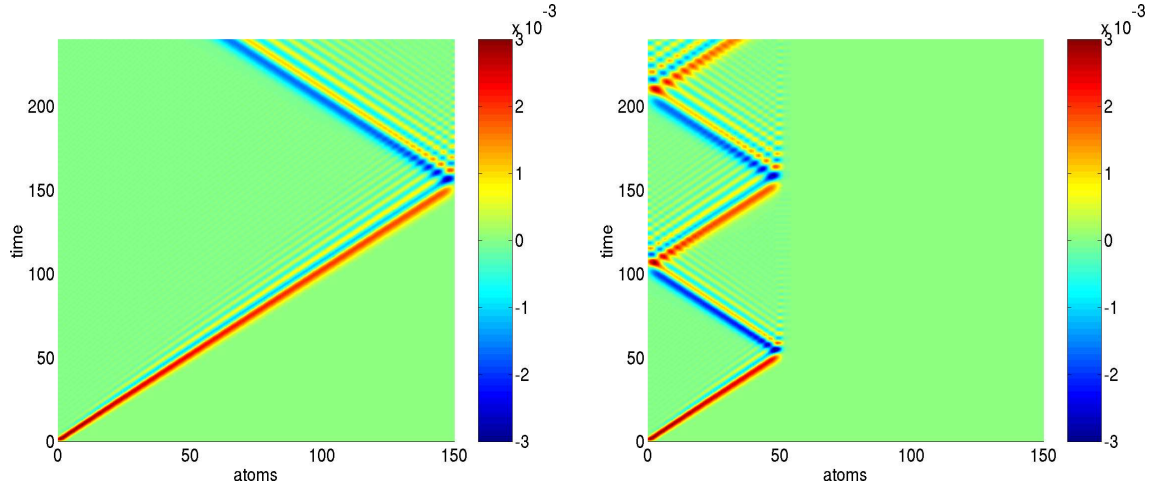


Figure 3.1: stress at the atomistic equilibrium positions, full (left) and reduced (right) system

single atom, which provides also a measure of wave reflection at the interface between atomistic and approximated region. Figure 3.2 shows in the left panel, that in the fully atomistic simulation, the energy  $E_{\text{at}}$  reaches zero, when the perturbation leaves the region of the real atoms. The behaviour is different for the reduced system, as can be seen in the left panel of figure 3.3. The energy of the real atoms is constant in time, since there is no possibility for energy exchange. The red line is thereby the kinetic, the blue one the potential and the green line the total energy.

In the right panel of figures 3.2 and 3.3, the displacement of the 40th atom from its equilibrium position is given over time. In the fully atomistic simulation, the perturbation passes this atom only once, and afterwards the displacement is fluctuating around a constant value, whereas in the reduced system, the perturbation is reflected at the boundary of the real atoms and the displacement of the atom is increased whenever the perturbation passes.

**Numerical example 2** In the second numerical example, we consider again a chain of 151 atoms with 51 real atoms. Again, all initial displacements are zero, but the initial momenta are sampled from a Gaussian distribution with mean zero, i.e.

$$p_i \sim N(0, 2k_B T m), \quad i \in \{1, \dots, n\}$$

with temperature  $T = 10^{19}$ .

We consider again the energy over time for the 51 real atoms and compare the mean values over 50 samples for the different approximations. In figure 3.4, it can be seen that for a fully atomistic simulation the mean value of the energy of the real atoms is nearly constant over time, since we have energy exchange between the first 51 and the other atoms. This example serves as a test if a given temperature can be kept constant in the approximation. For this example, there would be nearly no difference between the simulation of the full and the reduced system. Also the

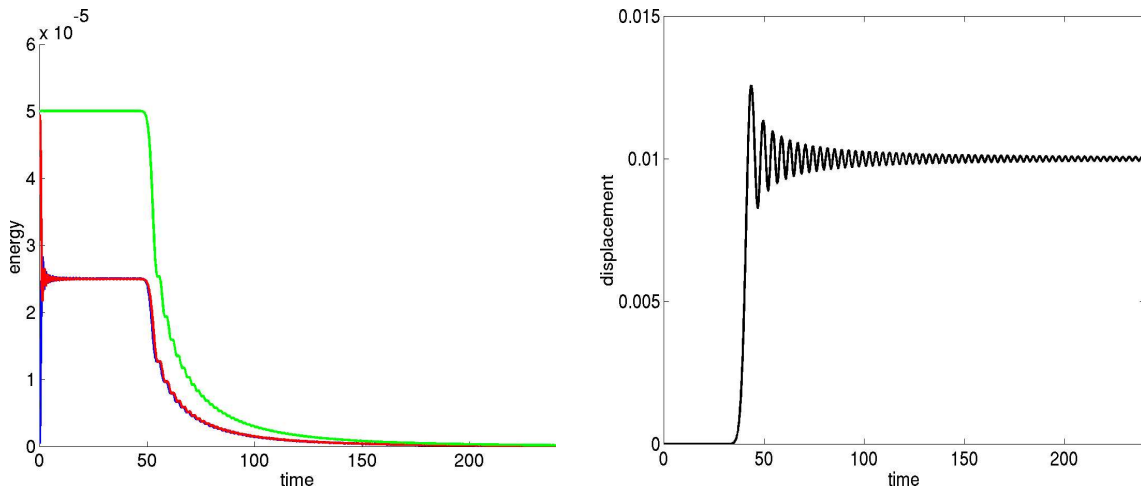


Figure 3.2: atomistic energy (left) and displacement of 40th atom (right) for fully atomistic system

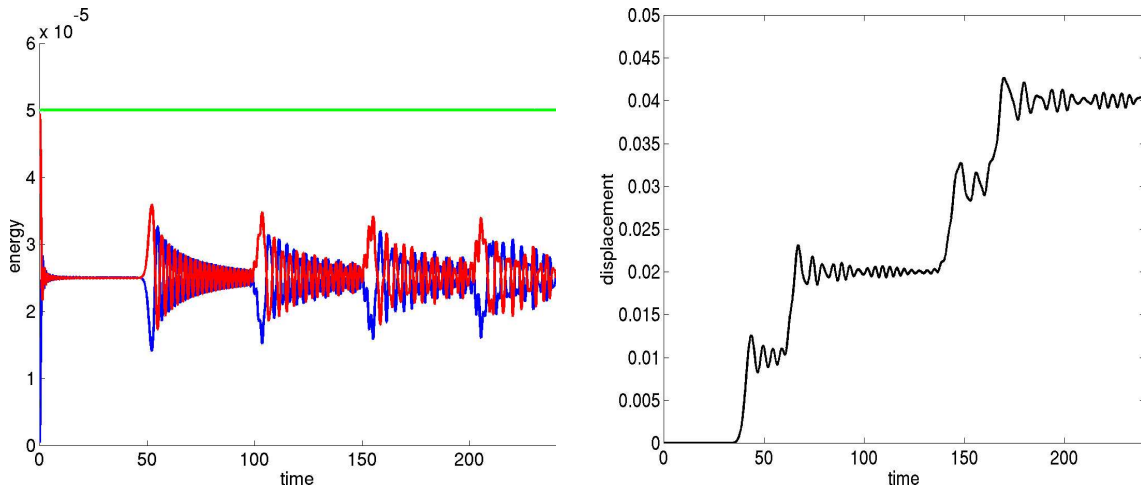


Figure 3.3: atomistic energy (left) and displacement of 40th atom (right) for reduced system

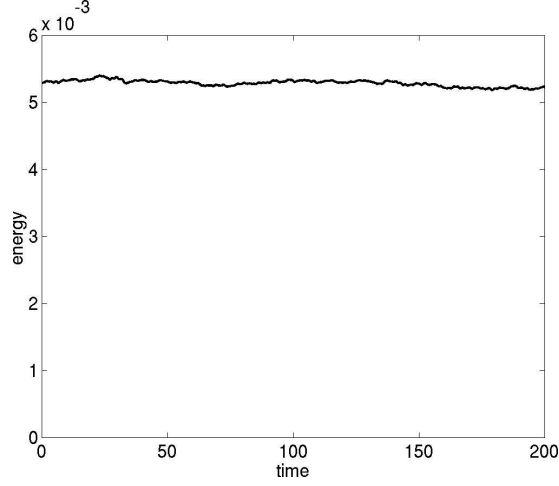


Figure 3.4: atomistic energy for fully atomistic system in numerical example 2

reduced system is a Hamiltonian system, i.e. the initial energy is constant over time. The only difference to the fully atomistic simulation is, that we do not have small fluctuations, since we have no energy exchange with other than the 51 real atoms.

### 3.1.1 Concurrent coupling of length scales method

To use the concurrent coupling of length scales approximation, we first have to define the appropriate Hamiltonian. For the one dimensional model problem, we have to determine the elasticity constant  $C$  and the mass density  $\rho$  for the finite element region. If we use piecewise linear hat functions for the finite elements, the non-zero coefficients in (2.8) for an element  $k$ , which is the interval  $[x_i, x_{i+1}]$ , are

$$\begin{aligned} M_{i,i}^k &= M_{i+1,i+1}^k = \frac{\rho(x_{i+1} - x_i)}{3}, \\ M_{i,i+1}^k &= M_{i+1,i}^k = \frac{\rho(x_{i+1} - x_i)}{6}, \\ K_{i,i}^k &= K_{i+1,i+1}^k = \frac{C}{x_{i+1} - x_i}, \\ K_{i,i+1}^k &= K_{i+1,i}^k = -\frac{C}{x_{i+1} - x_i}. \end{aligned}$$

Thereby denotes  $x_i$  the position of the finite element node  $i$ . If the lumped mass approximation is used, we get

$$M_{ii} = \rho(x_{i+1} - x_{i-1})/2, \quad M_{ij} = 0, \quad i \neq j$$

and the finite element Hamiltonian is

$$\mathcal{H}_{\text{FE}} = \frac{1}{2} \sum_{i \in I} \frac{\rho}{2} (x_{i+1} - x_{i-1}) \dot{u}_i^2 + \frac{1}{2} \sum_{i \in I} \frac{C(u_i - u_{i+1})^2}{(x_{i+1} - x_i)}. \quad (3.2)$$

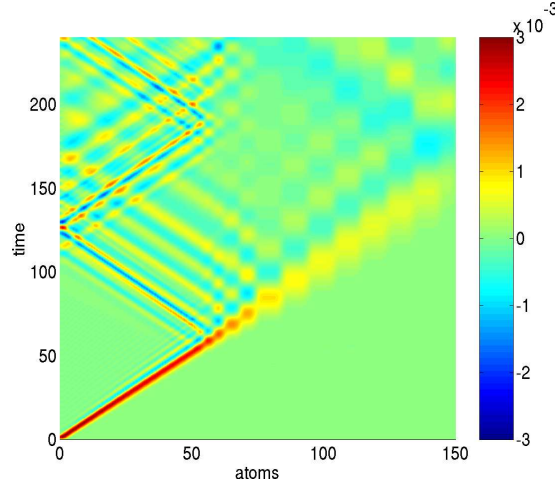


Figure 3.5: stress with concurrent coupling of length scales approximation for numerical example 1

The computation of the constant  $C$  from the atomistic model can be done according to [16]. This leads to a derivation of the elasticity constant similar to the derivation of the coarse scale force in the bridging scales approach (cf. section 3.1.2). However, for the model problem, we can get this constants directly, since the force calculation is linear not only in the finite elements but also in the atomistic region. We just have to consider the case that the distance of two nodes is the same as the atomic equilibrium distance  $x_{i+1} - x_i = a_0$ . If we choose the constants as

$$C = ka_0, \quad \rho = m/a_0, \quad (3.3)$$

the atomistic Hamiltonian (3.1) and the finite element Hamiltonian (3.2) are identical.

**Numerical example 1** The first numerical example is now computed with this approximation, using the same time step for atoms and nodes. In the transition region the distances of atoms and nodes are identical, in the finite element region the distances are increased stepwise from the atomic equilibrium distance  $a_0$  to  $10a_0$ . In figure 3.5, we see that whenever the distances of the nodes change, we get reflections back into the atomistic region. This can also be seen in the atomistic energy in figure 3.6. Whereas in the fully atomistic simulation all energy is leaving the real atoms, when the perturbation is travelling to the right, we can see here that not all energy is leaving this region and after a while the energy is increasing again, since part of the perturbation is reflected at the nodes. In the right panel of figure 3.6, the displacement changes not only once but every time the atom is reached by a reflected part of the perturbation. Concerning the velocity in the finite element region, we see in figure 3.5, that the velocity changes at the interface and the perturbation is slower in the finite element region. To be consistent with the stress calculation in the atomistic region, the stress in the finite element region was computed from linear interpolated values at the atomic positions.

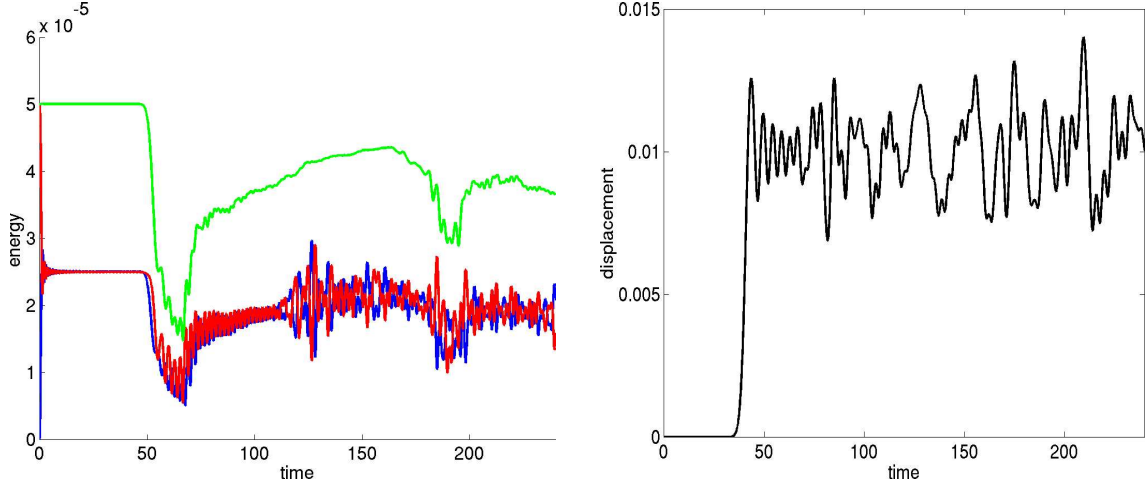


Figure 3.6: energy of the real atoms (left) and displacement of 40th atom (right) with concurrent coupling of length scales approximation

Both spurious effects, the reflection and the wrong velocity, can be explained by considering the different dispersion relations in the system. They are computed according to chapter 2.3 from the harmonic solutions  $u_j = \exp(i(\omega t + j\kappa\Delta x))$  in case of the continuous and  $u_j^n = \exp(i(\omega n\Delta t + j\kappa\Delta x))$  in case of the time discretised evolution equations in the finite element region with node distance  $\Delta x$ . As mentioned before, the atomistic and the finite element description for the model problem are in principle the same, only the space discretisation is different. Therefore, we get also the same dispersion relation, depending only on the space discretisation  $\Delta x$ :

$$\omega^2 = 4 \frac{C}{\rho \Delta x^2} \sin^2 \left( \frac{\kappa \Delta x}{2} \right), \quad (3.4)$$

$$\sin^2 \left( \frac{\omega \Delta t}{2} \right) = \frac{\Delta t^2 C}{\Delta x^2 \rho} \sin^2 \left( \frac{\kappa \Delta x}{2} \right). \quad (3.5)$$

The first is the dispersion relation for the continuous system, the second that for the time discretised system with time step  $\Delta t$  and

$$\ddot{u}(t) \approx \frac{1}{\Delta t^2} (u(t + \Delta t) - 2u(t) + u(t - \Delta t)).$$

The space discretisation is  $\Delta x = a_0$  for the atomistic equations. In the left panel of figure 3.7, the scaled velocity according to (2.7) is given for different values of the space discretisation, all multiples of the atomistic equilibrium distance  $a_0$ .

The smaller the wave number, the smaller is the difference in the velocities of the different discretisations. In the limit  $\kappa \rightarrow 0$  the velocity is the same for all discretisations. If we have a wave with wave number  $\kappa = \pi/(2a_0)$ , it is faster in a simulation with atomic distance  $\Delta x = a_0$  than in one with  $\Delta x = 2a_0$ . In a simulation with  $\Delta x = 3a_0$ , we cannot even represent this wave, since we need at least two discretisation points per wave length. Therefore, the space discretisation



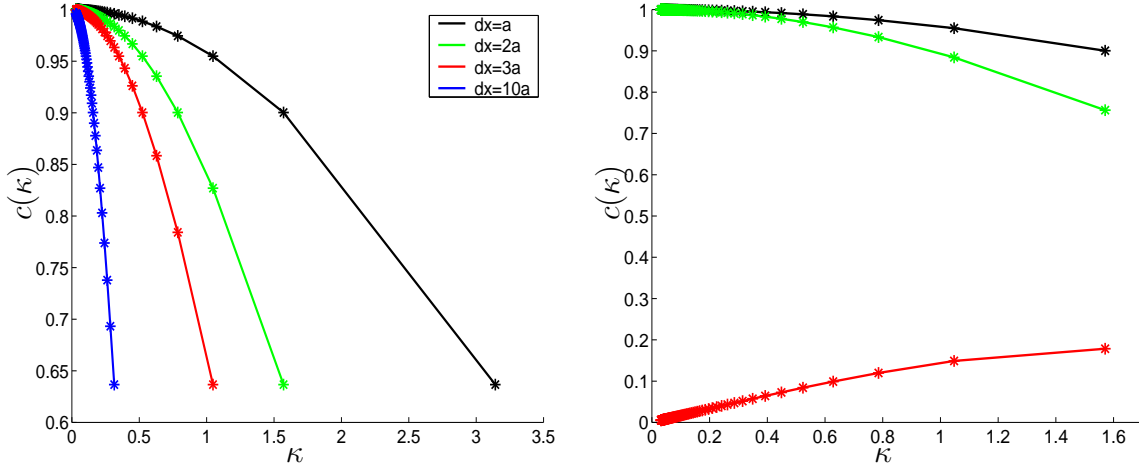


Figure 3.7: dispersion relation for different values of  $\Delta x$  (left) and for a coupling node (right) for first numerical example with coupling of length scales approximation

used for the finite elements determines the dispersion relation and the maximum wave vector in the approximate system. This is the reason why we get reflections at the interface and in the finite element region, everywhere the space discretisation is changing and why the speed of the perturbation in the finite element region is wrong. In fact, we get a different dispersion relation for every different discretisation, and the velocity of the perturbation does not only change once at the interface but everywhere the discretisation changes.

However, the reflected part of the perturbation consists not only of the waves with large wave numbers that cannot be resolved on a coarser grid. Even if the perturbation would consist only of waves with sufficiently small wave numbers, we would get some reflections at the nodes where the discretisation changes. In addition, we also get dissipation of energy there, since the frequencies  $\omega$  are complex for different space discretisations on both sides of the node.

In the right panel of figure 3.7, we see the real part (green) and the absolute value of the imaginary part (red) of the velocity at a node where the discretisation changes from  $\Delta x = a_0$  to  $\Delta x = 2a_0$ , compared again with the dispersion relation of the fully atomistic system (black). The dissipation, as well as the reflection, is decreasing for smaller wave numbers and is zero in the limit  $\kappa \rightarrow 0$ .

If we consider the Taylor expansion of the dispersion relation (3.4) around  $\kappa = 0$ ,

$$\omega^2 = \frac{C}{\rho} \left( \kappa^2 - \frac{\kappa^4 \Delta x^2}{12} + \frac{\kappa^6 \Delta x^4}{360} + \mathcal{O}(\kappa^8) \right),$$

and compare it with that of the atomistic dispersion relation

$$\omega^2 = 4 \frac{k}{m} \sin^2 \left( \frac{\kappa a_0}{2} \right) = \frac{k a_0^2}{m} \left( \kappa^2 - \frac{\kappa^4 a_0^2}{12} + \frac{\kappa^6 a_0^4}{360} + \mathcal{O}(\kappa^8) \right),$$

we can see that the choice of the parameters  $C$  and  $\rho$  according to (3.3) is necessary to get the same velocity in the limit  $\kappa \rightarrow 0$ . Therefore, the problem of wrong dispersion

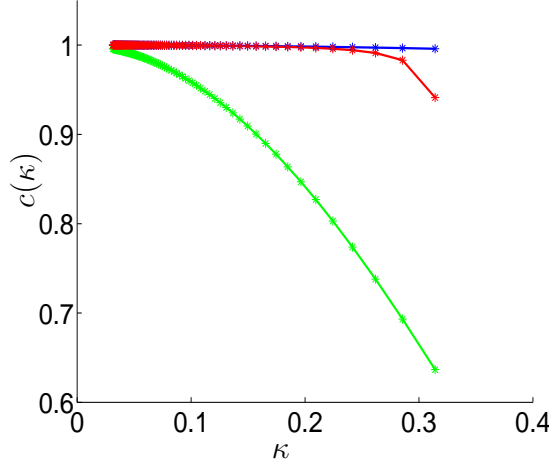


Figure 3.8: dispersion relation for the atomistic system (blue) and finite elements with  $\Delta x = 10a_0$  for different time discretisations,  $\Delta t = \Delta t_{\text{md}}$  (green) and  $\Delta t$  according to (3.6) (red)

relation in the finite element region and as a consequence also the reflection of small wave numbers, cannot be solved by choosing better parameters, since we have no free parameters left.

The situation changes if we do no longer consider the semi-discrete but the corresponding time discretised system, with the dispersion relation (3.5). In this system, we have one more degree of freedom, the time step  $\Delta t$ . If we define  $c$  as the limit of the velocity, i.e.

$$c := \lim_{\kappa \rightarrow 0} \frac{\omega(\kappa)}{\kappa},$$

we get as Taylor expansion of  $\omega$  in (3.5)

$$\omega = c\kappa + \frac{1}{24} (c^3 \Delta t^2 - c \Delta x^2) \kappa^3 + \mathcal{O}(\kappa^5).$$

As before, the first coefficient is independent of the discretisation. With  $\Delta t_{\text{md}}$  denoting the atomistic time step, we get the identical coefficient for  $\kappa^3$  for atomistic and coarse space discretisation,

$$c^3 \Delta t_{\text{md}}^2 - c a_0^2 = c^3 \Delta t^2 - c \Delta x^2,$$

for

$$\Delta t = \sqrt{\Delta t_{\text{md}}^2 + \frac{1}{c^2} (\Delta x^2 - a_0^2)}. \quad (3.6)$$

In figure 3.8, the dispersion relation for the atomistic system (blue) is shown together with that of the finite element nodes with  $\Delta x = 10a_0$  for the same time step (green) and for the time discretisation according to (3.6) (red). The error in the dispersion relation for the larger time step is much smaller than for the atomistic time step, only for large wave numbers we can observe a difference. Therefore, using

a larger time step in the finite element region can solve the problem of the wrong dispersion relation there. Nevertheless, it does not solve the problem that large wave numbers cannot be resolved in the finite element region and therefore will be reflected at the interface.

The larger the distance of the finite element nodes  $\Delta x$  is, the smaller is the difference between the optimal finite element time step  $\Delta t = \sqrt{\Delta t_{\text{md}}^2 + (\Delta x^2 - a_0^2)/c^2}$  and the maximum possible time step  $\Delta t_{\text{max}} = \Delta x/c$  for that the numerical scheme

$$\frac{1}{\Delta t^2}(u_j^{n+1} - 2u_j^n + u_j^{n-1}) = \frac{c^2}{\Delta x^2}(u_{j+1}^n - 2u_j^n + u_{j-1}^n) \quad (3.7)$$

is stable. This maximum time step is known as the CFL (Courant-Friedrichs-Lewy) stability criteria. For the time step  $\Delta t_{\text{max}}$ , we get for all wave numbers the same wave speed  $c$ .

All waves travelling with the same velocity is exactly the behaviour of the solution of the linear one dimensional wave equation,

$$\frac{\partial^2 u}{\partial x^2} - \frac{\partial^2 u}{\partial t^2} = 0,$$

that can also be solved numerically using scheme (3.7). The only difference is the time step used for the solution. The reason is, that the dispersion relations for the linear, time and space continuous, wave equation and the only time continuous molecular dynamics system are different. Since the dispersion relations of both discretised systems should not differ much from the continuous ones, different time steps are necessary for the solution.

For large  $\Delta x$ , the solution of the linear wave equation is a better approximation for waves with small wave numbers than the solution of the coarse equations in the finite element region. Using a larger time step reduces then not only the computation time but also the error in the dispersion relation.

For the analysis of finite difference schemes with asymptotic methods cf. e.g [41].

**Numerical example 2** To compute the second numerical example with this approximation, we sample first an initial momentum only for the 51 real atoms. In the left panel of figure 3.9, we see that the energy of the real atoms is decreasing at the beginning of the simulation. It is the energy of waves with large wave length that are not reflected at the interface and therefore can pass to the finite element region. They are reflected at the end of the finite element region and return to the atomistic region after a while.

The result changes if we sample also an initial momentum for the finite element nodes (figure 3.9, right). Again, waves with large wave length can pass the interface in both directions. But since all waves from the finite element region can enter the atomistic region, whereas the fine scale waves from the left are reflected, the energy is increasing at the beginning of the simulation. After a while, the energy of the waves with large wave length is again distributed equally over the whole domain. If we would run the simulation for a longer time interval, we would notice also some

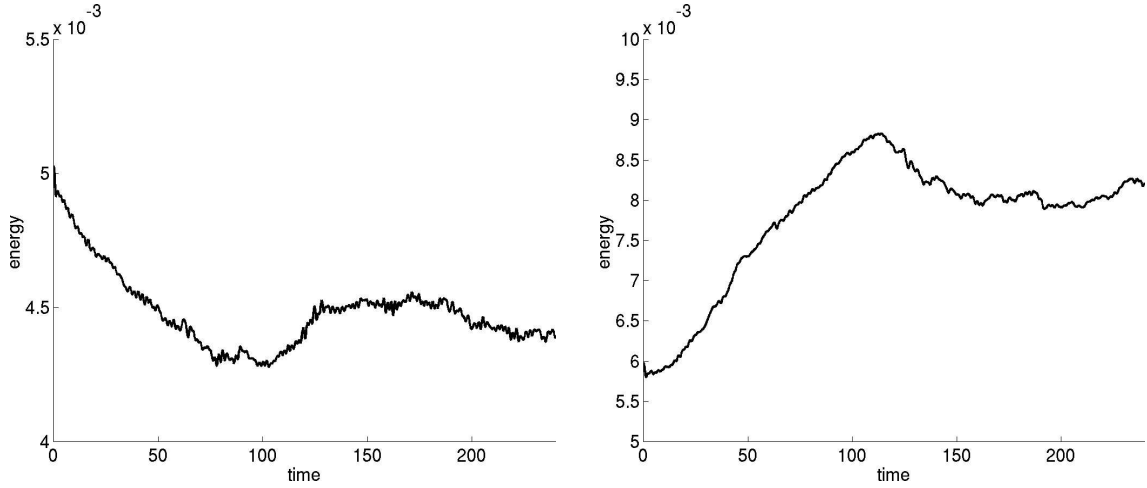


Figure 3.9: energy of the real atoms for numerical example 2 in case of initial momentum only for the atoms (left) and initial momentum for atoms and nodes (right) in concurrent coupling of length scales approximation

small decay in the energy due to numerical diffusion at the nodes where the space discretisation is changing.

If we want to compute only the total energy in the system, the overall kinetic and potential energy can be corrected by an offset, depending on the missing degrees of freedom in the finite element region [16]. However, it is then not possible to model an energy transfer between both regions.

### 3.1.2 Bridging scales approximation

Now, we consider the bridging scales approximation for the model problem. For the one dimensional harmonic nearest neighbour interaction, the potential energy in (2.12) is

$$\Phi(u) = \frac{1}{2} u^T K u,$$

with the tridiagonal matrix

$$K = k \begin{bmatrix} 1 & -1 & \dots & 0 & 0 \\ -1 & 2 & \dots & 0 & 0 \\ \vdots & & \ddots & & \vdots \\ 0 & 0 & \dots & 2 & -1 \\ 0 & 0 & \dots & -1 & 1 \end{bmatrix},$$

i.e.

$$\Phi(Nd + Qu) = (Nd + Qu)^T K (Nd + Qu).$$

To neglect the fine scale information for one part of the domain, we have to compute the memory kernel (2.18) and the coarse scale force (2.20) outside of the atomistic region.

The memory kernel can be computed according to [71] as follows. To obtain  $\theta(t)$ , we need the inverse Laplace transformation of the inverse of the matrix  $A = [s^2 I + M_2^{-1} K_{22}]$ . Since all atomic masses are identical,  $M = mI$ , the matrix is tridiagonal, with entries  $a = s^2 + 2k/m$  on the main diagonal and  $b = -k/m$  on the secondary diagonals. Fortunately, we do not need the whole matrix of the inverse Laplace transformation but only the first entry, since the matrix is multiplied from the left with  $K_{12}$  and from the right with  $K_{21}$ . These are the sub-matrices of  $K$  for the interaction of the real atoms and the atoms in the pure coarse scale region. Both matrices have only one non-zero entry,  $K_{12}$  in the lower left and  $K_{21}$  in the upper right corner. Taking the inverse  $\tilde{A} = A^{-1}$  for  $n \rightarrow \infty$  leads to the following representation of the first column

$$\begin{aligned}\tilde{A}_{1,1} &= -\frac{Z}{b}, \\ \tilde{A}_{1,N} &= -Z\tilde{A}_{1,N-1} = -\frac{1}{b}Z^N, \quad N > 1,\end{aligned}$$

with  $Z$  the continued fraction

$$Z = -\frac{b}{a - \frac{b^2}{a - \frac{b^2}{a - \dots}}},$$

which is equivalent to

$$Z = -\frac{b}{a + bZ} \quad \Rightarrow \quad Z = -\frac{1}{2b}(a - \sqrt{a^2 - 4b^2}).$$

The inverse Laplace transformation of this value is

$$\begin{aligned}L^{-1}\{\tilde{A}_{1,1}\} &= -\frac{1}{b}L^{-1}\left\{-\frac{1}{2b}(a - \sqrt{a^2 - 4b^2})\right\} \\ &= \frac{m}{k}L^{-1}\left\{\frac{m}{2k}\left(s^2 + 2\frac{k}{m} - s\sqrt{\frac{4k}{m} + s^2}\right)\right\} \\ &= \frac{2m}{k} \frac{J_2(2\sqrt{k/m} t)}{t},\end{aligned}$$

where  $J_k$  denotes the  $k$ th order Bessel function of the first kind.

Since this derivation is valid only in the limit  $n \rightarrow \infty$ , with  $n$  the number of atoms, the obtained memory kernel is the same as for the interaction of a long chain of atoms with one heavy particle [31]. An alternative derivation of the memory kernel, which can be used also for longer ranging harmonic potentials, is given in section 3.2.

We also have to compute the forces in the pure coarse scale region. According to section 2.5, we need the derivative of the energy density  $W_\alpha$  with respect to the deformation gradient  $\bar{F}_\alpha$ . For linear finite element hat functions as interpolation

functions, this deformation gradient is defined only between two coarse scale nodes, not at the nodes themselves. But since the energy density of all atoms between two nodes is the same for a harmonic potential, we use this value also for the atoms that are nodes. With

$$\bar{F}_\alpha = 1 + \frac{1}{\tilde{n}a_0} (d_{j+1} - d_j), \quad \text{for } q_{\text{eq},\alpha} \in (x_j, x_{j+1}),$$

we can determine the distance of two atoms for this deformation, the energy density and its derivative as

$$\begin{aligned} r_{\alpha(\alpha+1)} &= (\bar{F}_\alpha - 1)a_0 = \frac{1}{\tilde{n}} (d_{j+1} - d_j), \\ W_\alpha &= \frac{k}{4a_0} [(u_\alpha - u_{\alpha-1})^2 + (u_{\alpha+1} - u_\alpha)^2] = \frac{k}{4a_0} [(r_{(\alpha-1)\alpha})^2 + (r_{\alpha(\alpha+1)})^2] \\ &= \frac{k}{2a_0} \frac{1}{\tilde{n}^2} (d_{j+1} - d_j)^2 = \frac{ka_0}{2} (\bar{F}_\alpha - 1)^2, \\ \frac{\partial W_\alpha}{\partial \bar{F}_\alpha} &= ka_0 (\bar{F}_\alpha - 1) = \frac{k}{\tilde{n}} (d_{j+1} - d_j), \end{aligned}$$

and obtain finally the coarse scale forces for the nodes according to (2.20)

$$-(N^T \Phi'(u))_j = \frac{k}{\tilde{n}} (d_{j+1} - 2d_j + d_{j-1}).$$

Here,  $\tilde{n}$  denotes again the number of atoms from one node to the next. For higher order hat functions as interpolation functions, the deformation gradient  $\bar{F}_\alpha$  depends on more than two nodal displacements, but this is the only difference in the derivation. Therefore, in case of a harmonic potential, the coarse scale force derived in this way is the same than just neglecting the term  $Qu$  in the force calculation in (2.13),

$$N^T M N \ddot{d} = -N^T K N d - N^T K Q u \approx -N^T K N d, \quad (3.8)$$

since the matrix  $N^T K N$  has the same entries than  $K$ , divided by  $\tilde{n}$ . Because of  $[K, Q] = KQ - QK \neq 0$ , this is only an approximation. Since the coarse scale force computed in this way is for this example the same than neglecting the fine scale influence, it does not solve the problem of wrong dispersion relation. This is shown in the following.

**Numerical example 1** The first example is computed with linear interpolation functions and  $\tilde{n} = 10$ . In figure 3.11, we see the local stress for this approximation. In the coarse scale region, it is computed from the interpolated coarse scale values at the atomic positions.

Again, we have the same problem as with the concurrent coupling of length scales approximation, the velocity of the perturbation in the coarse scale region is not correct. Now, it is faster than in the fully atomistic simulation. But the problem of wave reflections at the interface is solved quite well with the reflectionless boundary

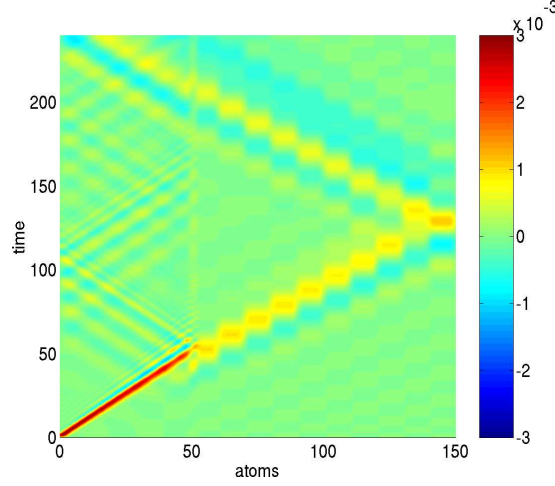


Figure 3.10: stress in bridging scales approximation

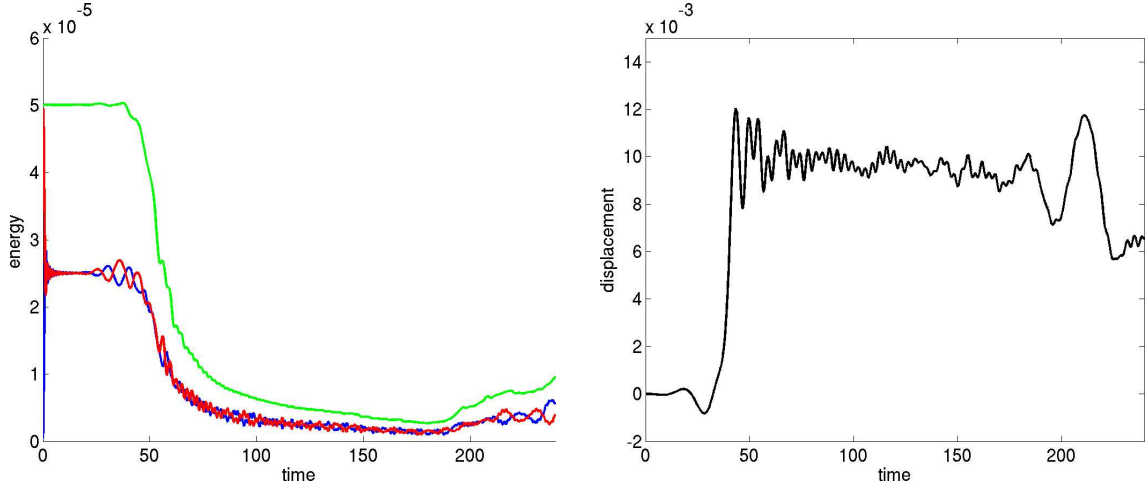


Figure 3.11: energy of real atoms (left) and displacement of 40th atom (right) in bridging scales approximation

condition. We computed the memory integral with the trapezoidal rule over 40 time steps. For this example, we do not have to take care of the term  $R(t)$  in (2.19). Since all initial values are zero, only the first atom has a non-zero initial momentum, especially all initial conditions for the atoms in the coarse scale region are zero.

If we take a look at the energy of the real atoms in the left panel of figure 3.11, it looks similar to that of the fully atomistic system in the left panel of figure 3.2. Only when the perturbation reaches the interface, i.e. when the energy starts to decrease, the energy differs a bit from that of the fully atomistic simulation. The energy increase at the end of the simulation results from the fact that the perturbation is too fast in the coarse scale region and reaches the first 51 atoms again during the simulation time. The better behaviour of the solution at the interface can also be seen in figure 3.10, where we see only little reflection of waves. But, instead of wave reflections, we get some deviation from the fully atomistic stress, even before the

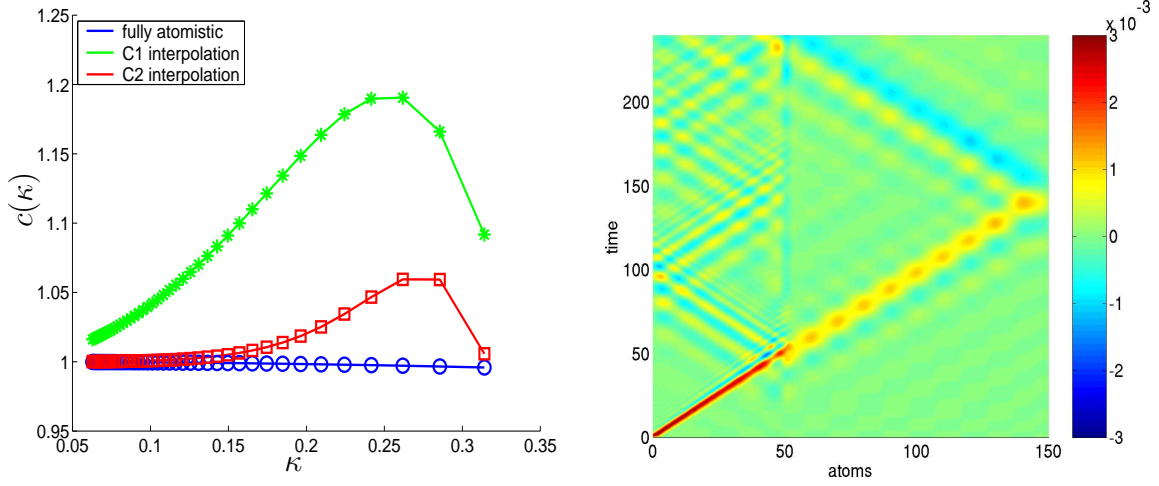


Figure 3.12: left: dispersion relation for  $C^1$  (green) and  $C^2$  (red) hat functions in bridging scales approximation, compared to atomistic dispersion relation (blue), right: stress for  $C^2$  hat functions

perturbation reaches the interface. The reason for this is the fact that the derivation of the reflectionless boundary condition for the bridging scales approximation leads to a system that is not energy conserving. We will discuss this in detail in section 4.1.

We consider the dispersion relation of the approximation, to explain the wrong speed of the perturbation in the coarse scale region. It is computed from the harmonic solutions  $d_j = \exp(i(\omega t + j\kappa\tilde{n}a_0))$  of (3.8). In figure 3.12 (left), we compare the dispersion relation of the atomistic system (blue) with that of the bridging scales approximation in the coarse scale region (green). As already observed in the stress plot, the wave speed for large wave numbers on the coarse grid is larger than in the atomistic system. Since the coarse scale mass matrix is not diagonal for this approximation, the dispersion relations differ not only due to the different space discretisations. We get

$$\omega^2 = \frac{4k}{\tilde{n}} \frac{\sin^2(\frac{\kappa\tilde{n}a_0}{2})}{2m_1 \cos(\kappa\tilde{n}a_0) + m_2},$$

with

$$m_1 = \frac{(\tilde{n}^2 - 1)m}{6\tilde{n}} \quad \text{and} \quad m_2 = \frac{(2\tilde{n}^2 + 1)m}{3\tilde{n}}$$

denoting the entries of the coarse scale mass matrix on the main and the secondary diagonals. Unfortunately, we cannot get a better dispersion relation here by taking a larger time step on the coarse scale for the time discretised system.

One possibility to improve the dispersion relation is to use interpolation functions of higher order. If we use quadratic instead of linear interpolation (red line in the left panel of figure 3.12), the error in the dispersion relation is already much smaller than for linear interpolation (green). However, if we increase the interpolation order by one, we get two additional non-zero off-diagonals in the coarse scale mass matrix



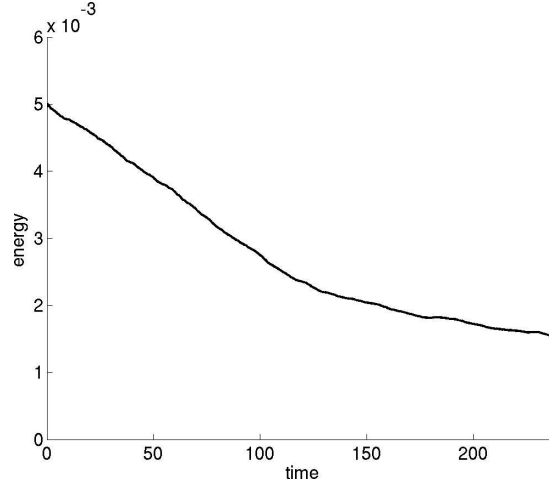


Figure 3.13: energy of real atoms in numerical example 2 for bridging scales approximation

$N^T M N$ , and in the coarse scale force matrix  $N^T K N$ . Solving the system numerically gets computationally more expensive, but the error of the dispersion relation in the coarse scale region is reduced.

Other possibilities for getting better dispersion relations will be discussed in sections 3.1.2.1 and 4.6.

**Numerical example 2** For the computation of the second numerical example, we sample initial momenta for all 151 atoms and compute the initial coarse scale velocities from the projection of the corresponding atomistic values. Displacements on the coarse scale can pass the interface in both directions. Since fine scale displacements can leave the atomistic region due to the reflectionless boundary condition, and we have no fine scale displacements that pass the interface from right to left, the energy during the simulation decreases.

The fine scale influences from the coarse scale region to the atomistic region are given by the term  $R(t)$  in the boundary condition (2.19). To be able to run simulations with constant temperature in the bridging scales approximation, it is therefore necessary to consider the term  $R(t)$ . However, since the bridging scales approximation leads to an approximate system that is not energy conserving (cf. section 4.1), even the exact computation of  $R(t)$  from the initial conditions cannot lead to a completely energy conserving system. We will explain in section 4.4 how we can sample initial conditions in the coarse scale region and compute  $R(t)$  for an energy conserving approximation.

### 3.1.2.1 Wave speed correction with combined mass matrix

In the dispersion analysis of the concurrent coupling of length scales approximation scheme, we found that using a larger time step for a coarser space discretisation reduces the difference in the dispersion relation compared to a fully atomistic system. In the bridging scales approximation, the situation is different. Since the coarse

scale mass matrix is  $N^T M N$ , it is a diagonal matrix only for piecewise constant interpolation functions. If they are piecewise linear or of higher order, we get a band matrix, a so called distributed mass matrix.

We compute the dispersion relation for the time discretised evolution equations in the pure coarse scale region,

$$\frac{1}{\Delta t^2} N^T M N (d^{n+1} - 2d^n + d^{n-1}) = N^T K N d^n,$$

from the harmonic solutions  $d_j^n = \exp(i(\omega n \Delta t + j \kappa \tilde{n} a_0))$  and get

$$\omega = \frac{2}{\Delta t} \arcsin \left( \sqrt{\frac{\Delta t^2 k}{\tilde{n}} \frac{\sin^2(\frac{\kappa \tilde{n} a_0}{2})}{2m_1 \cos(\kappa \tilde{n} a_0) + m_2}} \right). \quad (3.9)$$

There is no time step that gives the exact solution of the wave equation, and the maximal possible time step to get a stable, energy conserving system, i.e.  $\omega$  is not complex, is

$$\Delta t_{\max} = \sqrt{\frac{m(\tilde{n}^2 + 2)}{3k}}.$$

One possibility to overcome this problem in the pure coarse scale region, is to change the mass matrix by mass lumping to a diagonal matrix  $M_l$ , like in the concurrent coupling of length scales approximation. If we use the optimal time step (3.6), we can get a very small error in the dispersion relation. Since we have already a separation of fine and coarse scale evolution equations in the bridging scales approximation, a simulation with different time steps for the two different scales is even easier than in the concurrent coupling of length scales approximation, where the time step has to be changed every time the space discretisation is changing. The problem here is, that the mass matrix cannot be changed everywhere, since the distributed mass matrix is necessary in the atomistic region. There, we do not have the dispersion relation (3.9) but get the correct wave speed already from the influence of the fine scale displacements on the coarse scale forces. Therefore, we get again the problem of coupling different regions with different time steps.

If we want to avoid using the optimal time step on the coarse scale, we can use a combination of the lumped mass  $M_l$ , and the distributed mass matrix  $M_d = N^T M N$ , to get a combined mass matrix  $M_c$  (cf. [8]),

$$M_c = \lambda M_l + (1 - \lambda) M_d, \quad \lambda \in (0, 1).$$

Since the wave speed is too slow if we use the lumped mass matrix, with a time step smaller than the optimal one, and too fast with a distributed mass matrix, a combination of both can reduce the error for an arbitrary time step. If we consider the Taylor expansion of the dispersion relation for the combined mass matrix,

$$\begin{aligned} \omega &= \frac{2}{\Delta t} \arcsin \left( \sqrt{\frac{\Delta t^2 k}{\tilde{n}} \frac{\sin^2(\frac{\kappa \tilde{n} a_0}{2})}{\lambda m + (1 - \lambda)(2m_1 \cos(\kappa \tilde{n} a_0) + m_2)}} \right) \\ &= \sqrt{\frac{k}{m}} a_0 \kappa + \frac{a_0^3}{24} \sqrt{\frac{k}{m}} \left( \frac{\Delta t^2 k}{m} - 2 + 2\lambda + (1 - 2\lambda) \tilde{n}^2 \right) \kappa^3 + \mathcal{O}(\kappa^5), \end{aligned}$$

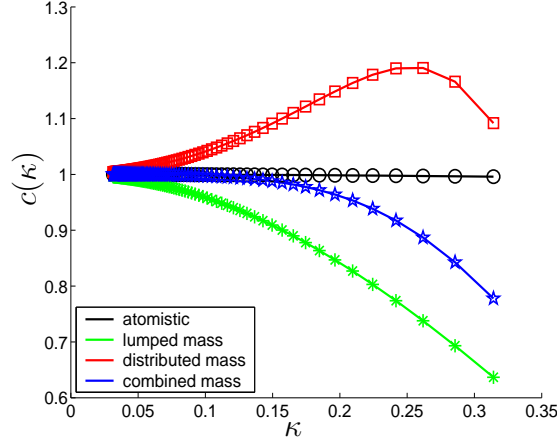


Figure 3.14: dispersion relation for combined mass matrix with  $\lambda = 0.5$ ,  $\Delta T = \Delta t$

we get the same coefficient of  $\kappa^3$  than in the atomistic case if

$$\lambda = \frac{k/m(\Delta t_{\text{md}}^2 - \Delta t^2) + 1 - \tilde{n}^2}{2 - 2\tilde{n}^2}.$$

If we use the same time step for the atomistic and the coarse scale system, we get  $\lambda = 0.5$ . An example of the different dispersion relations for  $\tilde{n} = 10$  is shown in figure 3.14. Choosing the mass matrix to get the correct dispersion relation in two dimensional simulations is considered e.g. in [51, 39, 20].

Another idea is to derive the coarse scale Hamiltonian from the energy of the atomistic system, averaged over all fine scale displacements and momenta, consistent with the coarse scale values [58, 60, 21]. Interpolation and projection are defined as in the bridging scales approximation and we get the same coarse scale mass matrix  $N^T M N$ . But we get a different coarse scale force matrix,  $\tilde{K} = ((N^T N)^{-1} N^T K^{-1} N (N^T N)^{-1})^{-1}$ , instead of  $N^T K N$ , leading to a better dispersion relation than in the concurrent coupling of length scales or in the bridging scales approximation [58, 60]. Since we average over the fine scale values, we get no evolution equations for them to derive a reflectionless boundary condition. In this case, we get reflection of waves with small wave length that cannot be resolved in coarser regions and reflections and diffusion due to changing and complex dispersion relations whenever the space discretisation changes. However, this approach can also be used for non-uniform coarse scale grids.

## 3.2 Longer ranging harmonic and anharmonic potentials

We want to discuss now, how the results of the two approximations change if the atomic interaction gets more complicated. The first case that we want to consider is still a harmonic potential but now with interaction to the nearest and second

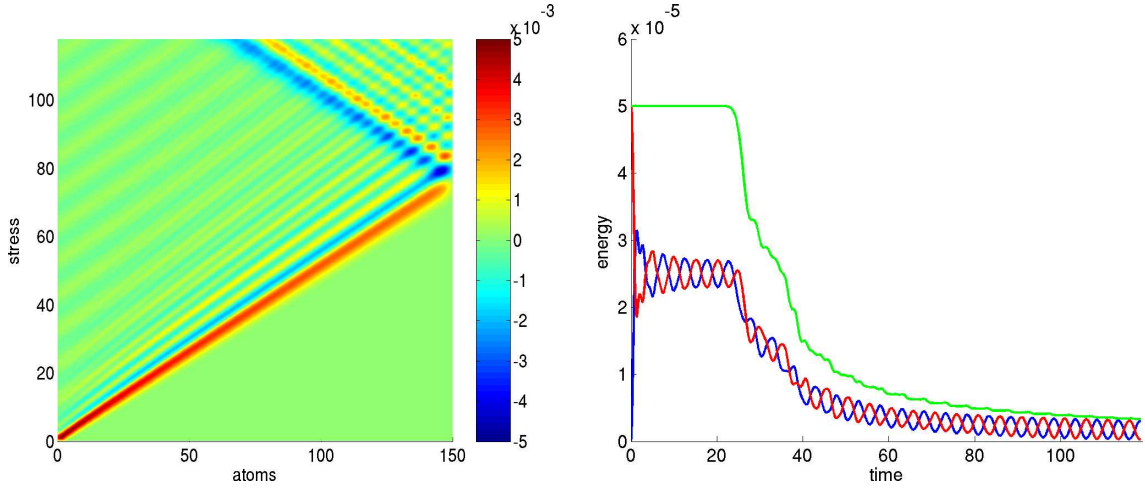


Figure 3.15: stress and energy of real atoms for fully atomistic system with longer ranging harmonic potential

nearest neighbours,

$$\mathcal{H}_1 = \frac{1}{2} \sum_{i=1}^n \frac{p_i^2}{m} + \frac{1}{2} \sum_{i=2}^n k_1 (q_i - q_{i-1} - a_0)^2 + \frac{1}{2} \sum_{i=3}^n k_2 (q_i - q_{i-2} - 2a_0)^2.$$

As second case, we consider an anharmonic nearest neighbour interaction,

$$\mathcal{H}_2 = \frac{1}{2} \sum_{i=1}^n \frac{p_i^2}{m} + \sum_{i=2}^n \left( \frac{k_1}{2} (q_i - q_{i-1} - a_0)^2 + \frac{k_2}{4} (q_i - q_{i-1} - a_0)^4 \right).$$

As numerical example we choose  $k_1 = 0.1$  and  $k_2 = 1$  for the harmonic Hamiltonian  $\mathcal{H}_1$ . The local stress and the energy of the real atoms for this example are shown in figure 3.15. The difference to the harmonic potential with only nearest neighbour interaction in section 3.1 is, that we get more dispersion of the different wave length and that the decay of the energy of the real atoms is slower. For realistic examples, the interaction with the second nearest neighbours would not be stronger than the nearest neighbour interaction, but since everything is linear for harmonic potentials and our main interest is to find out how the different approximations deal with longer ranging interactions, we choose a setting like this.

The initial conditions are the same as for the model problem in section 3.1, and we use the time step  $\Delta t = 1/10\sqrt{k_1 + 4k_2}$  for the numerical solution of the evolution equations.

As an example for the anharmonic potential, we take  $k_1 = 1$ ,  $k_2 = 10$  and  $p_1(0) = 0.3$  as initial momentum of the first atom. All other values are again initially zero. The momentum of the first atom is larger than for the harmonic examples, since the influence of the anharmonic term gets stronger for larger values. The local stress and the energy of the real atoms for this example are shown in figure 3.16. The stress plot looks similar to that of the harmonic nearest neighbour interaction in section 3.1, but the energy decays a little bit faster.

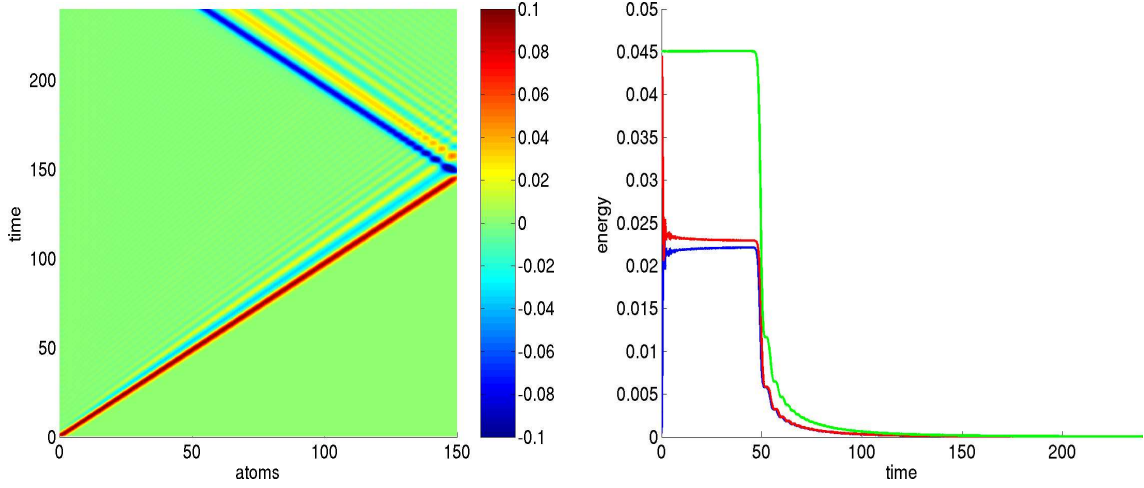


Figure 3.16: stress and energy of real atoms for fully atomistic system with anharmonic potential

### 3.2.1 Concurrent coupling of length scales

In this approximation, the only thing we have to do, is to compute the appropriate coarse scale elasticity constant  $C$ , according to the atomic interaction. For the case of a harmonic potential, we can compute it again from the limit  $\kappa \rightarrow 0$  of the velocity  $c(\kappa)$  of the atomistic model. Using the dispersion relation of the atomistic system,

$$\omega^2 = \kappa^2 a_0^2 \left( \frac{k_1}{m} \text{sinc}^2 \left( \frac{\kappa a_0}{2} \right) + 4 \frac{k_2}{m} \text{sinc}^2(\kappa a_0) \right), \quad \text{sinc}(x) = \frac{\sin(x)}{x},$$

we get

$$c = \lim_{\kappa \rightarrow 0} \frac{\omega(\kappa)}{\kappa} = \sqrt{\frac{a_0^2}{m} (k_1 + 4k_2)}.$$

Since only the potential energy is changed, the density  $\rho = ma_0$  is the same as before, and we get the new elasticity constant

$$C = a_0 (k_1 + 4k_2).$$

This elasticity constant is again identic with that calculated by the Cauchy-Born rule. The dispersion relation on the coarse scale is the same as for nearest neighbour interaction (3.4) with a new elasticity constant. If we normalize again the wave speed with the inverse of its limit  $\kappa \rightarrow 0$ ,

$$\tilde{c}(\kappa) = \sqrt{\frac{m}{a_0^2 (k_1 + 4k_2)}} c(\kappa),$$

the coarse scale dispersion relation is independent of the parameters  $k_i$ . In figure 3.17, we compare it with the atomistic dispersion relation, which is not independent of the parameters, for  $k_1 = 1$ ,  $k_2 = 0$  (blue) and  $k_1 = 0$ ,  $k_2 = 1$  (green). If we choose both values non zero, we end up with a dispersion relation in between. The

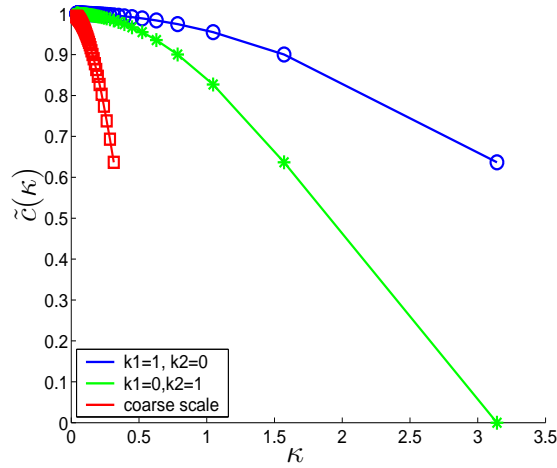


Figure 3.17: dispersion relation for longer ranging harmonic potential in coupling of length scales approximation

larger the value of  $k_2$ , the smaller the error between atomistic and coarse scale velocity. The error in the dispersion relation is therefore not increased by considering longer ranging harmonic interactions.

The error in the dispersion relation on the coarse scale is smaller for the numerical example with  $k_1 = 0.1$  and  $k_2 = 1$  than for the harmonic potential with only nearest neighbour interaction. But we get more wave reflection at the interface, as can be seen both on the stress and on the energy plot in figure 3.18. The reason is, that even if we choose the node distances at the interface as the atomic equilibrium distances, atomistic and finite element forces are not the same there, since the finite element forces range only over one element and the molecular forces range over two. The forces of the last three atoms, which are included in the atomistic energy calculation, are already mixed atomistic and finite element forces, since the interface region includes now more than two atoms due to longer ranging atomic interaction.

For the example with anharmonic potential, the coarse scale force is computed according to the Cauchy-Born rule. For an atom with equilibrium position between the finite element nodes  $j$  and  $j + 1$  with node distance  $\Delta x_j$ , we get for the energy density, with a calculation similar to that in section 3.1.2,

$$\begin{aligned}
 \bar{F}_\alpha &= 1 + \frac{1}{\Delta x_j} (d_{j+1} - d_j), \\
 r_{\alpha(\alpha+1)} &= \frac{a_0}{\Delta x_j} (d_{j+1} - d_j), \\
 W_\alpha &= \frac{k_1}{2} a_0 (\bar{F}_\alpha - 1)^2 + \frac{k_2}{4} a_0^3 (\bar{F}_\alpha - 1)^4, \\
 \frac{\partial W_\alpha}{\partial \bar{F}_\alpha} &= \frac{k_1 a_0}{\Delta x_j} (d_{j+1} - d_j) + \frac{k_2 a_0^3}{\Delta x_j^3} (d_{j+1} - d_j)^3.
 \end{aligned}$$

From the energy density and equation (2.20), we can compute the force on node  $j$ ,

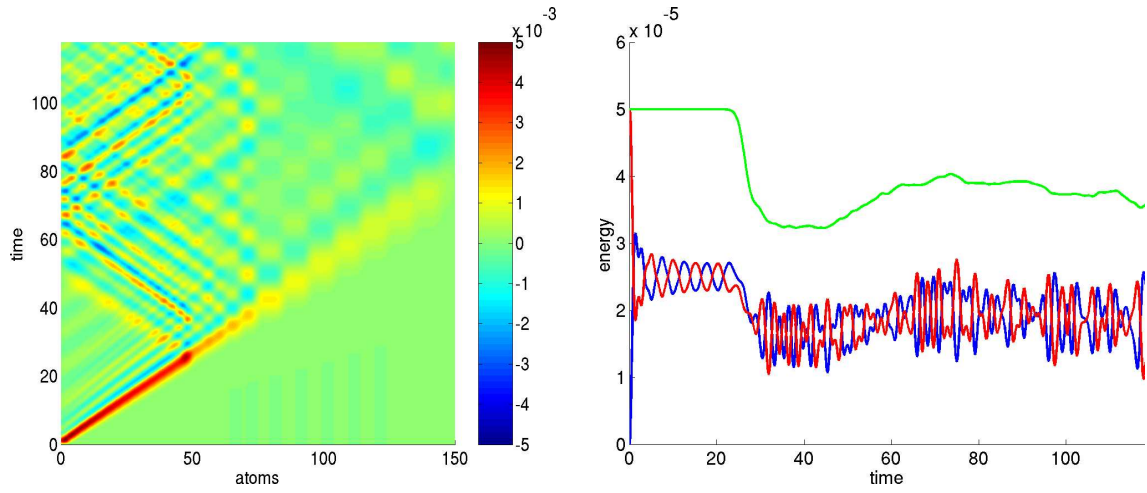


Figure 3.18: stress and energy of real atoms for longer ranging harmonic potential in coupling of length scales approximation

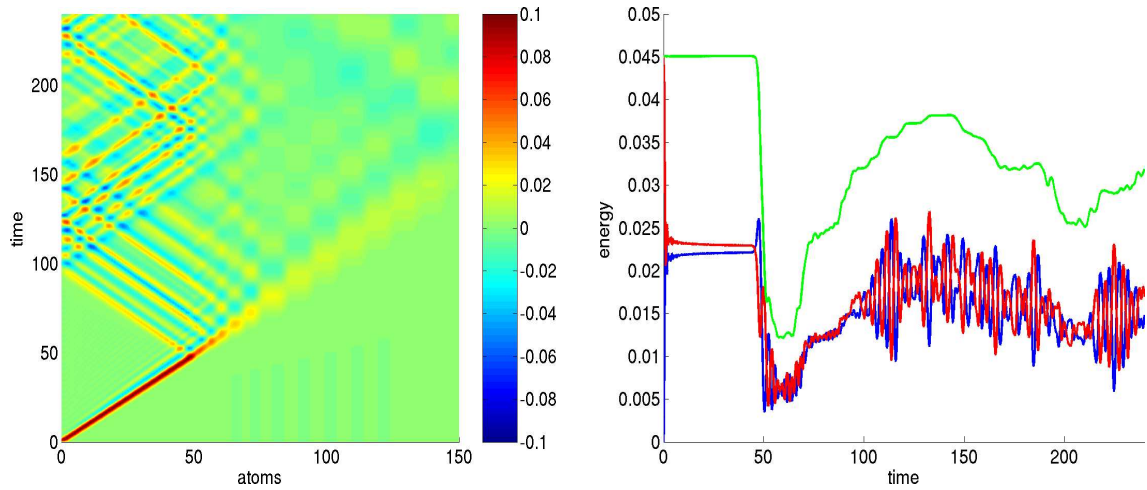


Figure 3.19: stress and energy of real atoms for anharmonic potential for coupling of length scales approximation

$f_j$ , and the potential energy  $E_{\text{pot}}$  in the finite element region,

$$f_j = k_1 a_0 \left( \frac{d_{j+1} - d_j}{\Delta x_j} + \frac{d_{j-1} - d_j}{\Delta x_{j-1}} \right) + k_2 a_0^3 \left( \frac{(d_{j+1} - d_j)^3}{\Delta x_j^3} + \frac{(d_{j-1} - d_j)^3}{\Delta x_{j-1}^3} \right),$$

$$E_{\text{pot}} = \sum_j \left( \frac{k_1}{2} \frac{a_0}{\Delta x_j} (d_{j+1} - d_j)^2 + \frac{k_2}{4} \frac{a_0^3}{\Delta x_j^3} (d_{j+1} - d_j)^4 \right),$$

where, in contrast to the bridging scales approximation, the node distances  $\Delta x_{j-1}$  and  $\Delta x_j$  can be different. If a linear elasticity model is used in the finite element region, only the quadratic terms in the potential energy are taken into account, i.e. the linear terms in the force calculation. However, also the non-linear forces can be used.

In the right panel of figure 3.19, we see that nearly two third of the energy can first leave the atomistic region, but a lot is reflected at the nodes where the space discretisation changes. Due to the anharmonic term in the force calculation, we have more reflections than for the example with harmonic nearest neighbour interaction. This can also be seen in the stress plot in the left panel of the figure.

### 3.2.2 Bridging scales approximation

For the bridging scales approximation, we have to compute again the memory kernel  $\theta(t)$  and the coarse scale forces.

To get the memory kernel, we have to determine

$$\theta(t) = K_{12} L^{-1} \{ [s^2 I + M_2^{-1} K_{22}]^{-1} \}$$

for a matrix  $K$  with two secondary diagonals. This can be done using the following lemma, which gives the inverse Laplace transformation for an arbitrary matrix  $M_2^{-1} K_{22}$ .

**Lemma 3.1** *The inverse Laplace transformation of*

$$(s^2 I + M)^{-1},$$

*with  $M$  a positive definite matrix and  $I$  the identity matrix, is given by*

$$L^{-1} \{ (s^2 I + M)^{-1} \} = M^{-1/2} \sin(M^{1/2} t).$$

**Proof:** If  $P$  is the orthogonal projection matrix of  $M$ ,

$$M = P \Lambda P^{-1},$$

the square root of the matrix is defined as

$$M^{1/2} = P \Lambda^{1/2} P^{-1}.$$



$\Lambda^{1/2}$  denotes the matrix obtained from the diagonal matrix  $\Lambda$  by taking the square root of each entry. We can write the Laplace transformation of the right hand side with this projection,

$$\begin{aligned} L\{M^{-1/2} \sin(M^{1/2}t)\} &= L\{(P\Lambda^{1/2}P^{-1})^{-1} \sin(P\Lambda^{1/2}P^{-1}t)\} \\ &= (P\Lambda^{-1/2}P^{-1}) \int_0^\infty e^{-st} \sin(P\Lambda^{1/2}P^{-1}t) dt, \end{aligned}$$

and remove the projection from the integral,

$$\begin{aligned} &= (P\Lambda^{-1/2}P^{-1}) \int_0^\infty e^{-st} \sum_{i=0}^\infty (-1)^i \frac{1}{(2i+1)!} (P\Lambda^{1/2}P^{-1}t)^{(2i+1)} dt \\ &= (P\Lambda^{-1/2}P^{-1}) \int_0^\infty e^{-st} \sum_{i=0}^\infty (-1)^i \frac{t^{2i+1}}{(2i+1)!} P(\Lambda^{1/2})^{(2i+1)} P^{-1} dt \\ &= P\Lambda^{-1/2} \int_0^\infty e^{-st} \sin(\Lambda^{1/2}t) P^{-1} dt. \end{aligned}$$

Since the matrix  $\Lambda$  is diagonal, we can compute the Laplace transformation of each entry separately and get the left hand side of the equation

$$\begin{aligned} &= P\Lambda^{-1/2} \int_0^\infty e^{-st} (\sin(\sqrt{\lambda_i} t))_{i=1:n} P^{-1} dt \\ &= P\Lambda^{-1/2} \left( \int_0^\infty e^{-st} \sin(\sqrt{\lambda_i} t) dt \right)_{i=1:n} P^{-1} \\ &= P\Lambda^{-1/2} \left( \frac{\sqrt{\lambda_i}}{s^2 + \lambda_i} \right)_{i=1:n} P^{-1} \\ &= P \left( \frac{1}{s^2 + \lambda_i} \right)_{i=1:n} P^{-1} \\ &= P(s^2 I + \Lambda)^{-1} P^{-1} = (P(s^2 I + \Lambda)P^{-1})^{-1} \\ &= (s^2 I + P\Lambda P^{-1})^{-1} = (s^2 I + M)^{-1}, \end{aligned}$$

where  $(a_i)_{i=1:n}$  denotes a diagonal  $n \times n$  matrix with the entries  $a_i$ .  $\square$

If the coarse scale force, for interpolation with linear hat functions, is computed according to the Cauchy-Born rule, we get the same coarse scale force as in the concurrent coupling of length scales approximation, now with identical node distance everywhere,

$$-(N^T \Phi'(u))_j = C(d_{j+1} - 2d_j + d_{j-1}), \quad C = a_0(k_1 + 4k_2).$$

For more than nearest neighbour interaction, this is no longer the same than just neglecting the term  $Qu$  in the force calculation (3.8), since  $N^T K N$  has now more than three non-zero diagonals.

We get again a different dispersion relation than for the concurrent coupling of length scales approximation, since the mass matrix of the bridging scales approximation is tridiagonal. The wave speed on the coarse scale is again larger than in

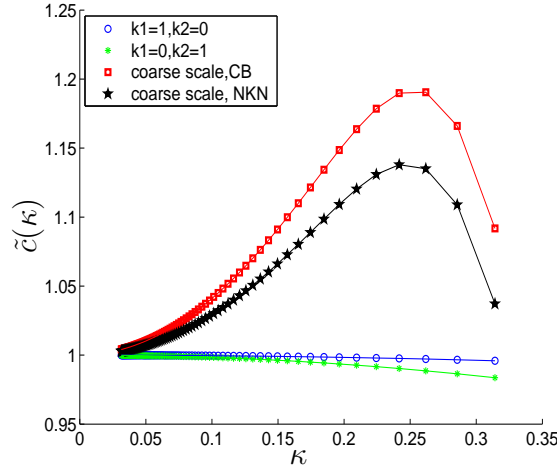


Figure 3.20: dispersion relation for longer ranging harmonic potential in bridging scales approximation

the atomistic region and, if normalized with its limit for  $\kappa \rightarrow 0$ , the same as for a harmonic potential with nearest neighbour interaction.

If we compute the coarse scale forces with the matrix  $N^T K N$ , we get also on the coarse scale an interaction of the second nearest neighbours, and the error in the dispersion relation is reduced.

In figure 3.20, the dispersion relations for the two possible force calculations in the coarse scale region are shown, together with the relation for the atomistic model with  $k_1 = 0$ ,  $k_2 = 1$  and  $k_1 = 1$ ,  $k_2 = 0$ . For both force calculations, the error in the dispersion relation gets larger if we increase the value of  $k_2$ .

In figures 3.21 and 3.22, we can see that in the atomistic region the reflection of waves and the energy is nearly the same for both force calculations, but the error in the coarse scale region is larger if we use the force calculation according to the Cauchy-Born rule.

For the example with anharmonic potential, the force can be computed only according to the Cauchy-Born rule. We get again the same force calculation as for the concurrent coupling of length scales approximation, now for equidistant nodes,

$$-(N^T \Phi'(u))_j = \frac{k_1}{\tilde{n}}(d_{j+1} - 2d_j + d_{j-1}) + \frac{k_2}{\tilde{n}^3}((d_{j+1} - d_j)^3 + (d_{j-1} - d_j)^3).$$

Results of the numerical example are shown in figure 3.23. The coarse scale force is no longer linear and has the same structure as the atomistic force calculation with scaled parameters. However, since the coefficient of the cubic term is much smaller than in the atomistic region and has hardly an influence on the coarse scale wave speed, it can also be neglected here.

We showed in this section, that the essential effects of the approximations are still the same if we consider more complicated interatomic interaction. Especially, the behaviour on the coarse scale is not changed significantly, but the reflections of waves at the interface get larger for longer ranging harmonic or anharmonic interaction. In the concurrent coupling of lengths scales approximation, this is due

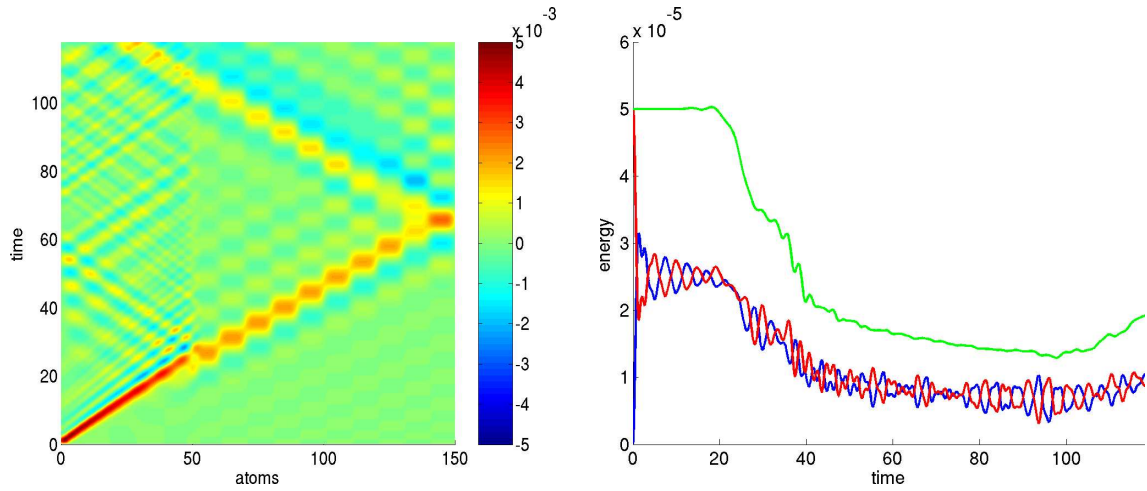


Figure 3.21: stress and energy of real atoms for longer ranging harmonic potential with  $N^T K N$  in bridging scales approximation

to the fact that force calculations at the interface are different in the atomistic and finite element description. In the next chapter, we show that the problem in the bridging scales approximation is, that it leads to an approximate system that is not energy conserving. Therefore, it is not possible to neglect the reflections at the interface completely by reducing the numerical error in the integration of the memory integral. We will derive a similar, but energy conserving approximation that reduces this reflections at the interface and therefore gives better results also for longer ranging harmonic interaction in the next chapter.

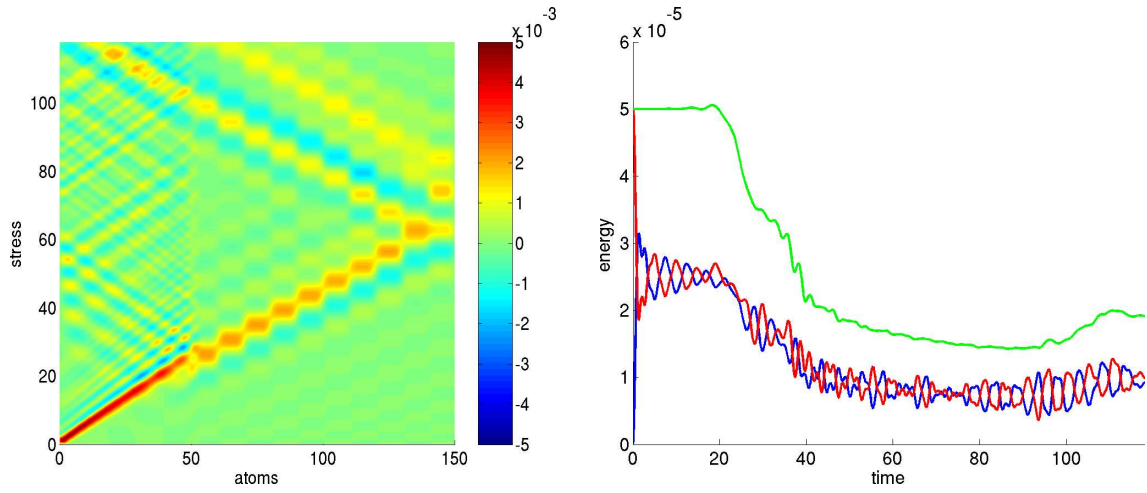


Figure 3.22: stress and energy of real atoms for longer ranging harmonic potential with Cauchy-Born rule in bridging scales approximation

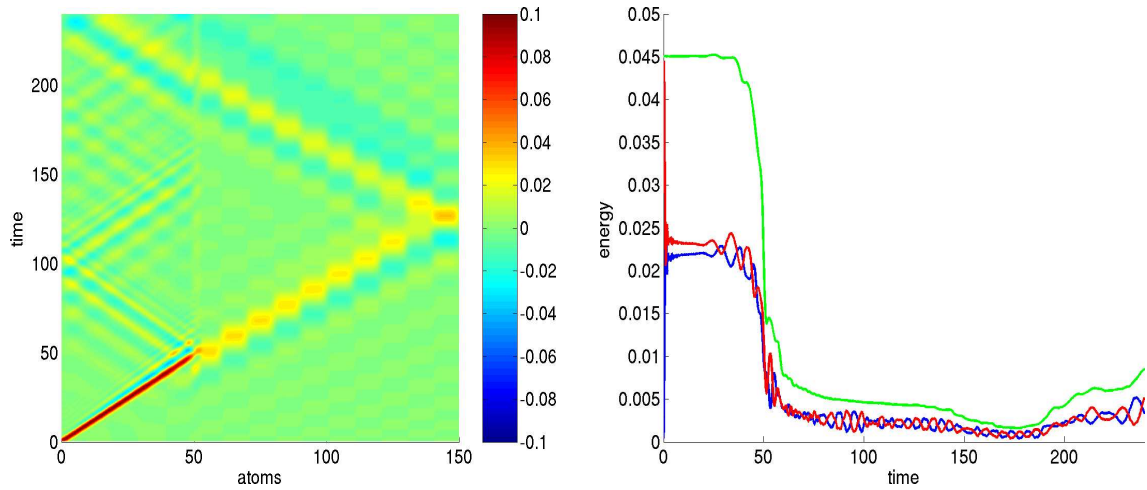


Figure 3.23: stress and energy of real atoms for anharmonic potential in bridging scales approximation



## Chapter 4

# Hamiltonian formulation, boundary conditions and interpolation functions

Since the evolution equations for the atoms are derived from a Hamiltonian and therefore are energy conserving, this should also hold for the approximation. In the concurrent coupling of length scales approximation, the coarse scale equations are derived from a continuum Hamiltonian, whereas the coupling conditions are not derived from the transition from atomistic to coarse scale. In the bridging scales approximation, we get the coupling directly from the displacement splitting, but we cannot derive the approximated equations together with the reflectionless boundary condition from a Hamiltonian. Therefore, this approximation leads to a system of equations that is not energy conserving. In section 4.1, we explain why this is the case and present in section 4.2 an idea how to overcome this difficulty using variables with interpolation weights in orthogonal subspaces. Some technical problems are discussed, and the choice of the subspaces for the coupling of an atomistic and a coarse scale region are presented in section 4.3. In section 4.4, we show, how we can use this Hamiltonian formulation for simulating systems at non-zero temperature. We give an alternative derivation of the equations based on the Mori-Zwanzig projection operator formalism in section 4.5 and show in section 4.6, how we can choose the interpolation weights from coarse to fine scale, to solve the problem of wrong dispersion relation in the coarse scale region. The new system of equations is then not only energy conserving but solves also the problems of wave reflection at the interface and wrong dispersion relation in the coarse scale region. Approximations in the Hamiltonian and numerical approximations in the solution of the system will be discussed in chapter 5.

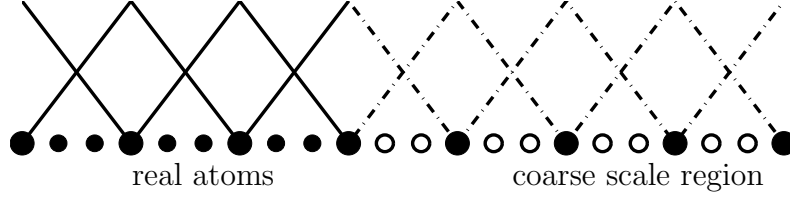


Figure 4.1: splitting of the hat functions for the real atoms (solid lines on the left) and for the coarse scale region (dash-dotted lines on the right)

## 4.1 Bridging scales approximation not energy conserving

To show that the bridging scales method cannot be derived directly from a Hamiltonian or Lagrangian, we consider first the case that the atoms are split in two parts. In one part we keep the fine scale information and in the other part we calculate only the movement of the coarse scale nodes, without reflectionless boundary condition at the interface. The problem is, that the matrix  $Q = I - P = I - N(N^T M N)^{-1} N^T M$ , which defines the projection on the fine scale (cf. section 2.5) is a fully occupied matrix, so we cannot split the matrix into two parts, according to the partitioning of atoms.

Without reflectionless boundary condition, we can overcome this problem by calculating the projection matrix  $Q$  only from the interpolation weights of the real atoms,  $i = 1, \dots, n_1$ . With the corresponding projection matrix  $N_1$ , consisting of the values on the thick black lines in figure 4.1, we can write the fine scale projection  $Q_1$  as  $Q_1 = I_1 - P_1 = I_1 - N_1(N^T M N)^{-1} N_1^T M$ , with

$$N_{1,ij} = \begin{cases} N_{ij}, & i = 1, \dots, n_1 \\ 0, & i = n_1 + 1, \dots, n \end{cases}, \quad I_{1,ij} = \begin{cases} 1, & i = j, i = 1, \dots, n_1 \\ 0, & i \neq j \text{ or } i > n_1 \end{cases}.$$

Since the projection matrix  $P_1$  has only non-zero entries on the upper left sub-matrix of size  $n_1 \times n_1$ , the same holds for  $Q_1$ . If we use the approximation  $Q \approx Q_1$  for the Lagrangian,

$$\mathcal{L}_1 \approx \frac{1}{2} \dot{d}^T N^T M N \dot{d} + \frac{1}{2} \dot{q}^T Q_1^T M Q_1 \dot{q} - \frac{1}{2} (N d + Q_1 q)^T K (N d + Q_1 q),$$

according to (2.12), we get the evolution equations

$$\begin{aligned} N^T M N \ddot{d} &= -N^T K (N d + Q_1 q), \\ Q_1^T M Q_1 \ddot{q} &= -Q_1^T K (N d + Q_1 q). \end{aligned}$$

Since the entries of the matrix  $Q_1$  of the atoms in the coarse scale region are zero, the corresponding fine scale values do not appear in the equations at all.

If we formulate the approximation in this way, we have to face two problems. First,  $P q + Q_1 q = N d + Q_1 q \neq q$ , even for the real atoms, since the projection

matrix  $P = N(N^T M N)^{-1} N^T M$  is derived from the values of all interpolation functions, in contrast to  $Q_1$ . The second problem is, that with this representation we cannot directly get the Hamiltonian from the Lagrangian description with Legendre transformation. We would have to compute the momenta

$$p = \frac{\partial \mathcal{L}}{\partial \dot{q}} = Q_1^T M Q_1 \dot{q}, \quad \mathcal{P} = \frac{\partial \mathcal{L}}{\partial \dot{d}} = N^T M N \dot{d},$$

where the matrix  $Q_1^T M Q_1$  is singular and the inverse can be determined only in the subspace  $\{q | Nd = 0\}$ .

The situation gets even worse if additionally we want to add the reflectionless boundary condition. It is computed according to section 2.5 with Laplace transformation from the evolution equations of the fine scale displacements of the atoms in the coarse scale region. In the derivation of the boundary condition, it was assumed, that the coarse and fine scale displacements decouple, i.e. the coarse scale evolution equations do not depend on the fine scale displacements. If we use this approximation in the Lagrangian, we get a system of decoupled evolution equations. We loose not only the coupling between the two scales but also end up with the wrong evolution equations in the atomistic region. However, without this approximation in the Lagrangian, we cannot derive the boundary condition, therefore the bridging scales approximation cannot be energy conserving.

If the approximated system of equations is not energy conserving, simulations with constant temperature are not possible by sampling the term  $R(t)$  in the reflectionless boundary condition (2.19) with the correct autocorrelation.

The forces in the coarse scale region and the reflectionless boundary condition are derived from different approximations. If we solve the fine scale system of equations, according to section 2.5, by computing the fully atomistic solution of the real atoms, the corresponding coarse scale part evolves according to another evolution equation than the coarse scale equations. It is therefore unavoidable to update the total displacements of the real atoms after several time steps with the solution of the coarse scale equations. Otherwise, the difference between the solution of the coarse scale equations and the projection to the coarse scale from the atomistic values would grow in every time step. This was observed in [71].

## 4.2 Orthogonal displacement splitting

We present now a method to split the displacements by projection in several orthogonal subspaces. This displacement splitting allows the derivation of a reflectionless boundary condition directly from the Lagrangian, as well as the derivation of energy conserving approximations. We derive the system of equations for displacements in an arbitrary space dimension  $\tilde{m}$  and for an arbitrary number of different subspaces  $k$ . Two examples for  $k = 3$  and  $k = 2$  in one dimension will be presented in the next section.

Starting from the atomistic Lagrangian,

$$\mathcal{L} = \frac{1}{2} \dot{u}^T M \dot{u} - \Phi(u), \quad \dot{u}, u \in \mathbb{R}^{\tilde{m}}, \quad (4.1)$$



with  $n$  the number of atoms, we split the displacements  $u$  into  $k$  different kinds of variables,  $a_1, \dots, a_k$ , with the corresponding projection matrices  $A_1, \dots, A_k$ , i.e.

$$u = A_1 a_1 + \dots + A_k a_k, \quad (4.2)$$

according to the conditions:

1. The vector of variables  $a_l$  has  $n_l$  entries,  $l \in \{1, \dots, k\}$ ,  $a_l \in \mathbb{R}^{\tilde{m}n_l}$ , with  $n_1 + \dots + n_k = n$ .
2. The corresponding projection matrices  $A_l : \mathbb{R}^{\tilde{m}n_l} \mapsto \mathbb{R}^{\tilde{m}n}$ ,  $l \in \{1, \dots, k\}$ , are orthogonal with respect to the atomistic mass matrix  $M$ ,

$$(A_l, A_j)_M = A_l^T M A_j = 0, \quad \text{for } l \neq j, \quad l, j \in \{1, \dots, k\}. \quad (4.3)$$

We need this condition to get decoupling of the kinetic energy in the Lagrangian.

The first condition allows to change from the Lagrangian to the Hamiltonian formulation with Legendre transformation, since the matrices  $A_l^T M A_l$ ,  $l \in \{1, \dots, k\}$ , are invertible.

In the following, we show that we can derive the evolution equations for the different variables and a boundary condition from one of the subspaces directly from this Lagrangian or the corresponding Hamiltonian if this two conditions are fulfilled.

We can write the Lagrangian (4.1) using (4.2) as

$$\mathcal{L} = \frac{1}{2}(\dot{a}_1^T A_1^T M A_1 \dot{a}_1 + \dots + \dot{a}_k^T A_k^T M A_k \dot{a}_k) - \Phi(A_1 a_1 + \dots + A_k a_k), \quad (4.4)$$

and we derive the evolution equations

$$A_l^T M A_l \ddot{a}_l = -\frac{\partial \Phi}{\partial a_l} = -A_l^T \frac{\partial \Phi}{\partial u}, \quad l \in \{1, \dots, k\}. \quad (4.5)$$

We obtain the corresponding Hamiltonian formulation from Legendre transformation of the Lagrangian, with the momenta defined as

$$\mathcal{A}_l := \frac{\partial \mathcal{L}}{\partial \dot{a}_l} = (A_l^T M A_l) \dot{a}_l, \quad l \in \{1, \dots, k\}.$$

From the Hamiltonian,

$$\begin{aligned} \mathcal{H} &= \dot{a}_1^T \mathcal{A}_1 + \dots + \dot{a}_k^T \mathcal{A}_k - \mathcal{L}(\dot{a}_1(\mathcal{A}_1), \dots, \dot{a}_k(\mathcal{A}_k), a_1, \dots, a_k) \\ &= \frac{1}{2}(\mathcal{A}_1^T (A_1^T M A_1)^{-1} \mathcal{A}_1 + \dots + \mathcal{A}_k^T (A_k^T M A_k)^{-1} \mathcal{A}_k) + \Phi(A_1 a_1 + \dots + A_k a_k), \end{aligned}$$

the Hamiltonian system of equations can be derived,

$$\begin{aligned} \dot{a}_l &= \frac{\partial \mathcal{H}}{\partial \mathcal{A}_l} = (A_l^T M A_l)^{-1} \mathcal{A}_l, \quad l \in \{1, \dots, k\} \\ \dot{\mathcal{A}}_l &= -\frac{\partial \mathcal{H}}{\partial a_l} = -A_l^T \frac{\partial \Phi}{\partial u}, \quad l \in \{1, \dots, k\}. \end{aligned}$$

The values of the variables  $a_1, \dots, a_k$ , corresponding to a given value of  $u$ , are calculated again as the least square fit,

$$(u - A_l a_l)^T M (u - A_l a_l) \mapsto \min, \quad l \in \{1, \dots, k\},$$

leading to the following relation

$$A_l a_l = P_l u = A_l (A_l^T M A_l)^{-1} A_l^T M u.$$

Since

$$P_l^2 = P_l P_l = A_l (A_l^T M A_l)^{-1} A_l^T M A_l (A_l^T M A_l)^{-1} A_l^T M = P_l$$

holds,  $P_l$  are linear projections.

To solve the system of equations, without explicitly solving the evolution equations of the variables  $a_k$  of the Lagrangian system (4.5), a first approximation in the Lagrangian function (4.1) is necessary. We expand the potential energy  $\Phi$  with respect to the variables  $a_k$  and neglect the terms of higher than second order. With  $K$  the matrix of the corresponding coefficients for the second order terms, the last equation of the Lagrangian system is then

$$A_k^T M A_k \ddot{a}_k = -A_k^T K (A_1 a_1 + \dots + A_k a_k).$$

With Laplace transformation, we can calculate from this equation

$$a_k(t) = \int_0^t \theta(\tau) A_k^T K (A_1 a_1 + \dots + A_{k-1} a_{k-1})(t - \tau) d\tau + R(t), \quad (4.6)$$

with

$$\theta(t) = L^{-1} \{ [A_k^T M A_k s^2 + A_k^T K A_k]^{-1} \}, \quad (4.7)$$

$$R(t) = \dot{\theta}(t) A_k^T M A_k a_k(0) + \theta(t) A_k^T M A_k \dot{a}_k(0). \quad (4.8)$$

If we use equation (4.6) for the other equations of (4.5), which are now all linear in  $a_k$ , the system can be solved without explicit computation of  $a_k$ . In the next section, we use this for the derivation of a reflectionless boundary condition. The memory kernel  $\theta(t)$  in (4.7) can be written using lemma 3.1 as

$$\begin{aligned} \theta(t) &= L^{-1} \{ [A_k^T M A_k s^2 + A_k^T K A_k]^{-1} \} \\ &= \sum_{l=0}^{\infty} \frac{(-1)^l}{(2l+1)!} [(A_k^T M A_k)^{-1} (A_k^T K A_k)]^l t^{2l+1} (A_k^T M A_k)^{-1}. \end{aligned}$$

We should keep in mind, that if the potential energy function is already quadratic in  $a_k$ , we need no approximation to derive (4.6) and even if the system of equations (4.5) looks complicated, we still get the correct atomistic solution.

The advantage is, that we can think now of different approximations in the Lagrangian (4.4) and derive an approximating system of equations which is always energy conserving. The approximation error compared to the fully atomistic system can be determined directly by comparing the Lagrangian or Hamiltonian functions. Like this, it is possible to distinguish between errors due to approximations in the Lagrangian and numerical errors in solving the approximated system. We will discuss this in detail in chapter 5.

### 4.3 Coupling of atomistic and coarse scale region

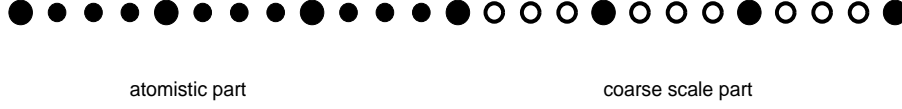


Figure 4.2: coupling of an atomistic and a coarse scale region

We use now the method presented in the previous section for the coupling of an atomistic and a coarse scale region [66, 67]. Like in the bridging scales approximation, we choose a coarse scale node at the equilibrium position of every  $\tilde{n}$ th atom and split the total atomistic displacements  $u$  into the contribution from the coarse scale  $u_c$ , and the remaining fine scale displacements  $u_f$ . The coarse scale part is given by the interpolation of the displacements of the coarse scale nodes, which we denote again by  $d$ ,  $N$  is again the matrix of the interpolation weights, i.e.  $u_c = Nd$ . How to choose this interpolation weights is discussed in section 4.6. We can use e.g. linear finite element hat functions on the coarse scale and evaluate them at the atomistic equilibrium positions, like in the bridging scales approximation.

In the  $\tilde{m}$  dimensional case with  $n$  atoms, the total displacement has  $n\tilde{m}$  degrees of freedom. If we have  $n_c$  coarse scale nodes,  $\tilde{m}(n - n_c)$  additional degrees of freedom are necessary to represent the fine scale displacements  $u_f$ . We denote them by the vector  $b$  and have to determine the interpolation weights  $B$  for the atoms to get the total displacements as

$$u = Nd + Bb.$$

According to (4.3), the interpolation matrices  $N$  and  $B$  have to be orthogonal with respect to the mass matrix, that is

$$N^T M B = 0.$$

Since we want to keep the fine scale information only in one part of the domain, we have to split the variables  $b$  into two parts,  $b_1$  and  $b_2$ , according to the fine scale degrees of freedom which we want to keep and those that we want to neglect. The two corresponding interpolation matrices  $B_1$  and  $B_2$  have also to be orthogonal, i.e.

$$B_1^T M B_2 = 0.$$

In terms of the previous section, we have now three orthogonal subspaces ( $k = 3$ ), and the total atomistic displacement can be written as

$$u = Nd + B_1 b_1 + B_2 b_2.$$

Before we explain the splitting of the matrix  $B$ , we have to choose the entries of this matrix. We do this in such a way that  $B$  has only few non-zero entries to make the numerical solution of the corresponding system of equations easier. In order to simplify things, we consider the computation of interpolation weights for the one

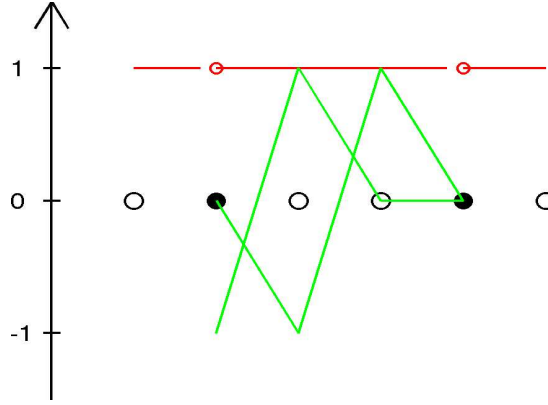


Figure 4.3: one dimensional example: piecewise constant interpolation functions from the coarse scale nodes (red) and corresponding fine scale interpolation functions (green) for  $\tilde{n} = 3$

dimensional case and  $M = mI$ . However, the general procedure is similar for higher dimensions or different atomic masses.

We start with the easiest possible interpolation from the coarse scale values to the atoms: constant interpolation between two nodes (marked red in figure 4.3). If we have a coarse scale node at the equilibrium position of every  $\tilde{n}$ th atom, we need  $\tilde{n} - 1$  variables  $b_l$  at the atoms in between. Since the corresponding interpolation weights have to be orthogonal to the one column of  $N$  with non-zero entries for this element, we get the  $\tilde{n} - 1$  vectors as solution of the equation

$$b_1 + b_2 + \dots + b_{\tilde{n}} = 0.$$

An example is shown in figure 4.3. Each of the two orthogonal vectors corresponding to the two green lines has two non-zero entries. Both together have non-zero entries at the left node of the element and at the atoms between the nodes. In this case, it is easy to split the matrix  $B$  in two parts, since the non-zero entries in each element do not overlap.

The situation gets more complicated if we have  $l$  coarse scale interpolation functions in each element. Then, the linear system of equations that defines the interpolation weights  $B$  needs  $\tilde{n} - 1 + l$  unknowns to have a  $\tilde{n} - 1$  dimensional solution. E.g. for linear finite element hat functions as interpolation functions, we have two non-zero weights of  $N$  at each atom. Therefore, we need  $\tilde{n} + 1$  non-zero entries of  $B$  in each element to construct  $\tilde{n} - 1$  vectors orthogonal to both vectors of  $N$ . The system of equations to solve in every element is

$$\begin{aligned} b_0 + \frac{\tilde{n}-1}{\tilde{n}}b_1 + \dots + \frac{1}{\tilde{n}}b_{\tilde{n}-1} &= 0 \\ \frac{1}{\tilde{n}}b_1 + \dots + \frac{\tilde{n}-1}{\tilde{n}}b_{\tilde{n}-1} + b_{\tilde{n}} &= 0. \end{aligned}$$

The vectors of adjacent elements will now overlap, since the variables  $b_0$  and  $b_{\tilde{n}}$  will appear also in the corresponding system of equations for the neighbouring elements. Setting one or both of them to zero is not possible, since we should not only fulfil

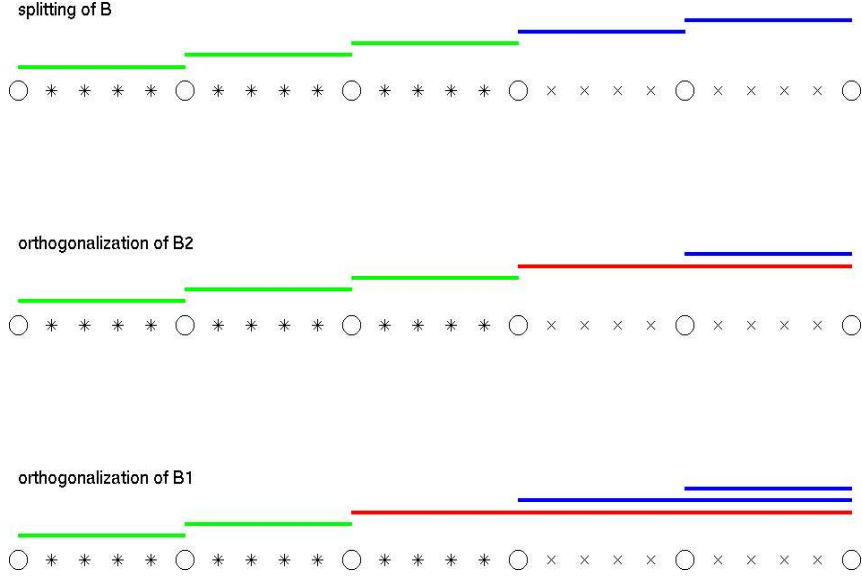


Figure 4.4: splitting the matrix B in two orthogonal parts

both equations, but the solution should also have dimension  $\tilde{n} - 1$ . Splitting the matrix B in such a way that  $B_1$  represents the fine scale part of the real atoms and  $B_2$  the fine scale part which we want to neglect, is therefore not a problem, but the two matrices will not be orthogonal.

One possibility to solve this problem is, to split the matrix  $B = B_1 + B_2$  in such a way that the entries correspond to the geometrical separation of the atoms and to orthogonalize the matrix  $B_2$ . If we finally orthogonalize the last block of  $B_1$ , that is the entries of  $B_1$  corresponding to the element next to the interface, with respect to the orthogonal entries of  $B_2$ ,  $B_1^T B_2 = 0$  holds. This procedure is shown in figure 4.4. Green lines in the first picture indicate the support of the vectors given by the columns of  $B_1$ , blue lines that of the columns of  $B_2$  for an example with 6 nodes and  $\tilde{n} = 5$ . The vertical distances of the lines in the picture are only to show that the supports of the entries of different blocks overlap at the node in between. Only the entries of the last block of  $B_1$  are not orthogonal to the entries of  $B_2$  at the beginning, due to overlapping supports.

In the first step, the entries of  $B_2$  are orthogonalized, by orthogonalizing the entries of the first block of  $B_2$  with respect to that of the second block. Thereby, the red line indicates the new support of the entries of the first block of  $B_2$ . Then, the entries of the last block of  $B_1$  are orthogonalized with respect to  $B_2$ , again the red line indicates the change in the support. The entries of the last block of  $B_1$  are not local any more after the orthogonalization but they are now non-zero everywhere in the coarse scale region. Since they decrease very fast away from the interface, this does not matter much, and, for the numerical solution, it is enough to consider only the entries of the first elements after the interface. We will see in the next section, that we can even perform this orthogonalization only for the first two or three elements after the interface, leading to still satisfactory results.

If we have different atomic masses, i.e.  $M \neq mI$ , we have to orthogonalize the

vectors with respect to the mass matrix  $M$  in order to fulfil (4.3).

In the following, we give the Lagrangian together with the corresponding evolution equations and the reflectionless boundary condition for the coupling of atomistic and coarse scale region with harmonic potential.

Lagrangian:

$$\begin{aligned} \mathcal{L} = & \frac{1}{2}(\dot{d}^T N^T M N \dot{d} + \dot{b}_1^T B_1^T M B_1 \dot{b}_1 + \dot{b}_2^T B_2^T M B_2 \dot{b}_2) - \\ & - \frac{1}{2}(N d + B_1 b_1 + B_2 b_2)^T K (N d + B_1 b_1 + B_2 b_2), \end{aligned} \quad (4.9)$$

evolution equations:

$$N^T M N \ddot{d} = -N^T K (N d + B_1 b_1 + B_2 b_2), \quad (4.10)$$

$$B_1^T M B_1 \ddot{b}_1 = -B_1^T K (N d + B_1 b_1 + B_2 b_2), \quad (4.11)$$

boundary condition:

$$b_2(t) = \int_0^t \theta(\tau) B_2^T K (N d + B_1 b_1)(t - \tau) d\tau + R(t), \quad (4.12)$$

$$\begin{aligned} \theta(t) &= L^{-1} \{ [B_2^T M B_2 s^2 + B_2^T K B_2]^{-1} \} \\ &= \sum_{l=0}^{\infty} \frac{(-1)^l}{(2l+1)!} [(B_2^T M B_2)^{-1} (B_2^T K B_2)]^l t^{2l+1} (B_2^T M B_2)^{-1}, \end{aligned} \quad (4.13)$$

$$R(t) = \dot{\theta}(t) B_2^T M B_2 b_2(0) + \theta(t) B_2^T M B_2 \dot{b}_2(0). \quad (4.14)$$

We consider again the first numerical example from chapter 3. In figure 4.5, we show the stress of the fully atomistic system, the stress calculated with the bridging scales approximation and of the system with the orthogonal displacement splitting, together with a plot of the energy of the first 50 atoms for the three simulations.

In contrast to the bridging scales approximation, an error in the solution does not occur, before the perturbation reaches the interface between atomistic and pure coarse scale region. Then, we see a slightly different behaviour compared to the fully atomistic system, since a small part of the perturbation is reflected due to numerical errors in the calculation of the memory kernel.

Another difference to the bridging scales approximation is, that the dispersion relation is correct if we keep the reflectionless boundary condition in the equations for  $d$ . However, keeping the boundary condition also in the coarse scale equations is not exactly what we want, since computing the boundary condition everywhere is not cheaper than a fully atomistic simulation. Choosing the interpolation functions in such a way that we do not need the boundary condition in (4.10) will be discussed in section 4.6, numerical approximations in the memory kernel and the memory integral in chapter 5.

To compute the exact memory kernel  $\theta(t)$ , we use the orthogonal transformation of the matrix  $(B_2^T M B_2)^{-1} (B_2^T K B_2)$  to a diagonal matrix. With the transformation matrix  $\hat{P}$  and the diagonal matrix

$$\Lambda = \hat{P}^T (B_2^T M B_2)^{-1} (B_2^T K B_2) \hat{P},$$

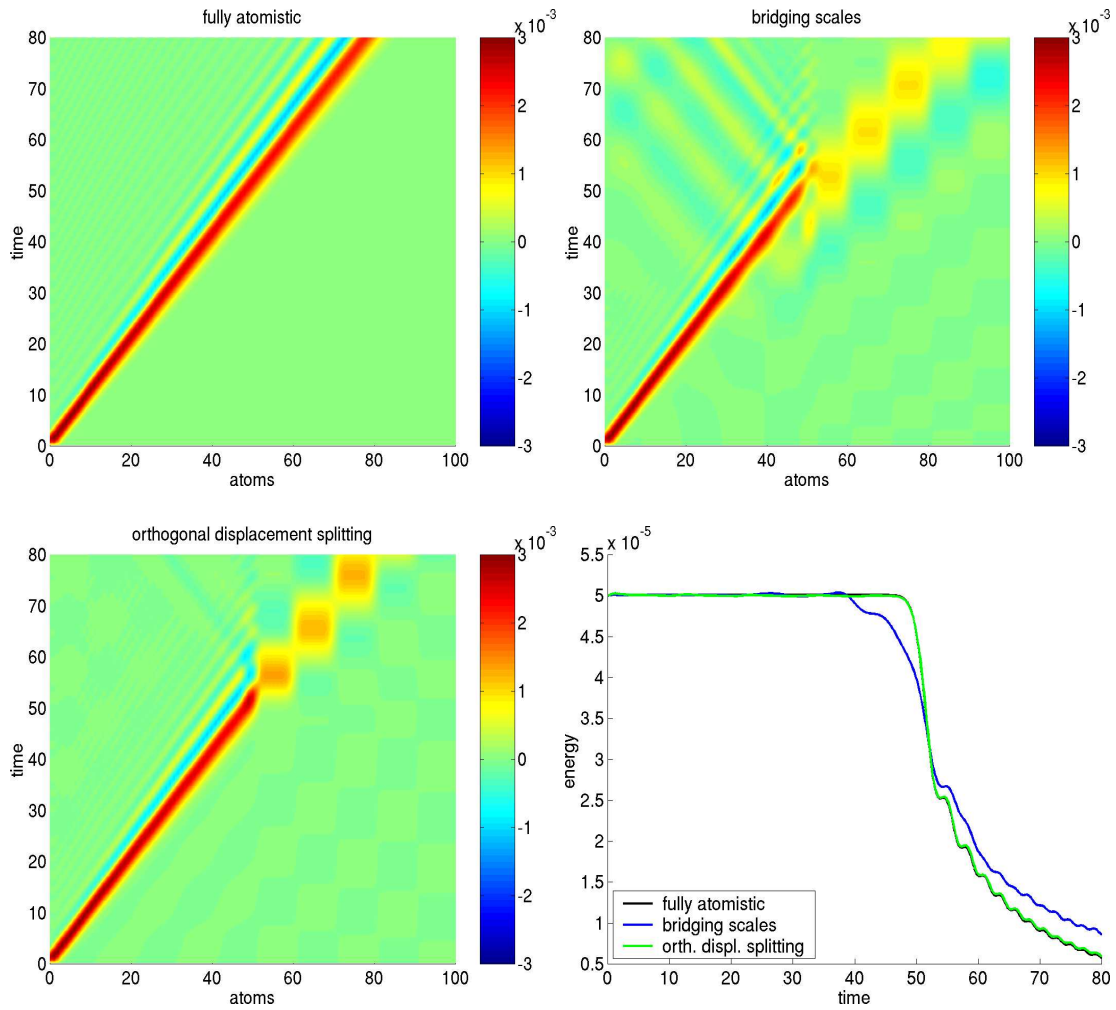


Figure 4.5: stress and energy with fully atomistic system, bridging scales approximation and orthogonal displacement splitting

we can write the memory kernel as

$$\begin{aligned}
 \theta(t) &= L^{-1} \{ [B_2^T M B_2 s^2 + B_2^T K B_2]^{-1} \} \\
 &= \sum_{l=0}^{\infty} \frac{(-1)^l}{(2l+1)!} [(B_2^T M B_2)^{-1} (B_2^T K B_2)]^l t^{2l+1} (B_2^T M B_2)^{-1} \\
 &= \hat{P} \sum_{l=0}^{\infty} \frac{(-1)^l}{(2l+1)!} \Lambda^l t^{2l+1} \hat{P}^T (B_2^T M B_2)^{-1} \tag{4.15} \\
 &= \hat{P} \Lambda^{-1/2} \sin(\Lambda^{1/2} t) \hat{P}^T (B_2^T M B_2)^{-1}. \tag{4.16}
 \end{aligned}$$

Since the matrix  $(B_2^T M B_2)^{-1} (B_2^T K B_2)$  is positive definite, all entries of  $\Lambda$  are positive. We can compute now the sine function of every entry of the diagonal matrix separately.

If we use the orthogonal displacement splitting for two subspaces on the same scale, we can derive a reflectionless boundary condition for a small atomistic region, without the coupling to a coarse scale region,

$$u = B_1 b_1 + B_2 b_2.$$

E.g. for a one dimensional splitting of atoms in two parts, we get the matrices

$$B_1 = \begin{pmatrix} I_1 & 0 \\ 0 & 0 \end{pmatrix}, \quad B_2 = \begin{pmatrix} 0 & 0 \\ 0 & I_2 \end{pmatrix},$$

with the identity matrices  $I_1$  and  $I_2$  for the two kinds of atoms.

The splitting of the matrix  $B$  is now no problem, since all vectors have only one non-zero entry and are therefore all pairwise orthogonal. Such a coupling of an atomistic and a continuum region is considered e.g. in [3, 57, 75].

## 4.4 Calculation of the random force

In the second numerical example in chapter 3, we studied the behaviour of the bridging scales approximation for initial conditions sampled from a normal distribution according to a given temperature  $T$ . Neglecting the term  $R(t)$  in the reflectionless boundary condition of the bridging scales approximation leads to an energy decrease of the real atoms. To be able to run simulations for non-zero temperature, we therefore need  $R(t)$ . But, since the bridging scales approximation is not energy conserving, even with the exact function  $R(t)$  we would not get the correct energy in the real atoms. However, with the modified approach of the orthogonal displacement splitting, this is no problem anymore, since the system is derived, together with the boundary condition, from the Lagrangian (4.9).

We use a method similar to that proposed in [75] to compute

$$R(t) = \dot{\theta}(t) (B_2^T M B_2) b_2(0) + \theta(t) (B_2^T M B_2) \dot{b}_2(0)$$

as a random force by sampling the initial conditions and calculating  $R(t)$  from this initial conditions in every time step. Since we do not know the distribution of the



initial conditions in the variables  $b_2$ , we make a coordinate transformation of  $b_2$  to the corresponding normal modes for the interaction of this degrees of freedom,

$$\begin{aligned} x &:= \hat{P}^T b_2, \\ b_2^T B_2^T K B_2 b_2 &= b_2^T \hat{P} \Lambda \hat{P}^T b_2 = x^T \Lambda x, \end{aligned}$$

with  $\Lambda$  the diagonal matrix of eigenvalues of  $B_2^T K B_2$  and  $\hat{P}$  consisting of the corresponding eigenvectors. Furthermore, we use the fact that the entries of the matrix  $B_2$  can be chosen orthonormal with respect to the mass matrix  $M$ ,

$$B_2^T M B_2 = I, \quad \dot{x} = \hat{P}^T \dot{b}_2 \Rightarrow \dot{b}_2^T B_2^T M B_2 \dot{b}_2 = \dot{b}_2^T \hat{P} \hat{P}^T \dot{b}_2 = \dot{x}^T \dot{x}.$$

In this new coordinates, the part of the Hamiltonian of the interaction of  $b_2$  is given by

$$\dot{b}_2^T B_2^T M B_2 \dot{b}_2 + b_2^T B_2^T K B_2 b_2 = \frac{1}{2} \dot{x}^T \dot{x} + \frac{1}{2} x^T \Lambda x.$$

The normal mode coordinates  $x$  are now independent from each other. The coordinates  $\dot{x}_i$  and  $x_i$  can therefore be sampled from a Gaussian distribution,

$$\dot{x}_i \sim N(0, k_B T), \quad x_i \sim N\left(0, \frac{k_B T}{\lambda_i}\right), \quad i \in \{1, \dots, n\}.$$

If we sample initial displacements and velocities independently, we can compute the random force directly from the transformation above as

$$\begin{aligned} R(t) &= \theta(t) \dot{b}_2(0) + \dot{\theta}(t) b_2(0) \\ &= \hat{P} \Lambda^{-1/2} \sin(\Lambda^{1/2} t) \hat{P}^T \dot{b}_2(0) + \hat{P} \cos(\Lambda^{1/2} t) \hat{P}^T b_2(0) \\ &= \hat{P} \Lambda^{-1/2} \sin(\Lambda^{1/2} t) \dot{x}(0) + \hat{P} \cos(\Lambda^{1/2} t) x(0) \end{aligned} \quad (4.17)$$

if we use the representation of the memory kernel in equation (4.16).

If the memory integral and the random force (4.17) are computed exactly, the solution of (4.10) and (4.11) is the same than for a fully atomistic simulation. But, since the computation of the memory integral is very time consuming, we have to approximate the memory kernel. We show in chapter 5, that for simulations at zero temperature, we can cut the memory kernel in time and reduce the simulation time drastically, without creating a too large numerical error. The situation is different for non-zero temperature simulations, i.e. if we consider also  $R(t)$ . This random force gives a periodic excitation of the normal modes of the missing degrees of freedom  $b_2$  that are damped by the memory integral. If we cut the memory kernel in time and/or in space, the damping of some normal modes can be changed, and the energy of this normal modes can grow exponentially. To avoid this, we can use the method proposed in [75]. With integration by parts, we can rewrite

$$\begin{aligned} b_2(t) &= \int_0^t \theta(\tau) B_2^T K (N d + B_1 b_1)(t - \tau) d\tau \\ &= \Theta(t) B_2^T K (N d + B_1 b_1)(0) - \int_0^t \Theta(\tau) B_2^T K (N \dot{d} + B_1 \dot{b}_1)(t - \tau) d\tau, \end{aligned}$$

where

$$\Theta(t) := \int_0^t \theta(\tau) d\tau.$$

With

$$d = (N^T M N)^{-1} N^T M u, \quad b_1 = (B_1^T M B_1)^{-1} B_1^T M u \quad (4.18)$$

and the harmonic solutions of  $u$ ,

$$u = u_0 \exp(-i\omega t),$$

we can rewrite the memory integral

$$\begin{aligned} & - \int_0^t \Theta(\tau) B_2^T K (N(N^T M N)^{-1} N^T M \dot{u} + B_1(B_1^T M B_1)^{-1} B_1^T M \dot{u}) (t - \tau) d\tau \\ &= - \int_0^t \Theta(\tau) B_2^T K (I - B_2(B_2^T M B_2)^{-1} B_2^T M) \dot{u}(t - \tau) d\tau \\ &= i\omega \int_0^t \Theta(\tau) B_2^T K (I - B_2(B_2^T M B_2)^{-1} B_2^T M) u_0 \exp(-i\omega(t - \tau)) d\tau \\ &= i\omega \exp(-i\omega t) \int_0^t \Theta(\tau) B_2^T K (I - B_2(B_2^T M B_2)^{-1} B_2^T M) \exp(i\omega\tau) d\tau u_0 \\ &= i\omega \exp(-i\omega t) \int_0^t \Theta(\tau) B_2^T K (I - B_2(B_2^T M B_2)^{-1} B_2^T M) (\cos(\omega\tau) + i \sin(\omega\tau)) d\tau u_0. \end{aligned}$$

Since

$$\Theta(t) = \hat{P}(I - \cos(\Lambda^{1/2}t))\hat{P}^T, \quad (4.19)$$

the term with the sine function is zero. If we rewrite the left hand side of equations (4.10) and (4.11) also with (4.18) and consider only the terms with the memory integral on the right hand side, we get

$$\begin{aligned} & \begin{pmatrix} N^T M N \ddot{d} \\ B_1^T M B_1 \ddot{b}_1 \end{pmatrix} = \begin{pmatrix} N^T \\ B_1^T \end{pmatrix} \ddot{u}(t) \\ &= - \begin{pmatrix} N^T \\ B_1^T \end{pmatrix} K B_2 \int_0^t \Theta(\tau) B_2^T K (I - B_2(B_2^T M B_2)^{-1} B_2^T M) \cos(\omega\tau) d\tau i\omega e^{(-i\omega t)} u_0 \\ &= \begin{pmatrix} N^T \\ B_1^T \end{pmatrix} \int_0^t K B_2 \Theta(\tau) B_2^T K (I - B_2(B_2^T M B_2)^{-1} B_2^T M) \cos(\omega\tau) d\tau \dot{u}(t) \\ &= \begin{pmatrix} N^T \\ B_1^T \end{pmatrix} \gamma(\omega) \dot{u}(t). \end{aligned}$$

To get a damping in the memory integral, the matrix  $\gamma(\omega)$  has to be negative semi-definite. This is the case if we compute  $\Theta(t)$  according to (4.19). But, if we cut the function after time  $T$ , or we cut the matrix  $B_2$  in space, the negative semi-definiteness can no longer be guaranteed.

One possibility to overcome this problem, is to compute the function

$$K B_2 \Theta(t) B_2^T K (I - B_2(B_2^T M B_2)^{-1} B_2^T M) \quad (4.20)$$

over the time interval  $[0, T]$ , with  $T$  long enough that the entries of the matrix have decayed, diagonalize the matrix, compute the real part of its Fourier transformation and set the positive values to zero. With inverse Fourier transformation, we can compute an update of (4.20). Possibly, the entries of the matrix do now not decay in the given time interval  $[0, T]$  and in space. The procedure is therefore repeated till the matrix entries decay and the matrix has the required negative semi-definiteness. This method was tested in [75] for the coupling of a small atomistic to a continuum region.

To reduce the computation time effectively, without reducing the number of degrees of freedom in  $b_2$ , we would have to take  $R(t)$  into account only in some probabilistic way as a random force in every time step. Since the values of  $R(t)$  in different points in time are related to each other, it is not enough to sample  $R(t)$  with the correct mean value  $\langle R(t) \rangle$  and the correct variance  $\langle R(t)^T R(t) \rangle$ , but we need also the correct autocorrelation  $\langle R(0)^T R(t) \rangle$ . As described in [4] for the coupling of an atomistic and a continuum region, we can compute the autocorrelation function of the random force by taking the time derivative of  $R(t)$  and multiplying with  $\dot{b}_2$  which leads to

$$\dot{R}(t)\dot{b}_2^T(0) = \dot{\theta}(t)B_2^T M B_2 b_2(0)\dot{b}_2^T(0) + \ddot{\theta}(t)B_2^T M B_2 \dot{b}_2(0)\dot{b}_2^T(0).$$

Taking the ensemble average, we get

$$\begin{aligned} \langle \dot{R}(t)\dot{b}_2^T(0) \rangle &= \langle \ddot{\theta}(t)B_2^T M B_2 b_2(0)\dot{b}_2^T(0) \rangle + \langle \dot{\theta}(t)B_2^T M B_2 \dot{b}_2(0)\dot{b}_2^T(0) \rangle \\ &= \langle \dot{\theta}(t)B_2^T M B_2 \dot{b}_2(0)\dot{b}_2^T(0) \rangle \\ &= \dot{\theta}(t)B_2^T M B_2 \langle \dot{b}_2(0)\dot{b}_2^T(0) \rangle \\ &= k_B T \dot{\theta}(t). \end{aligned}$$

If we solve for the derivative of the memory kernel,

$$\dot{\theta}(t) = \frac{1}{k_B T} \langle \dot{R}(t)\dot{b}_2^T(0) \rangle,$$

and integrate with respect to  $t$ , we get

$$\begin{aligned} \theta(t) &= \frac{1}{k_B T} \langle R(t)\dot{b}_2^T(0) \rangle \\ &= -\frac{1}{k_B T} \langle \dot{R}(t)b_2^T(0) \rangle, \end{aligned}$$

where the second equality is valid because the process  $R(t)$  is stationary. With another integration with respect to  $t$ , we finally get

$$\int_t^\infty \theta(\tau) d\tau = \frac{1}{k_B T} \langle R(t)b_2^T(0) \rangle = \frac{1}{k_B T} \langle R(t)R^T(0) \rangle,$$

where we get the last equation with  $R(0)$  according to (4.17). However, the sampling of this autocorrelation function, without the projection to normal mode coordinates, is still an open problem.

## 4.5 Mori-Zwanzig projection operator formalism

The Mori-Zwanzig projection operator formalism (cf. e.g. [31, 19]), developed about 40 years ago by H. Mori and R. Zwanzig, is a theoretical framework for the derivation of evolution equations for a subset of observables of a Hamiltonian system. In the following, we want to show, how we can obtain the evolution equations, the reflectionless boundary condition and the random force of the orthogonal displacement splitting for a harmonic system, as derived in section 4.2, also from this formalism. If we once have derived these equations for the special case of observables that are linear combinations of the atomic displacements or momenta, it is much easier to determine the appropriate evolution equations for special linear combinations (like the displacement splitting  $u = Nd + B_1b_1 + B_2b_2$ ) than deriving the equations for every setting from the Mori-Zwanzig equations. Since they are designed for a more general setting, using them for a special choice of the variables is not straightforward.

We first give a short overview of the Mori-Zwanzig projection operator formalism, following the representation in [31], but since we are dealing only with classical mechanics systems, we will use the notation for classical instead of quantum mechanical Hamiltonians. Then, we derive the reflectionless boundary condition and the random force for the case of two orthogonal subspaces in this formalism, following the example 16.1 in [31], where the equations are derived for a heavy particle in an elastic chain.

First, we have to choose a set of observables  $A = \{A_l\}_{l \in \{1, \dots, k\}}$  for the Hamiltonian system under consideration. These observables should be linearly independent and depend on time only through the time dependence of the momenta  $p$  and positions  $q$ . Their evolution for the dynamic with the Liouville operator  $\hat{L}$  is given according to section 1.2 by

$$A(t) = e^{i\hat{L}t}A(0). \quad (4.21)$$

Furthermore, we need the projector  $P$  for the projection of atomistic values on the set of variables  $A$ ,

$$P := \sum_{\mu\nu} |A_\mu\rangle a_{\mu\nu} \langle A_\nu|, \quad (4.22)$$

with  $a_{\mu\nu}$  the inverse of the symmetric matrix  $(A_\mu|A_\nu)$  defined by

$$\sum_{\alpha} a_{\mu\alpha} (A_\alpha|A_\nu) = \delta_{\mu\nu}.$$

The chosen projection  $P$  depends therefore not only on the set of observables  $A$ , but also on the choice of the scalar product  $(\cdot | \cdot)$ . Usually, the used scalar product is the Mori scalar product. If the chosen operators  $A$  are a subset of the coordinates, this scalar product is the correlation of the coordinates with respect to the probability distribution of the given ensemble (cf. section 1.3). The operator  $Q$ , orthogonal to  $P$ , is given by

$$Q := I - P.$$

From the equations of motion for the observables  $A_l$ ,

$$\dot{A}_l(t) = e^{i\hat{L}t}\dot{A}_l(0) = e^{i\hat{L}t}P\dot{A}_l(0) + e^{i\hat{L}t}Q\dot{A}_l(0), \quad l \in \{1, \dots, k\},$$

together with the identity

$$e^{i\hat{L}t} = i \int_0^t e^{i\hat{L}(t-\tau)} P \hat{L} e^{iQ\hat{L}\tau} d\tau + e^{iQ\hat{L}t},$$

we obtain

$$\dot{A}_l(t) = e^{i\hat{L}t} P \dot{A}_l(0) + i \int_0^t e^{i\hat{L}(t-\tau)} P \hat{L} e^{iQ\hat{L}\tau} Q \dot{A}_l(0) d\tau + e^{iQ\hat{L}t} Q \dot{A}_l(0).$$

With the definition of  $P$  in (4.22) and  $A_l(t) = e^{i\hat{L}t} A_l$ , we derive

$$\dot{A}(t) = i\Omega A(t) - \int_0^t \gamma(\tau) A(t-\tau) d\tau + f(t),$$

with the following definitions:

$$i\Omega := (A|A)^{-1} (A|i\hat{L}A), \quad (4.23)$$

$$f(t) := i e^{iQ\hat{L}t} Q \hat{L} A, \quad (4.24)$$

$$\gamma(t) := (A|A)^{-1} (f(0)|f(t)).$$

Now we want to proof, that the memory integral and the random force of section 4.2 can be derived alternatively with the Mori-Zwanzig projection operator formalism if we choose a special subset of observables with the corresponding scalar product. Since an approximation is neither in the derivation in section 4.2 nor in the Mori-Zwanzig formalism necessary, both methods are exact and should therefore lead to the same equations. If the observables are a subset of the atomistic momenta, such a derivation is carried out e.g. in [57] and [75].

As the subset of observables, we choose here  $n_d$  arbitrary linear combinations of the atomistic momenta,

$$\mathcal{P} := N^T p, \quad \mathcal{P}_i = \sum_{j=1}^n N_{ji} p_j, \quad i \in \{1, \dots, n_d\},$$

with  $n$  the total number of atoms, and we use the same matrix notation as in section 4.2. This definition of the coarse scale momenta  $\mathcal{P}$  corresponds to that of the space discretised version of the local momenta in section 2.2, with the only difference, that we have now a non differentiable and not time dependent weight function. The projection matrix  $P$  is defined as the canonical ensemble average,

$$P := \frac{|\mathcal{P}\rangle\langle\mathcal{P}|}{\langle\mathcal{P}|\mathcal{P}\rangle} = \frac{|N^T p\rangle\langle N^T p|}{\langle N^T p|N^T p\rangle} = \frac{|N^T p\rangle\langle N^T p|}{N^T(p|p)N} = \frac{|N^T p\rangle\langle N^T p|}{k_B T N^T M N},$$

and the displacements corresponding to this momenta are

$$d = (N^T M N)^{-1} N^T M u.$$

With  $b$  we denote once more the displacements in the subspace orthogonal to the space spanned by  $d$ , with the corresponding momenta  $\mathcal{B}$  and interpolation matrix  $B$

orthogonal to  $N$ ,  $N^T M B = 0$ . The Hamiltonian for the whole system with harmonic interaction is given by

$$\mathcal{H} = \frac{1}{2} (\mathcal{P}^T (N^T M N)^{-1} \mathcal{P} + \mathcal{B}^T (B^T M B)^{-1} \mathcal{B} + (N d + B b)^T K (N d + B b)).$$

With the following identities

$$\begin{aligned} \mathcal{P} &= (N^T M N) i \hat{L} d, \\ (\mathcal{F} | \hat{L} \mathcal{G}) &= i k_B T \langle \{\mathcal{F}^T, \mathcal{G}\} \rangle, \\ (\mathcal{P} | \mathcal{P}) &= k_B T (N^T M N), \end{aligned} \tag{4.25}$$

$$\begin{aligned} Q \hat{L} \mathcal{F} &= \hat{L} \mathcal{F} - P \hat{L} \mathcal{F} = \hat{L} \mathcal{F} - \mathcal{P}^T \frac{(\mathcal{P} | \hat{L} \mathcal{F})}{(\mathcal{P} | \mathcal{P})} \\ &= \frac{1}{i} \{\mathcal{F}, \mathcal{H}\} - i \mathcal{P}^T (N^T M N)^{-1} \langle \{\mathcal{P}, \mathcal{F}\} \rangle \\ &= -\frac{1}{i} \{\mathcal{H}, \mathcal{F}\} + \frac{1}{i} \left\{ \frac{1}{2} \mathcal{P}^T (N^T M N)^{-1} \mathcal{P}, \mathcal{F} \right\} \\ &= -\frac{1}{i} \{\tilde{\mathcal{H}}, \mathcal{F}\} = \tilde{L} \mathcal{F}, \end{aligned} \tag{4.26}$$

taken from [31], a Hamiltonian  $\tilde{\mathcal{H}}$  for the evolution in the space orthogonal to the variables  $\mathcal{P}$  can be derived:

$$\tilde{\mathcal{H}} = \frac{1}{2} (\mathcal{B}^T (B^T M B)^{-1} \mathcal{B} + (B b + N d)^T K (B b + N d)),$$

where the equality (4.26) holds only if the observable  $\mathcal{F}$  is a linear combination of the atomic displacements and momenta. The Poisson brackets  $\{\cdot, \cdot\}$  in the preceding equations are defined as

$$\{\mathcal{F}, \mathcal{G}\} := \sum_{i=1}^n \frac{\partial \mathcal{F}}{\partial q_i} \frac{\partial \mathcal{G}}{\partial p_i} - \frac{\partial \mathcal{F}}{\partial p_i} \frac{\partial \mathcal{G}}{\partial q_i}.$$

According to (4.24), we can derive the residual force

$$f(t) = e^{iQ\hat{L}t} Q i \hat{L} \mathcal{P} = e^{i\tilde{L}t} i L \mathcal{P} = -e^{i\tilde{L}t} N^T K u = -e^{i\tilde{L}t} N^T K (N d + B b). \tag{4.27}$$

The projected Hamiltonian  $\tilde{\mathcal{H}}$  leads to the following evolution equations

$$\begin{aligned} \dot{d} &= 0, \\ \dot{B} = B^T M B \ddot{b} &= -B^T K (N d + B b). \end{aligned} \tag{4.28}$$

The dynamic of the residual force is therefore determined by the evolution of the orthogonal variables  $b$ , when the displacements  $d$  are fixed. As before, we can solve (4.28) with a Laplace transformation to obtain

$$b(t) = \int_0^t \theta(\tau) B^T K N d_0 d\tau + \theta(t) B^T M B \dot{b}(0) + \dot{\theta}(t) B^T M B b(0),$$

with

$$\theta(t) = L^{-1}\{[B^T M B s^2 + B^T K B]^{-1}\}.$$

We use the notation  $d_0$  to indicate that  $d$  does not change in time. Therefore, we can evaluate the integral with

$$\Theta(t) := \int_0^t \theta(\tau) d\tau.$$

From (4.27), we derive the following representation for the residual force

$$\begin{aligned} f(t) = & -N^T K N d_0 - N^T K B \Theta(t) B^T K N d_0 - \\ & -N^T K B \theta(t) B^T M B \dot{b}(0) - N^T K B \dot{\theta}(t) B^T M B b(0), \end{aligned}$$

and with the Kubo identity (4.25), we can obtain the memory kernel

$$\begin{aligned} \gamma(t) &= \frac{1}{(\mathcal{P}|\mathcal{P})} (f(0)|f(t)) = \frac{1}{(\mathcal{P}|\mathcal{P})} (iL\mathcal{P}|f(t)) \\ &= (N^T M N)^{-1} \langle \{\mathcal{P}, f(t)\} \rangle \\ &= (N^T M N)^{-1} \frac{\partial \mathcal{P}}{\partial \mathcal{P}} \frac{\partial f(t)}{\partial d} \\ &= -(N^T M N)^{-1} (N^T K N + N^T K B \Theta(t) B^T K N). \end{aligned}$$

Finally, we can determine the memory integral

$$\begin{aligned} \int_0^t \gamma(\tau) \mathcal{P}(t-\tau) d\tau &= \int_0^t \gamma(\tau) (N^T M N) \dot{d}(t-\tau) d\tau \\ &= (-N^T K N - N^T K B \Theta(t) B^T K N) d_0 + N^T K N d(t) \\ &\quad + \int_0^t N^T K B \theta(\tau) B^T K N d(t-\tau) d\tau, \end{aligned}$$

using integration by parts.

Since the function  $i\Omega$ , defined in (4.23), is zero for our definition of the observables, we finally end up with the evolution equations

$$\begin{aligned} \dot{\mathcal{P}} = (N^T M N) \ddot{d} &= - \int_0^t \gamma(\tau) \mathcal{P}(t-\tau) d\tau + f(t) \\ &= -N^T K N d - \int_0^t N^T K B \theta(\tau) B^T K N d(t-\tau) d\tau \quad (4.29) \\ &\quad - N^T K B \theta(t) B^T M B \dot{b}(0) - N^T K B \dot{\theta}(t) B^T M B b(0), \end{aligned}$$

which is exactly the same as in equations (4.10) - (4.14) if we do not split the displacement  $b$  into two parts.

Note, that the use of the term memory integral in the Mori-Zwanzig formalism differs from that used in previous subsections. There we used the expression only for the integral given by (4.29).

The derivation above is valid only for the case of a harmonic potential, since equation (4.26) is only valid if  $\mathcal{F}$  is a linear combination of positions and momenta. In the derivation in subsection 4.2, it was only necessary that the Hamiltonian is harmonic in the variables for which we want to derive the reflectionless boundary condition but not for the others. Furthermore, the derivation in section 4.2 is independent, whether we are in a equilibrium situation or not. In contrast to this, for the derivation with the Mori-Zwanzig projection operator formalism, we use the Mori scalar product which is only defined in equilibrium situations.

For the derivation of equations (4.10) - (4.14) in case of harmonic interaction from the Mori-Zwanzig formalism, define  $\mathcal{P} = (N^T p, B_1^T p)$  and the orthogonal variables as  $b_2$ .

## 4.6 Choosing the interpolation functions

So far, a coupling scheme was defined from a displacement splitting that allows to derive evolution equations together with reflectionless boundary conditions from the Lagrangian formulation. If it is used for the coupling of an atomistic and a coarse scale region, we get no reflections at the interface and the correct dispersion relation in the coarse scale region. However, solving the whole system (4.10) and (4.11), with exact calculation of the reflectionless boundary condition (4.12), is not cheaper than solving the whole atomistic system. Therefore, some approximations in the computation of the boundary condition are necessary.

For the evolution equations of the fine scale variables  $b_1$ , the influence of the reflectionless boundary condition is strong only near the interface, since the matrix  $B_1^T K B_2$  has only a few non-zero entries in the atomistic region, due to the local support of the interpolation functions. The boundary condition in this equations is necessary to suppress the reflection of waves with small wave length. Due to the local interaction, we can approximate the memory integral comparatively easy by integrating only over a small time interval or by neglecting the fine scale variables  $b_2$  with support more than a few nodes away from the interface. We study the error for such approximations together with the numerical error in chapter 5.

The situation becomes more complicated for the evolution equations of the coarse scale variables (4.10). The interaction between  $d$  and the fine scale variables  $b_2$  is the same everywhere in the coarse scale region. Approximations by neglecting most of the fine scale variables  $b_2$  are therefore not possible. Additionally, the decay of the corresponding entries in the memory kernel depends on the distance of the support of the interpolation function of a node from the support of the interpolation of a fine scale variable. The larger this distance, the later the memory kernel reaches its maximum value before decaying.

In the evolution equations of the coarse scale nodes, the reflectionless boundary condition is responsible for keeping the correct dispersion relation. Figure 4.6 shows on the left panel an example of the stress for  $\tilde{n} = 5$  (other parameters according to numerical example 1 in section 3.1) if the boundary condition is taken into account for both the fine scale (4.11), and the coarse scale evolution equations (4.10). The



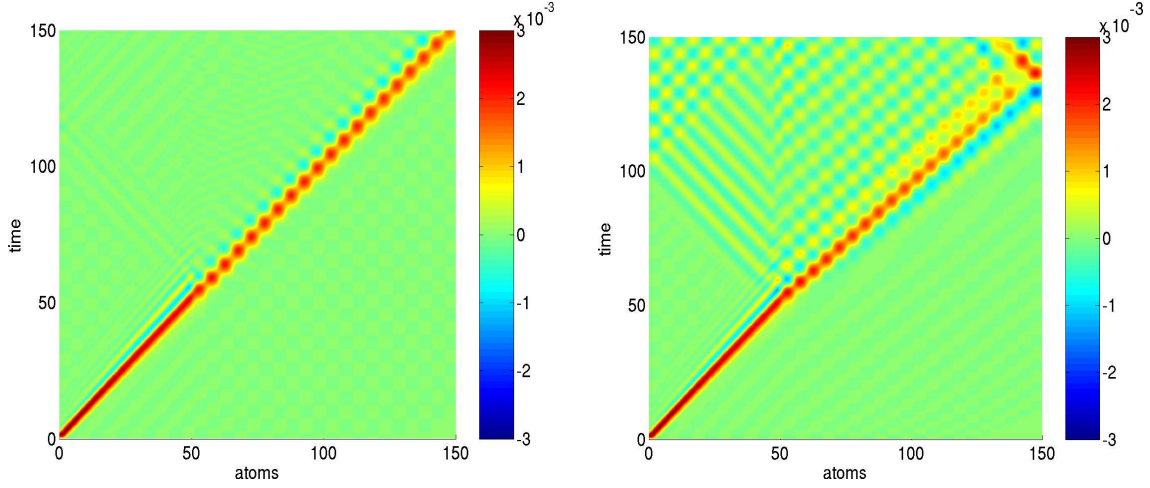


Figure 4.6: stress with and without boundary condition for equation (4.10) and interpolation with linear hat functions

dispersion relation in the coarse scale region is correct and we have nearly no reflection at the interface. On the right panel, the same example with boundary condition only for the fine scale part is shown. Now, the wave speed in the coarse scale region differs, since we get the wrong dispersion relation if we neglect the variables  $b_2$  in the equations. Additionally, we get reflections at each node. Since the total mass of the nodes in the coarse scale region is the same than the total mass of all atoms in this region whereas the wave speed is higher, we get a higher momentum. Due to the conservation of the overall momentum in a Hamiltonian system, part of the perturbation has to be reflected at the interface.

Of course, we cannot approximate the equations in the coarse scale region, keeping all the atomistic information, but the correct dispersion relation is what we require on the coarse scale. Therefore, we have to think of another possibility for conserving the dispersion relation, without the need of the reflectionless boundary condition. In section 3.1.2.1, we discussed already one possibility to correct the dispersion relation in the coarse scale region by changing the mass matrix. However, the resulting evolution equations cannot be derived from the Lagrangian. The only option that we still have in our coupling model, is a tuning of the interpolation functions from coarse to fine scale.

We explain now, how to choose the interpolation functions from coarse to fine scale in such a way that they provide already the correct dispersion relation, thus making the information in the boundary condition redundant for our application.

The new interpolation functions should fulfil the following conditions:

1. For  $M = mI$ , the interpolation function from each coarse scale node to the atoms should be symmetric to this node.
2. Partition of unity: the sum of all coarse scale interpolation weights at each atom should be one.

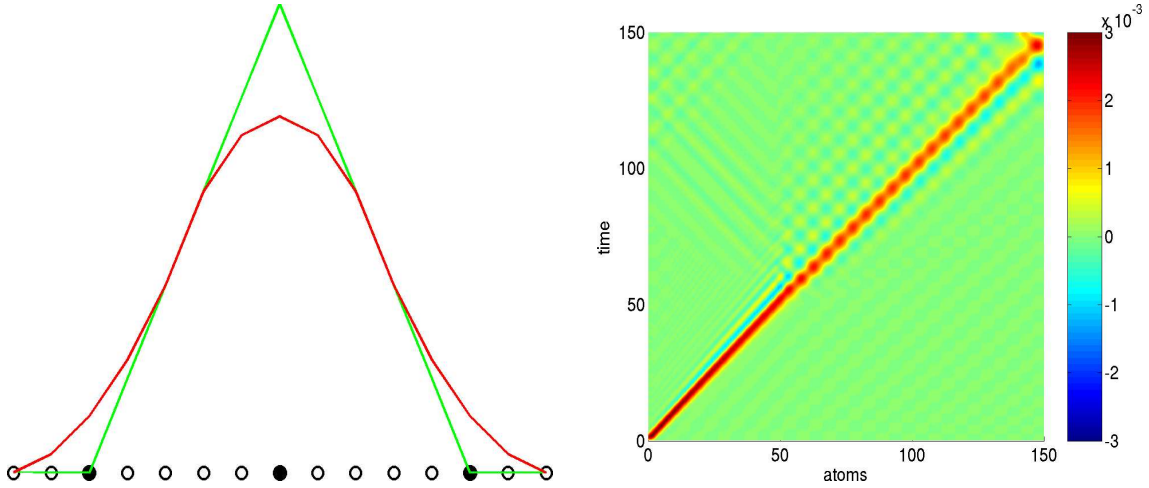


Figure 4.7: new interpolation function (red) compared to linear hat function (green) and stress with the new interpolation

3. The error in the dispersion relation of the coarse scale evolution equations, compared to the atomistic dispersion relation, should be as small as possible.
4. The interpolation from each coarse scale node to the atoms should be local, i.e. the interpolation weights are non-zero only in a small neighbourhood of each node.

Whereas the first and the second condition are general requirements, the third and the fourth condition are contradictory. To obtain the exact dispersion relation on the coarse scale, the projection from fine to coarse scale should provide a separation in fine and coarse scale wave length. However, such an interpolation would not be local anymore, hence leading to fully occupied matrices for the mass and the force calculation on both scales. This allows indeed a separation of fine and coarse scale displacements but no separation of the fine scale degrees of freedom in the atomistic and in the coarse scale region.

For linear finite element hat functions as interpolation functions, the error in the dispersion relation, between coarse scale and atomistic equations for a harmonic potential, was large for the largest wave vectors that can be represented on the coarse grid, (cf. figure 3.12). If we compute the Taylor expansion of both dispersion relations around  $\kappa = 0$ , the first term of both expansions is the same, since the limits  $\kappa \rightarrow 0$  are the same. We can start now with arbitrary interpolation weights that fulfil the first and second condition stated above and choose the weights in such a way that not only the first term is the same, but as many terms of the expansion as possible are the same. How many terms we can fit depends of course on the number of non-zero weights. We will show in chapter 5, that we get already quite good results, if the first two or three terms in the dispersion relation match. Of course, we can think of other criteria for better interpolation functions, e.g. the error for a special wave number can be reduced if this wave number is of special importance in the calculation.

In figure 4.7, we show an example for a new interpolation function (red) compared to the linear hat function (green) and the stress for the computation with this new interpolation. In the coarse scale region no reflectionless boundary condition was used. In contrast to the computation with linear hat functions in figure 4.6, the reflection at the interface is reduced, and also the wave speed in the coarse scale region is almost correct. The computation for this and other one dimensional new interpolation functions will be explained in chapter 5, and the corresponding dispersion relations are calculated. Two dimensional examples will be considered in chapter 6.

# Chapter 5

## Approximations and numerical results for one dimensional harmonic potentials

We concentrate in this chapter on the orthogonal displacement splitting for the coupling of an atomistic and a coarse scale region in one dimension in case of harmonic interaction with the same mass  $m$  and spring constant  $k$  for all atoms. In section 5.1, we construct a general procedure for computing interpolation weights with correct dispersion relation in the coarse scale region and give examples for this. One of the advantages of deriving the evolution equations for coarse and fine scale degrees of freedom from an orthogonal displacement splitting is, that we can make approximations directly in the Lagrangian and derive evolution equations that are still energy conserving. We will give some examples of such approximations in section 5.2. In section 5.3, we discuss numerical approximations for solving the system of equations by approximating the memory integral or using different time steps for the update of coarse and fine scale values. For the approximations of the memory kernel, we focus especially on the advantage of using coarse scale interpolation weights with correct dispersion relation. We show also results for the anharmonic example of section 3.2, computed with the orthogonal displacement splitting.

### 5.1 Computation of better interpolation weights

In section 4.6, we discussed the advantage of choosing the interpolation from the coarse scale in such a way that the error in the dispersion relation, compared to the fully atomistic system, is small. By choosing suitable coarse scale variables we get like this coarse scale equations that capture the essential atomistic features for our simulation and can therefore be used without the fine scale variables [66, 67]. Choosing the interpolation weights in such a way that some fine scale property is preserved is also used e.g. in multigrid simulations (e.g. cf. [13, 14, 15]).

We explain now for some examples, how we can compute interpolation weights that fulfil the requirements of section 4.6.

For linear finite element hat functions, the interpolation weights of each node are non-zero for the atom with equilibrium position at this node, as well as for the atoms in the two neighbouring elements. If we use a coarse scale node at the equilibrium position of every  $\tilde{n}$ th atom, we have  $2\tilde{n} - 1$  non-zero weights, and the evaluation of the linear hat functions at the equilibrium positions of the atoms gives already the best choice of the interpolation weights.

**Lemma 5.1** *For an interpolation with  $2\tilde{n} - 1$  non-zero weights, we cannot fit more than the first term in the coarse scale dispersion relation. This term is only the same as the corresponding atomistic value for interpolation with linear hat functions.*

**Proof:** With the requirement of symmetry to the weight in the center, we have  $\tilde{n}$  different weights which reduce to  $\lceil \frac{\tilde{n}-1}{2} \rceil$  independent weights with the partition of unity, according to section 4.6. In the following, we show for odd  $\tilde{n}$  that the best choice of these interpolation weights is according to linear hat functions, for even  $\tilde{n}$  the computation is similar. With the symmetry and the partition of unity, we get a vector of interpolation weights

$$N_i = [0, 1 - w_2, 1 - w_3, \dots, w_3, w_2, 1, w_2, w_3, \dots, 1 - w_3, 1 - w_2, 0]$$

for every node, from which we can compute the entries of the coarse scale mass matrix  $N^T M N$  and the coarse scale force matrix  $N^T K N$ . Both matrices are tridiagonal, and we denote the entries on the main diagonal with  $m_1$  and  $k_1$  respectively and that on the secondary diagonal with  $m_2$  and  $k_2$ . The values are related, since the sum of every row of the force matrix is zero, and the sum of every row of the mass matrix corresponds to the sum of all atomic masses in one element, i.e.

$$k_1 + 2k_2 = 0, \quad m_1 + 2m_2 = \tilde{n}m. \quad (5.1)$$

For the dispersion relation, we obtain for  $a_0 = 1$

$$\begin{aligned} \omega(\kappa) &= \sqrt{\frac{2k_2 \cos(\kappa \tilde{n}) + k_1}{2m_2 \cos(\kappa \tilde{n}) + m_1}} \\ &= \frac{1}{2} \sqrt{-2k_1 \tilde{n}} \kappa + \frac{1}{48} \sqrt{-2k_1 \tilde{n}} \tilde{n} (5\tilde{n} - 6m_1) \kappa^3 + \mathcal{O}(\kappa^5), \end{aligned}$$

where we used (5.1) and a Taylor expansion for the second equality. We show now, that choosing the weights according to linear hat functions is the only possibility to match the first term of the dispersion relation, i.e. that these are the only weights which fulfil

$$\begin{aligned} \frac{1}{2} \sqrt{-2k_1 \tilde{n}} - 1 &= 3 - \frac{1}{\tilde{n}} - 4w_2 - 4w_{(\tilde{n}+1)/2} - 4w_2 w_3 - 4w_3 w_4 - \dots \\ \dots - 4w_{(\tilde{n}-1)/2} w_{(\tilde{n}+1)/2} + 4w_2^2 + \dots + 4w_{(\tilde{n}-1)/2}^2 + 6w_{(\tilde{n}+1)/2}^2 &= 0. \end{aligned} \quad (5.2)$$

We show that for

$$w_2 = \frac{1}{\tilde{n}}, \quad w_3 = \frac{2}{\tilde{n}}, \quad \dots, \quad w_{(\tilde{n}+1)/2} = \frac{\tilde{n} - 1}{2\tilde{n}}, \quad (5.3)$$

the function

$$f(w_2, \dots, w_{(\tilde{n}+1)/2}) = 3 - \frac{1}{\tilde{n}} - 4w_2 - 4w_{(\tilde{n}+1)/2} - 4w_2w_3 - 4w_3w_4 - \dots \\ \dots - 4w_{(\tilde{n}-1)/2}w_{(\tilde{n}+1)/2} + 4w_2^2 + \dots + 4w_{(\tilde{n}-1)/2}^2 + 6w_{(\tilde{n}+1)/2}^2$$

has a global minimum. The only point where the gradient

$$\nabla f(w_2, \dots, w_{(\tilde{n}+1)/2}) = \begin{pmatrix} -4 - 4w_3 + 8w_2 \\ -4w_2 - 4w_4 + 8w_3 \\ -4w_3 - 4w_5 + 8w_4 \\ \vdots \\ -4w_{(\tilde{n}-3)/2} - 4w_{(\tilde{n}+1)/2} + 8w_{(\tilde{n}-1)/2} \\ -4 - 4w_{(\tilde{n}-1)/2} + 12w_{(\tilde{n}+1)/2} \end{pmatrix}$$

vanishes is given by (5.3). The Hessian  $H$  of this function,

$$H = \begin{pmatrix} 8 & -4 & 0 & \dots & \dots & 0 & 0 \\ -4 & 8 & -4 & 0 & & 0 & 0 \\ 0 & -4 & 8 & -4 & \ddots & 0 & 0 \\ \vdots & \ddots & \ddots & \ddots & \ddots & \ddots & \vdots \\ 0 & 0 & \ddots & -4 & 8 & -4 & 0 \\ 0 & 0 & \ddots & \ddots & -4 & 8 & -4 \\ 0 & 0 & \dots & \dots & 0 & -4 & 12 \end{pmatrix}.$$

is constant and positive definite. To prove the positive definiteness of  $H$ , we show that the determinant of every sub-matrix  $H_n = H(1 : n, 1 : n)$  is positive. This is true for  $n = 1$ . For  $n = 2, \dots, k - 1$ , with  $k \times k$  the size of  $H$  and  $|H_0| := 1$ , the determinant can be computed as

$$|H_n| = -16 |H_{n-2}| + 8 |H_{n-1}|.$$

This identity can be used recursively, to show that  $|H_n|$  is positive.

$$\begin{aligned} |H_{n-1}| &> 2 |H_{n-2}| =: x_{n-2} |H_{n-2}|, \\ \text{if } |H_{n-2}| &> \frac{16}{8-2} |H_{n-3}| =: x_{n-3} |H_{n-3}|, \\ \text{if } |H_{n-3}| &> x_{n-4} |H_{n-4}| \quad \dots \end{aligned} \tag{5.4}$$

with

$$x_{n-2} := 2, \quad x_k := \frac{16}{8 - x_{k+1}}, \quad k \in \{1, \dots, n-3\}.$$

The limit of this series is  $x_1 = 4$  for  $n \rightarrow \infty$ , and we have always  $x_k > x_{k+1}$ . Since  $|H_2| = 6|H_1|$ , the inequality (5.4) holds for all  $n$ . Due to  $|H| = |H_k| = -16|H_{k-2}| + 12|H_{k-1}| > -16|H_{k-2}| + 8|H_{k-1}| > 0$ , also the determinant of the whole matrix is positive.

Since the point given by (5.3) is the only minimum, it is a global one, and since  $f = 0$  in this point holds, choosing the interpolation weights on the linear hat functions is the only possibility to fulfil equation (5.2).  $\square$

Therefore, if we want to use an interpolation with better coarse scale dispersion relation, we need at least one more non-zero weight in each direction from the weight in the center. The easiest possibility to get such an interpolation, is to change the zero weights at the neighbouring nodes to a non-zero value. Due to the requirement of the partition of unity, we have to change also the weight 1 at the node itself. Instead of the interpolation weights of linear hat functions for each node,

$$N_{old} = \left[ 0, \frac{1}{\tilde{n}}, \frac{2}{\tilde{n}}, \dots, \frac{\tilde{n}-1}{\tilde{n}}, 1, \frac{\tilde{n}-1}{\tilde{n}}, \dots, \frac{2}{\tilde{n}}, \frac{1}{\tilde{n}}, 0 \right],$$

we use

$$N_{new} = \left[ \tilde{x}, \frac{1}{\tilde{n}}, \frac{2}{\tilde{n}}, \dots, \frac{\tilde{n}-1}{\tilde{n}}, x, \frac{\tilde{n}-1}{\tilde{n}}, \dots, \frac{2}{\tilde{n}}, \frac{1}{\tilde{n}}, \tilde{x} \right], \quad \text{with } 2\tilde{x} + x = 1,$$

where we have to find a better value than 1 for the parameter  $x$ . For an arbitrary value of  $x$ , we obtain the entries of the coarse scale mass matrix,

$$\begin{aligned} m_1(x) &= \frac{3}{2}x^2 - x - \frac{1}{2} + \frac{2\tilde{n}}{3} + \frac{1}{3\tilde{n}}, \\ m_2(x) &= x - x^2 + \frac{\tilde{n}}{6} - \frac{1}{6\tilde{n}}, \\ m_3(x) &= \frac{1}{4} - \frac{1}{2}x + \frac{1}{4}x^2, \end{aligned}$$

and of the coarse scale force matrix,

$$\begin{aligned} k_1(x) &= -3x^2 + 6x - \frac{6x}{\tilde{n}} - 3 + \frac{4}{\tilde{n}}, \\ k_2(x) &= 2x^2 - 4x + \frac{4x}{\tilde{n}} + 2 - \frac{3}{\tilde{n}}, \\ k_3(x) &= -\frac{x^2}{2} + x - \frac{x}{\tilde{n}} + \frac{1}{\tilde{n}} - \frac{1}{2}, \end{aligned}$$

where  $m_1$  and  $k_1$  denote the values of the main diagonal of the matrices, the other values that of the secondary diagonals. For the coarse scale dispersion relation for  $a_0 = 1$  it follows

$$\begin{aligned} \omega(\kappa) &= \left( -\frac{2k_3 \cos(2\kappa\tilde{n}) + 2k_2 \cos(\kappa\tilde{n}) + k_1}{2m_3 \cos(2\kappa\tilde{n}) + 2m_2 \cos(\kappa\tilde{n}) + m_1} \right)^{1/2} \\ &= \kappa + \left( \left( \frac{1}{4}x^2 - \frac{1}{2}x + \frac{1}{4} \right) \tilde{n}^3 + \left( \frac{1}{2}x - \frac{11}{24} \right) \tilde{n}^2 + \left( \frac{1}{2} - \frac{1}{2}x \right) \tilde{n} - \frac{1}{12} \right) \kappa^3 \\ &\quad + \mathcal{O}(\kappa^5). \end{aligned}$$

The first term in the expansion does not depend on  $x$ . To find  $x$  with the least square error in the second term of the dispersion relation, we compare it with the corresponding term of the Taylor expansion of the atomistic dispersion relation,

$$\omega(\kappa) = \kappa - \frac{1}{24}\kappa^3 + \mathcal{O}(\kappa^5).$$

We minimize the squared error, i.e.

$$\left( \frac{1}{4}\tilde{n}^3x^2 - \frac{1}{2}\tilde{n}^3x + \frac{1}{2}\tilde{n}^2x - \frac{11}{24}\tilde{n}^2 + \frac{1}{4}\tilde{n}^3 - \frac{1}{2}x\tilde{n} + \frac{1}{2}\tilde{n} - \frac{1}{24} \right)^2 \mapsto \min$$

and obtain

$$x = 1 - \frac{1}{\tilde{n}} + \frac{1}{\tilde{n}^2}.$$

In this case, the quadratic error for the second coefficient is given by

$$\left( \frac{1}{24}\tilde{n}^2 - \frac{1}{4}\tilde{n} + \frac{11}{24} - \frac{1}{4\tilde{n}} \right)^2,$$

compared to

$$\left( \frac{1}{24}\tilde{n}^2 - \frac{1}{24} \right)^2$$

for the linear hat function, i.e. for  $x = 1$ . Since

$$\begin{aligned} & \left( \frac{1}{24}\tilde{n}^2 - \frac{1}{4}\tilde{n} + \frac{11}{24} - \frac{1}{4\tilde{n}} \right)^2 - \left( \frac{1}{24}\tilde{n}^2 - \frac{1}{24} \right)^2 \\ &= -3(\tilde{n} - 1)^3(\tilde{n}^2 - 2\tilde{n} + 3) \leq 0, \end{aligned}$$

where the upper bound 0 is reached only for  $\tilde{n} = 1$ , the error is always reduced, although the second term of the dispersion relation is correct only for  $\tilde{n} \leq 3$ . However, this gives us the possibility to obtain a better interpolation, just by changing the interpolation weights at the coarse scale nodes.

We give now two examples, how to compute interpolation weights, which match the second term or higher order terms in the dispersion relation for an arbitrary value of  $\tilde{n}$ .

First, we consider the case  $\tilde{n} = 5$  and two additional non-zero weights in every direction compared to linear hat functions [66]. On the left panel of figure 5.1, the linear hat function is shown for this example (green) with 9 non-zero weights and the new interpolation function with 13 non-zero weights (red). Due to the required symmetry, we have to determine 7 different weights. We denote them by  $w_i$ ,  $i = 1, \dots, 7$ , with  $w_1$  the value of the interpolation function in the center, i.e. the maximum in figure 5.1.

From the requirement that the sum of all weights for each atom should be unity, we get the following linear system of equations,

$$\begin{aligned} w_1 &= 1 - 2w_6, \\ w_2 &= 1 - w_5 - w_7, \\ w_3 &= 1 - w_4. \end{aligned}$$

The four free parameters left,  $w_4 - w_7$ , are now calculated from the dispersion relation of the coarse scale equations, using this new interpolation weights. The first term of the expansion of the coarse scale dispersion relation is

$$\sqrt{30w_4^2 + 20w_5^2 + 20w_7^2 - 20w_4 - 20w_4w_5 + 20w_4w_7 - 40w_5w_7 + 5} \kappa.$$



To match the first term of the atomistic dispersion relation, this coefficient should be one. Additionally, the weights should all be real, which implies

$$w_4 = \frac{2}{5}, \quad w_5 = \frac{1}{5} + w_7.$$

Taking this results into account for the calculation of the second term of the Taylor expansion of the coarse scale dispersion relation, this term simplifies to

$$\left(125w_6^2 + 250w_7^2 - 270w_6w_7 - 20w_6 + 10w_7 + \frac{23}{24}\right) \kappa^3.$$

If we require that this term matches also the atomistic dispersion relation and that again all weights are real, we finally get

$$w_6 = \frac{3}{25}, \quad w_7 = \frac{1}{25},$$

i.e. the new vector of interpolation weights

$$N_1 = \frac{1}{25} [0, 1, 3, 6, 10, 15, 18, 19, 18, 15, 10, 6, 3, 1, 0]. \quad (5.5)$$

If we take again two additional interpolation weights in each direction, we can choose weights which match also the third term in the dispersion relation, this leads to

$$N_2 = \frac{1}{125} [0, 1, 4, 10, 20, 35, 52, 68, 80, 85, 80, 68, 52, 35, 20, 10, 4, 1, 0]. \quad (5.6)$$

Both new interpolation functions are shown on the left panel of figure 5.1, where  $N_1$  is marked in red and  $N_2$  in blue. On the right panel of the figure, the corresponding dispersion relations are shown together with that of the atomistic system (black) and that of the linear hat functions (green). The error is drastically reduced with the new interpolation functions, from maximum 17.60% to maximum 6.49% with  $N_1$  and 3.22% with  $N_2$  respectively, and we get the maximum error always for the second largest wave number. We used Maple 10 for the computation of dispersion relations and interpolation weights above.

Thus, the computation of new interpolation weights divides into the following steps:

1. Determine the number of independent weights from the requirements of symmetry and partition of unity.
2. Compute the entries of the coarse scale mass  $N^T M N$  and force matrix  $N^T K N$ .
3. Compute the dispersion relation from the entries of the mass and force matrix.
4. Expand the dispersion relation around  $\kappa = 0$  and compare the coefficients with that of the fully atomistic case.

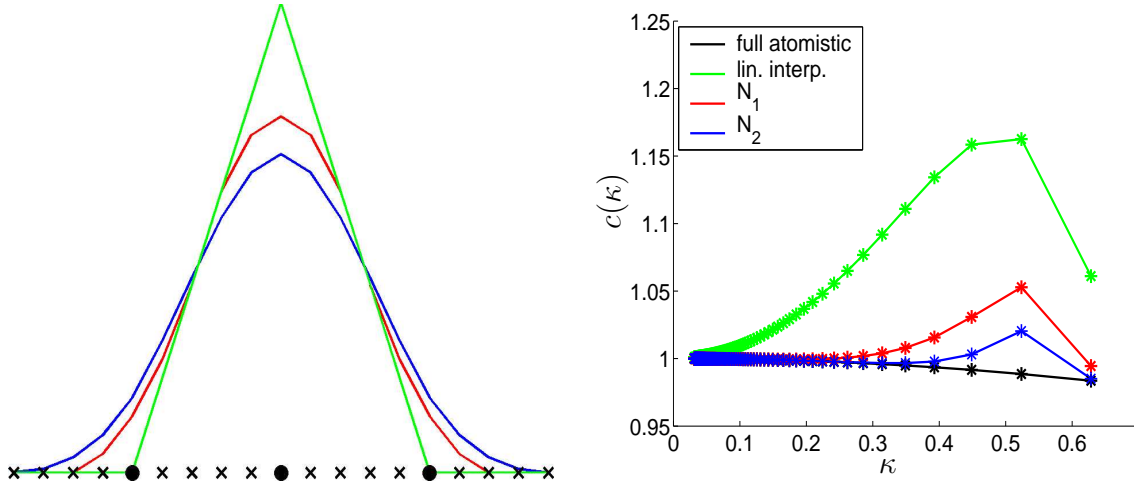


Figure 5.1: new interpolation weights (a) and dispersion relation (b)

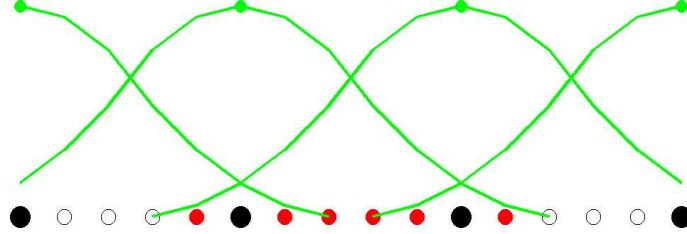


Figure 5.2: new interpolation functions (green) and atoms with non-zero entries of the fine scale interpolation (red) for fine scale variables in the element in the middle

Of course, we can think of other criteria to compare the atomistic and coarse scale dispersion relation. We can e.g. minimize the error with respect to a special wave number if this one is of special importance in the simulation.

Since the new interpolation functions do not end at a node, the interpolation weights at the boundary of the domain have to be changed, to guarantee the partition of unity everywhere. This can be done by changing only the values of the interpolation weights of the nodes directly at the boundary in such a way that the sum of all weights of each atom in the last elements is one.

If new interpolation functions are used, we also need appropriate interpolation weights for the fine scale variables  $b$ . The first question is, how many non-zero entries of the matrix  $B$  are necessary for the fine scale variables between two coarse scale nodes. This number depends on the number of non-zero coarse scale interpolation functions in each element. We denote this number by  $\hat{m}$ . Figure 5.2 shows an example with  $\hat{m} = 4$  for the interpolation weights  $N_1$  from (5.5). To get  $\tilde{n} - 1$  vectors of interpolation weights from the fine scale variables that are orthogonal to the  $\hat{m}$  non-zero vectors of  $N$  we need  $\tilde{n} - 1 + \hat{m}$  entries. For the example in figure 5.2, we choose the entries of the atoms marked red for the fine scale variables

of the element in the middle. We can choose them e.g. as

$$B = \begin{pmatrix} -1/6 & 0 & 0 & 0 \\ 0 & 1/3 & 0 & 0 \\ 1 & -1 & 0 & 0 \\ -4/3 & 1 & -1/3 & 1/2 \\ 1/2 & -1/3 & 1 & -4/3 \\ 0 & 0 & -1 & 1 \\ 0 & 0 & 1/3 & 0 \\ 0 & 0 & 0 & -1/6 \end{pmatrix}$$

or every arbitrary linear combination of this vectors.

**Discretisation in time** So far, we considered the computation of new interpolation weights for the time continuous system. If the first  $l$  terms of the coarse scale dispersion relation are correct, this is also true for the time discretised system with the same time step for coarse and atomistic system.

In the coupling of length scales approximation, the dispersion relation in the coarse scale region could be improved by choosing another time step. Therefore, the question arises, if we can use the coarse scale time discretisation  $\Delta T$  as an extra parameter to get better interpolation weights, i.e. if we can obtain a better dispersion relation with the same number of non-zero weights, by choosing an appropriate time step. Or if we can choose the interpolation weights in such a way that the dispersion relation is correct for large  $\Delta T$  compared to the atomistic time step.

Unfortunately, first attempts for the given examples showed that the extra parameter  $\Delta T$  cannot be used, since the interpolation weights depend on the atomistic time step, and we obtain real values only for  $\Delta T = \Delta t$ . In that case the values are equivalent to the weights for the time continuous case. To get interpolation weights that can be used for larger time steps in the coarse scale region, the requirement of fitting the first terms in the expansion of the dispersion relation should therefore be changed.

Nevertheless, if we use the interpolation weights optimized for the time continuous case and use a larger time step in the coarse scale region, the error compared to linear hat functions is reduced anyway, as shown in figure 5.3. It is therefore reasonable to use the new interpolation functions also for  $\Delta T > \Delta t$ , even if we still have some error in the dispersion relation.

## 5.2 Approximations in the Lagrangian for harmonic potential

In this section, we analyse the effect of several approximations in the Lagrangian for the coupling example with harmonic interaction which lead always to energy conserving evolution equations. We compare again the stress and energy for a fully atomistic simulation of the first numerical example of chapter 3 with that of the

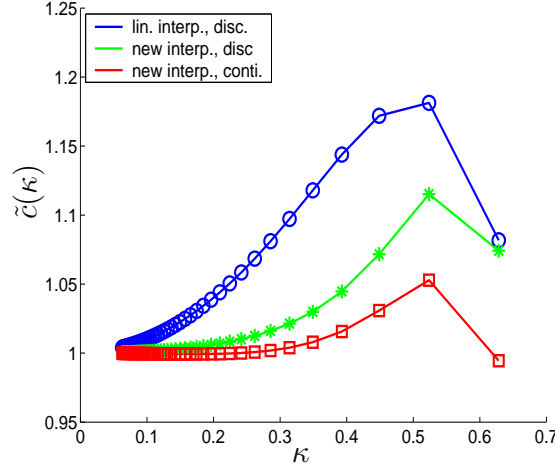


Figure 5.3: dispersion relation for time discretised system ( $\Delta T = 10\Delta t$ ) for linear hat functions (blue) and new interpolation weights  $N_1$  (green) compared to  $N_1$  for the time continuous case (red)

approximations. The only difference to chapter 3 is, that we use here  $\tilde{n} = 5$  and compute always the energy of the first 50 atoms. Like in the previous chapters, the red line in the energy plots is the kinetic energy, the blue line the potential energy and the green line the sum of both.

**1. Omit fine scale degrees of freedom in one part of the domain** The first approximation we can make, is to omit one part of the fine scale variables, i.e. for our coupling example, we omit the variables  $b_2$ . We get the Lagrangian

$$\mathcal{L} = \frac{1}{2}(\dot{d}^T N^T M N \dot{d} + \dot{b}_1^T B_1^T M B_1 \dot{b}_1) - \frac{1}{2}(Nd + B_1 b_1)^T K (Nd + B_1 b_1)$$

and the evolution equations

$$\begin{aligned} N^T M N \ddot{d} &= -N^T K (Nd + B_1 b_1), \\ B_1^T M B_1 \ddot{b}_1 &= -B_1^T K (Nd + B_1 b_1). \end{aligned}$$

Without reflectionless boundary condition, the fine scale part of the perturbation is of course reflected at the interface, but the energy of the variables  $d$  and  $b_1$  is constant over time. Whether the wave speed in the coarse scale region is correct, depends on the choice of the interpolation function. For the interpolation weights (5.5), stress and energy of the variables  $d$  and  $b_1$  are shown in figure 5.4. Again, we have no visible error compared to the fully atomistic solution (cf. left panel of figure 3.1) before the perturbation reaches the interface. The situation differs in the bridging scales approximation. As can be seen in figure 5.5, we have also reflection of one part of the perturbation, however the system is not energy conserving, and we have an error in the stress already before the perturbation reaches the interface. Additionally, we get a modified perturbation in the real atoms after the reflection,

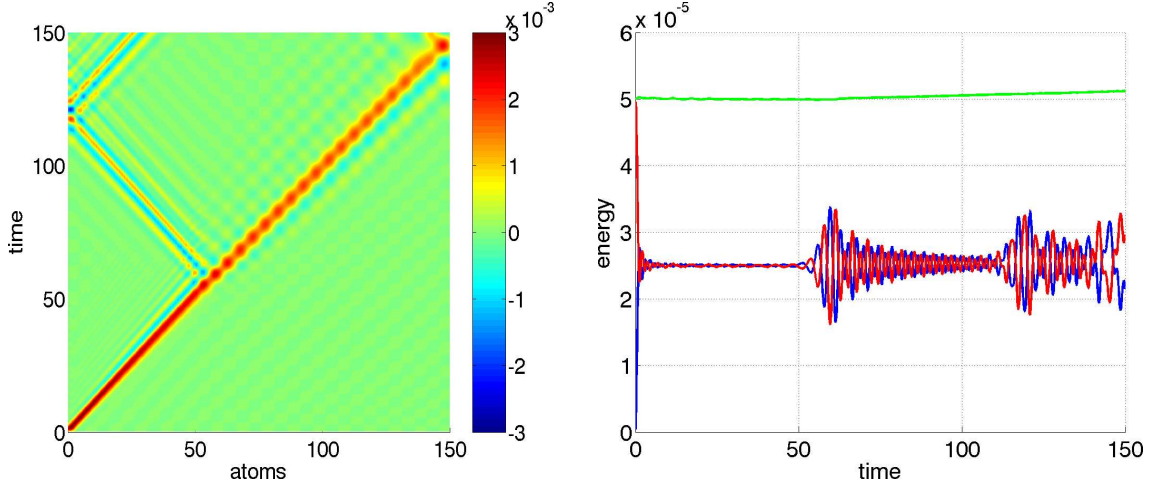


Figure 5.4: first approximation, omitting the variables  $b_2$  for orthogonal displacement splitting, stress (left) and energy of the variables  $d$  and  $b_1$  (right)

and the velocity of the perturbation is wrong in the coarse scale region, since we use linear hat functions for the interpolation.

In figure 5.6, we compare for both methods the energy of the first 50 real atoms with the fully atomistic simulation (blue). For the orthogonal displacement splitting (red), the energy is correct till the perturbation reaches the interface, whereas in the bridging scales approximation (green) we observe some earlier deviations. Contrary to this, the amount of energy that cannot pass the interface is a bit larger for the orthogonal displacement splitting.

**2. Omit coupling of coarse scale degrees of freedom  $d$  and fine scale variables  $b_2$**  Another approximation in the Lagrangian is to omit the interaction between the fine scale variables  $b_2$  and  $d$ . This interaction is the same for the whole coarse scale region. In contrast to this, the coupling of  $b_1$  and  $b_2$  gets weaker if we go away from the interface, and we can therefore approximate the memory integral by integrating not over the whole but a small time interval, thereby reducing the computational effort drastically. We study this numerical approximation in the next section. Here, we show the importance of interpolation weights with correct dispersion relation for this approximation. The Lagrangian is

$$\begin{aligned} \mathcal{L} = & \frac{1}{2}(\dot{d}^T N^T M N \dot{d} + \dot{b}_1^T B_1^T M B_1 \dot{b}_1 + \dot{b}_2^T B_2^T M B_2 \dot{b}_2) \\ & - \frac{1}{2}(N d + B_1 b_1)^T K (N d + B_1 b_1) - \frac{1}{2}(B_2 b_2)^T K (B_2 b_2) - (B_1 b_1)^T K (B_2 b_2), \end{aligned}$$

and the evolution equations are

$$\begin{aligned} N^T M N \ddot{d} &= -N^T K (N d + B_1 b_1), \\ B_1^T M B_1 \ddot{b}_1 &= -B_1^T K (N d + B_1 b_1 + B_2 b_2). \end{aligned}$$

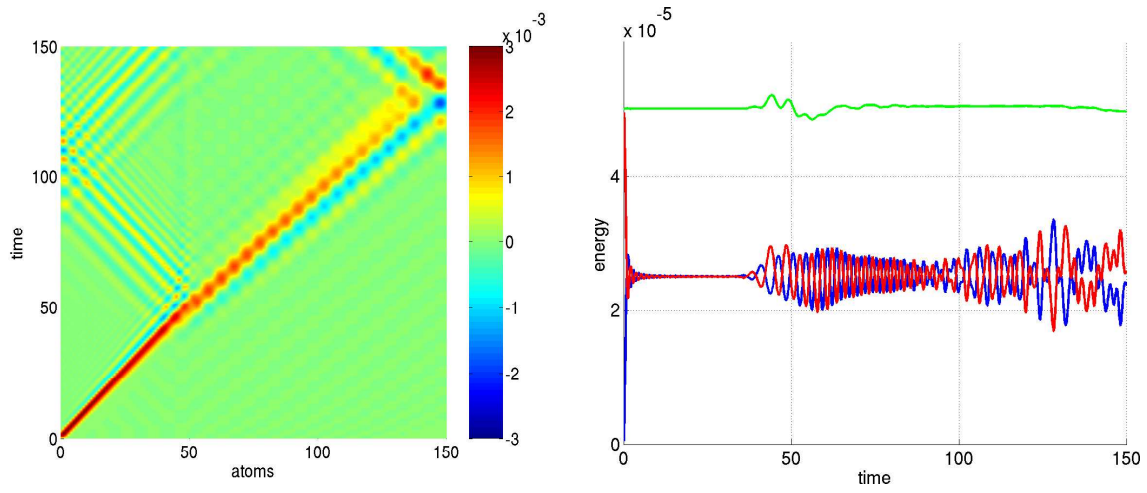


Figure 5.5: first approximation, omitting the variables  $b_2$  for the bridging scales approximation

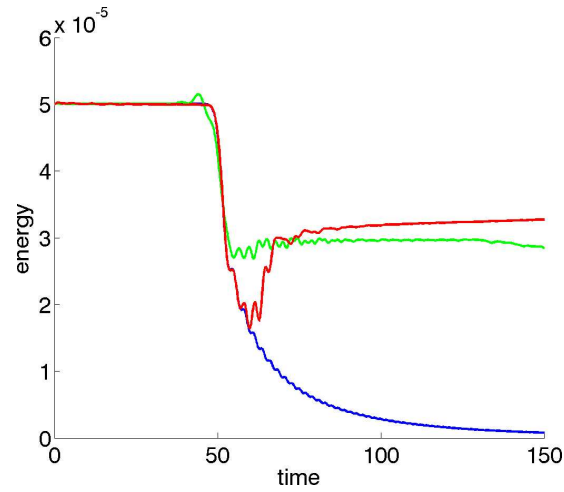


Figure 5.6: first approximation: energy in atomistic region for fully atomistic simulation (blue), orthogonal displacement splitting (red) and bridging scales approximation (green)

In the memory integral for the reflectionless boundary condition (4.12), we just have to omit the term  $Nd(t - \tau)$ . In figure 5.7, we see the stress and energy for this approximation for interpolation with linear hat functions (a) and the interpolation weights  $N_1$  (b). The difference in the error of the energy of the real atoms (c) at the end of the simulation is reduced from 6.42% to 2.03% by using the new interpolation. However, more important is, that the error in the wave speed in the coarse scale region is reduced. And, in contrast to using the whole Lagrangian (4.9) and neglecting the reflectionless boundary condition in the coarse scale evolution equations (4.10), this approximation is energy conserving.

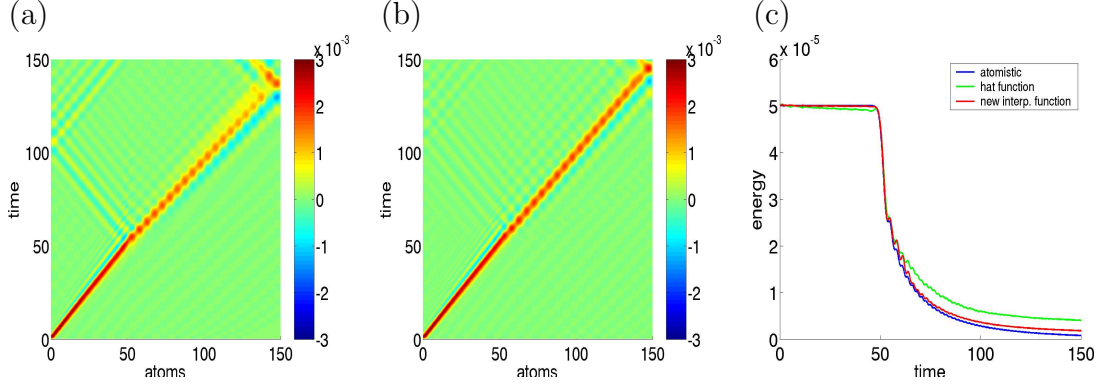


Figure 5.7: second approximation: stress for old (a) and new (b) interpolation function and energy compared to fully atomistic simulation (c)

**3. Truncation of matrix  $B_2$**  The last approximation in the Lagrangian which we want to consider, is neglecting not all fine scale variables  $b_2$  but only those with support of the interpolation function more than a few nodes away from the interface. For the remaining variables  $\tilde{b}_2$ , we keep the interaction with  $d$  and  $b_1$ . The corresponding interpolation matrix  $\tilde{B}_2$  is zero for the neglected variables. With the Lagrangian

$$\begin{aligned} \mathcal{L} = & \frac{1}{2}(\dot{d}^T N^T M N \dot{d} + \dot{b}_1^T B_1^T M B_1 \dot{b}_1 + \dot{\tilde{b}}_2^T \tilde{B}_2^T M \tilde{B}_2 \dot{\tilde{b}}_2) \\ & - \frac{1}{2}(Nd + B_1 b_1 + \tilde{B}_2 \tilde{b}_2)^T K (Nd + B_1 b_1 + \tilde{B}_2 \tilde{b}_2) \end{aligned}$$

and the evolution equations

$$\begin{aligned} N^T M N \ddot{d} &= -N^T K (Nd + B_1 b_1 + \tilde{B}_2 \tilde{b}_2), \\ B_1^T M B_1 \ddot{b}_1 &= -B_1^T K (Nd + B_1 b_1 + \tilde{B}_2 \tilde{b}_2), \\ \tilde{B}_2^T M \tilde{B}_2 \ddot{\tilde{b}}_2 &= -\tilde{B}_2^T K (Nd + B_1 b_1 + \tilde{B}_2 \tilde{b}_2), \end{aligned}$$

we obtain an energy conserving system if we ensure that  $B_1^T M \tilde{B}_2 = 0$  and  $\tilde{B}_2^T M (B_2 - \tilde{B}_2) = 0$ . In figure 5.8, we show an example for which we kept only the fine scale variables of the first five elements after the interface. In this case we do not get

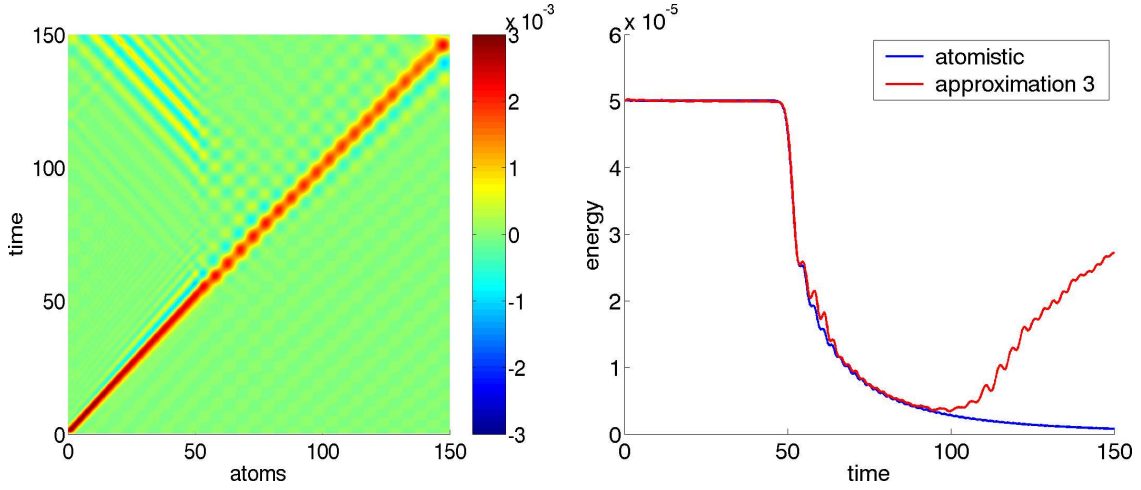


Figure 5.8: third approximation: stress (left) and energy of the real atoms compared to that of the fully atomistic system (right)

reflections directly at the interface, but at the end of the fine scale variables  $\tilde{b}_2$ , as can be seen on the left panel. On the right panel, we see the energy of the real atoms for this approximation (red) compared to that of a fully atomistic simulation (blue). Before we get reflections, both energies are nearly the same, but then the error increases strongly. In the next section, we show that combining the third approximation with a numerical approximation of the memory integral, we can use this approximation to reduce the simulation time significantly by increasing the error only slightly compared to a simulation with all variables  $b_2$ .

### 5.3 Numerical computation of memory integral and other numerical errors

The evolution equations of the coarse and fine scale variables, (4.10) and (4.11), are exact for harmonic potentials. However, we cannot solve the whole system of equations numerically, since the computational effort would be higher than solving the whole atomistic system, due to the necessary evaluation of the integral for the reflectionless boundary condition. In the previous section, we discussed some examples of possible approximations in the Lagrangian and the importance of the choice of the interpolation weights for this approximations. E.g. in the second approximation, we neglect the coupling between the variables  $d$  and  $b_2$ . This is only reasonable if we can also approximate the memory integral,

$$\int_0^t \theta(\tau) B_2^T K B_1 b_1(t - \tau) d\tau, \quad (5.7)$$

by an integral over a small time interval  $[0, t_I]$ . Like this, after the time  $t_I$  all necessary entries of  $\theta(t)$  are known, and no further evaluation of the function



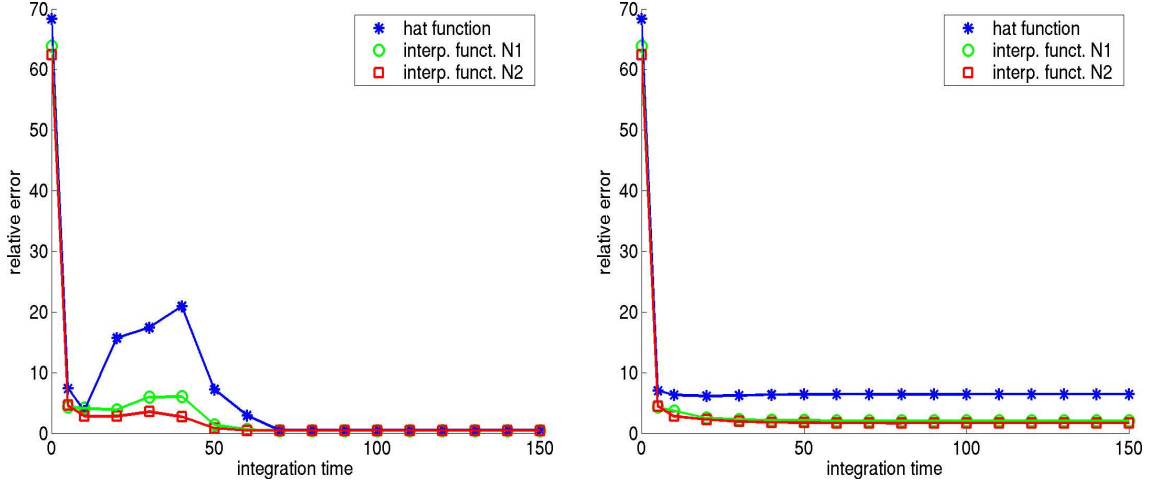


Figure 5.9: relative error in percent for different integration times of the memory integral, for reflectionless boundary condition for  $b_1$  and  $d$  (left) and for  $b_1$  (right)

is required. Otherwise, this approximation does not reduce the computational costs, since the computation of the memory integral makes the reflectionless boundary condition very time consuming. If we integrate over  $\theta(\tau)B_2^TKB_1b_1(t-\tau)$  or  $\theta(\tau)B_2^TK(Nd+B_1b_1)(t-\tau)$  is not that important in terms of computational costs.

In figure 5.9, we compare the relative error for different integration times  $t_I$ . On the left panel, we consider the system with reflectionless boundary condition for  $d$  and  $b_1$  and on the right panel the system with boundary condition only for  $b_1$  and the memory integral (5.7), both for  $\tilde{n} = 5$ . Parameters and initial conditions are chosen like in the first numerical example of chapter 3. We define the relative error by

$$\epsilon_r := \frac{E_{\text{end}} - E_{\text{ref,end}}}{E_0},$$

with  $E_{\text{end}}$  denoting the energy of the real atoms at the end of the simulation,  $E_{\text{ref,end}}$  the energy of the real atoms at the end of a fully atomistic simulation and  $E_0$  the initial energy. The figures in this chapter show this relative error in percent for a simulation over 1500 time steps  $\Delta t = 0.1$ .

In both panels of figure 5.9, we see that the error, compared to a simulation without boundary condition ( $t_I = 0$ ), is already drastically reduced for  $t_I = 5$ , i.e. for taking always the information of the last 50 time steps into account. If we keep the coupling between  $d$  and  $b_2$  (left panel), the error is first reduced, increases again, before decaying to less than 1% as the integration time increases. The reason can be seen in figure 5.10. The perturbation is now not reflected at the interface but at the first nodes that do not get the information of the fine scale displacements if we cut the integration time, since the dispersion relation of the system is changing there. This explains also the error reduction for longer integration. In this case, reflection occurs at nodes farer away from the interface, and the reflected perturbation does not reach the region of the real atoms again within our simulation time.

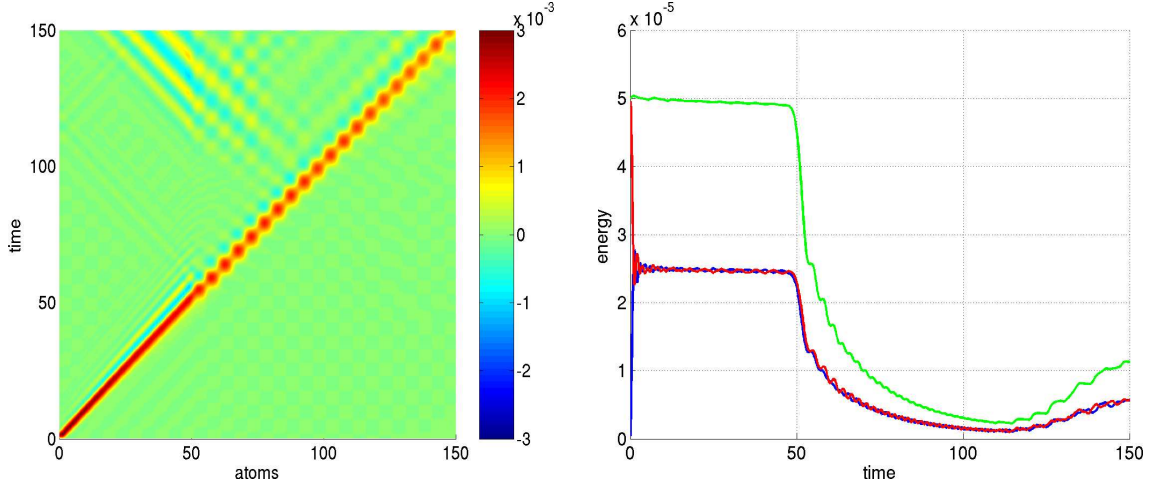


Figure 5.10: stress and energy for integration of the memory integral with  $t_I = 40$  using linear hat functions for interpolation

Therefore, the integration should be carried out for at least half of the time from the moment the perturbation reaches the interface till the end of the simulation. The general behaviour is the same for interpolation with linear hat functions and the new interpolation weights  $N_1$ , given by (5.5), and  $N_2$  according to (5.6). However, the maximum error gets smaller the better the new interpolation function is, since the change in the dispersion relation gets smaller.

For the second approximation, with boundary condition for  $b_1$ , the error reduction for integration over 50 time steps is nearly the same as with the boundary condition for  $d$  and  $b_1$ . The error is reduced further by longer integration and is nearly constant for  $t_I > 30$ . This is due to the fact that for this approximation the dispersion relation does not change in the coarse scale region. It changes at the interface, since without boundary condition for  $d$  we do not get the correct wave speed in the coarse scale region, but this reflection is not affected by the integration time. The fact that this reflection is much smaller for the new interpolation functions ( $\approx 2.07\%$  for  $N_1$ ,  $\approx 1.65\%$  for  $N_2$ ) as for linear hat functions ( $\approx 6.42\%$ ) shows that it depends indeed on the correctness of the dispersion relation. Therefore, choosing better interpolation functions is very important for this approximation. This behaviour of the error can also be seen for the simulation without reflectionless boundary condition. The difference in the error between linear hat functions and interpolation weights  $N_1$  for  $t_I = 0$  is 4.52%, compared to 4.35% for longer integration times. This shows also that this error does not depend on the memory integral but only on the dispersion relation in the coarse scale region. However, the large error reduction by integrating over a small time interval, instead of using no boundary condition at all, is due to the strong interaction between  $b_1$  and  $b_2$  near the interface, the corresponding entries of the memory kernel decay very fast.

In figure 5.11, we show the first entries of the memory kernel  $\theta(t)$  for interpolation with linear hat functions (left panel) and the interpolation weight  $N_1$  (right panel). The decay of the kernel depends on the interpolation, but both have in common,

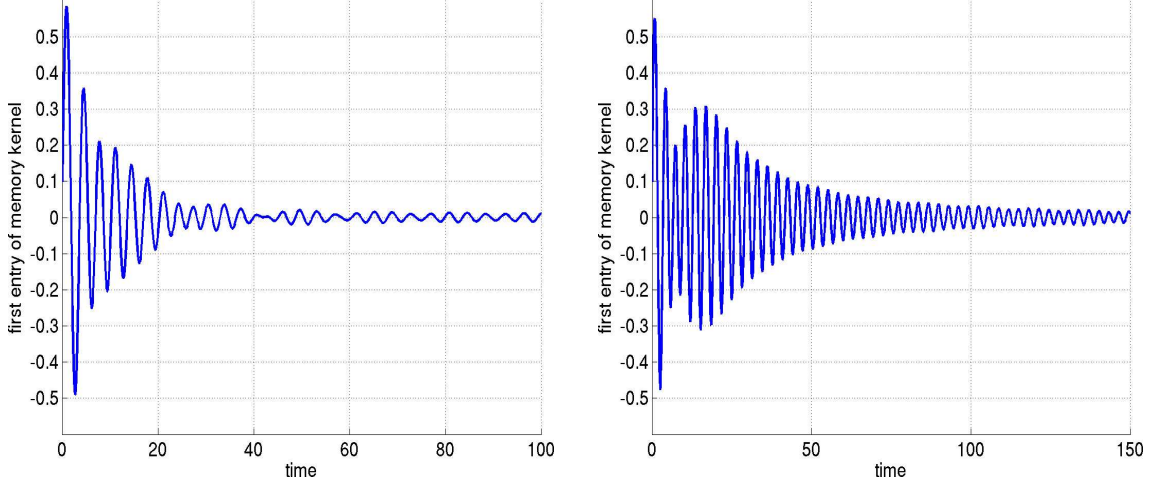


Figure 5.11: first entry of the memory kernel matrix over time for linear hat functions (left) and new interpolation function (right) for  $\tilde{n} = 5$

that they oscillate around some constant value after a while.

The integrals above were computed numerically with the trapezoidal rule

$$\int_0^{t_I} f(x) \approx \Delta t \left( \frac{y_0}{2} + y_1 + y_2 + \cdots + y_{n-1} + \frac{y_n}{2} \right), \quad y_i = f(t_i), \quad t_i = i\Delta t,$$

with quadratic error  $\mathcal{O}(\Delta t^2)$ . Since the memory integral is used in the force calculation, i.e. for the acceleration update, which is only second order accurate in the velocity Verlet algorithm (cf. section 1.4), a higher accuracy in the integration does not pay off. However the absolute error can be smaller for a higher order integration rule.

For the third approximation approach in the previous chapter, with only some of the fine scale degrees of freedom  $b_2$ , we found, that the very accurate solution at the beginning gets worse the longer we run the simulation. The perturbation is reflected at the node where we cut the fine scale variables  $b_2$ , since again the dispersion relation is changing there. We can correct this error, by integrating the memory integral again not over the whole but only a small time interval. This should be long enough, that the perturbation can leave the atomistic region, but not long enough, that it is reflected at the end of the fine scale variables and reaches the atomistic region again. The error for this approximation depends therefore strongly on the integration time  $t_I$ , as can be seen in figure 5.12. We used again the entries of  $b_2$  of the five elements directly on the right of the interface. If the integration interval is too long, we get huge errors. Nearly the whole perturbation is then reflected back into the atomistic region. The reflection depends on the interpolation, but the error for a long integration is nearly the same for all interpolation functions, since for this approximation we compute the memory integral from  $b_1$  and  $d$ .

Next, we want to consider, if the error behaviour for the second approximation depends on the initial perturbation. So far, only the first atom got a high initial momentum, now we compare this results with that for two to five atoms with initial

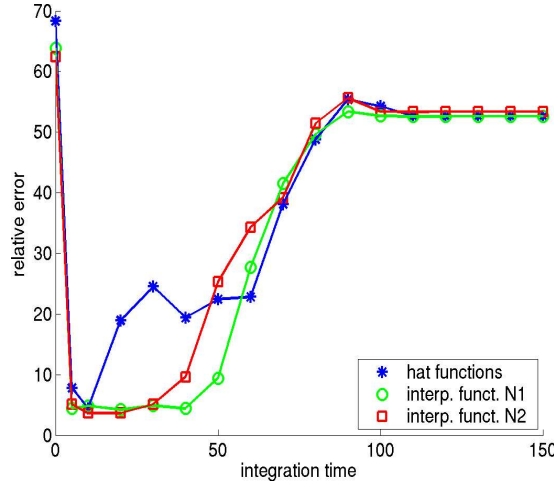


Figure 5.12: relative error for different integration times of the memory integral for third approximation approach given in section 5.2

b.c. for $d$ and $b_1$	b.c. for $b_1$	approx. in $B_2$	$t_I$	CPU time	rel. error
x	x	-	150	730	0.44%
x	x	-	60	377	0.59%
-	x	-	20	143	2.50%
x	-	x	20	19	4.21%
-	x	x	20	19	2.33%
-	-	-	0	9	63.83%

Table 5.1: CPU times for different boundary conditions and different integration times in the memory integral

momentum  $p_i(0) = 0.01$ . The results are shown in figure 5.13. The behaviour is in principle the same for all initial perturbations, but the error gets smaller the more atoms with initial momentum we have, since we have then initially more energy in the coarse scale degrees of freedom. Without boundary condition, i.e. for  $t_I = 0$ , the reflection at the interface is therefore reduced. Also with reflectionless boundary condition the error is smaller, since the boundary condition has to deal only with the, now smaller, fine scale part of the perturbation. Since the general behaviour of the error is the same, we can use the second approximation also for other initial conditions, and it is always enough to integrate over  $t_I$  between 20 or 30. If we consider systems with different atomic mass  $m$  and spring constant  $k$ , we get always a minimal error if we integrate the memory integral for the second approximation over  $t_I$  between  $20\sqrt{m/k}$  and  $30\sqrt{m/k}$ .

We compare now the computation times for computing the boundary condition for  $b_1$  and  $d$  over the whole simulation time, only over 600 time steps (i.e.  $t_I = 60$ ) and for the second and third approximation with integration over 200 time steps (i.e.  $t_I = 20$ ) in table 5.1. We see that we can reduce the effort significantly if we allow a little error in the energy at the end of the simulation. However, the CPU-time for

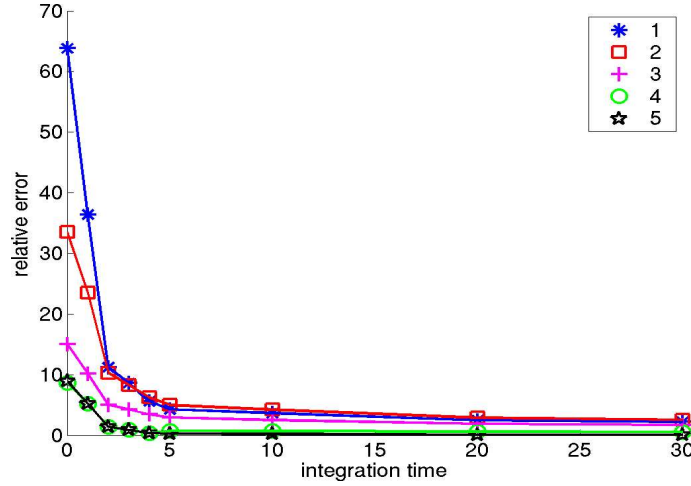


Figure 5.13: comparison of relative error for different number of atoms with initial momentum and different integration time, with second approximation approach given in section 5.2

the third approximation is only twice of that without boundary condition, thereby reducing the error from 63.83% to 2.33%. The computations were run on an Intel Xeon processor with 2.80 GHz with Matlab 6.5.

To be useful for the simulation of real systems, the computation of the projection matrices, the memory kernel, the memory integral and the solution of the whole system should be faster than solving the corresponding atomistic system. This depends especially on the numerical effort to compute the interatomic forces, which depends on the dimension of the system, the potential energy function and the number of interacting neighbours. For a one dimensional harmonic potential with interaction only between nearest neighbours, the force computation is as cheap as possible for an interacting system of atoms. Therefore, it is difficult to achieve lower computation time for a coupled system. However, potential energy functions of real systems are much more complicated, and the force calculation is usually the bottleneck in molecular dynamics simulations.

Since we are using a different space discretisation in the coarse scale and the atomistic region, it would save even more computation time if we could use also a coarser time step for the update of the coarse scale node values. In section 5.1, we discussed already the problem of finding interpolation weights with good dispersion relation for larger coarse scale time steps. Now, we use again the new interpolation weights  $N_1$  for  $\tilde{n} = 5$  and compute the coarse scale update not in each but only in every  $l$ th atomistic time step, for the full simulation and the second and third approximation. For the second approximation, the memory integral was computed over  $t_I = 60$ , for the third approximation over  $t_I = 20$ . The results are shown in figure 5.14. There is nearly no difference in the error, for  $l$  between 1 and 5 and even for  $l = 10$  it becomes only a little bit larger, no matter if we use the full simulation or an approximation. Since for  $l = 20$  it increases significantly, such a large time step should not be used for small values of  $\tilde{n}$  like 5. But choosing  $l = \tilde{n}$  for an atomistic time step  $\Delta t = \frac{1}{10}\sqrt{\frac{m}{k}}$  leads to good results and reduces the computation

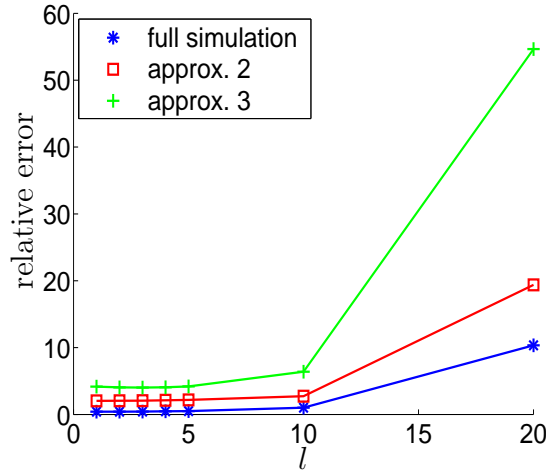


Figure 5.14: relative error for different coarse scale time steps

time significantly.

In section 3.2, we considered an anharmonic example with nearest neighbour interaction,

$$\mathcal{H}_2 = \frac{1}{2} \sum_{i=1}^n \frac{p_i^2}{m} + \sum_{i=2}^n \left( \frac{k_1}{2} (q_i - q_{i-1} - a_0)^2 + \frac{k_2}{4} (q_i - q_{i-1} - a_0)^4 \right),$$

with  $k_1 = 1$  and  $k_2 = 10$  and initial condition  $p_1(0) = 0.3$ . For the coupling of length scales approximation, we got a large error in the stress and the energy of the real atoms (cf. figure 3.19). The reflection of the perturbation was reduced significantly by using the bridging scales approximation, but due to the wrong wave speed in the coarse scale region, the energy at the end of the simulation was not correct. If we rerun the computation with the orthogonal displacement splitting for  $\tilde{n} = 5$ , with the interpolation weights  $N_1$ , we get nearly no reflection at the interface (left panel of figure 5.15) and only a small error in the energy of the real atoms at the end of the simulation (right panel of the figure), compared to the fully atomistic simulation. This small error at the end is caused by the small error left in the dispersion relation even with the new interpolation weights. But apart from that and a little energy increase before the perturbation reaches the interface, we have no deviations from the energy of the fully atomistic simulation.

Another question, that arises if we consider numerical aspects of the orthogonal displacement splitting, is how large the distance between the coarse scale nodes should be. So far, the node distance was always chosen as five or ten times the atomic equilibrium distance. If the distance is smaller, the part of the perturbation that is given by the coarse scale variables is larger and can pass the interface independent if we have a boundary condition or not. However, the reduction in the degrees of freedom is larger for a large node distance.

A problem with small node distances is, that for interpolation with linear hat functions, the energy in the atomistic region is not constant if we use the time step  $\Delta t$  of the simulations above. We can overcome this problem only with a much



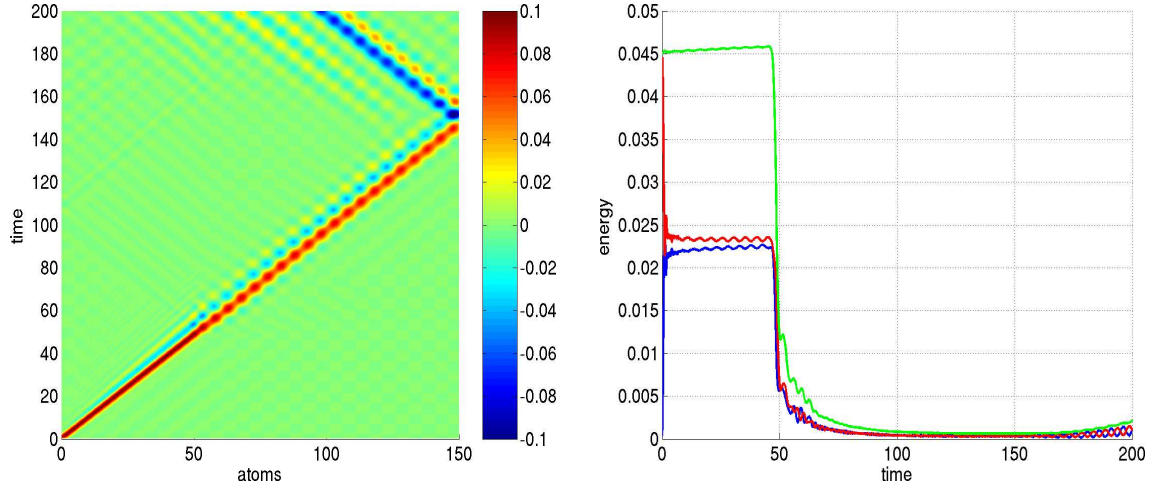


Figure 5.15: stress and energy for the anharmonic example computed with orthogonal displacement splitting and new interpolation function

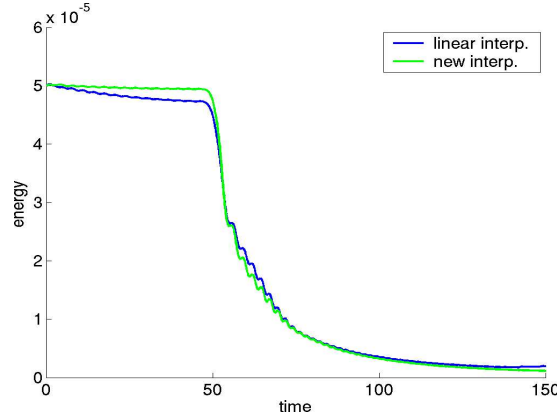


Figure 5.16: approximation with  $\tilde{n}=3$  for linear hat function (blue) and interpolation with correct dispersion relation (green)

smaller time step that increases the computation time drastically. The problem cannot be solved by using other interpolation functions from the fine scale variables to the atomic positions or by increasing the accuracy in the computation of the fine scale accelerations from the fine scale forces,

$$\ddot{b}_1 = (B_1^T M B_1)^{-1} B_1^T K (N d + B_1 b_1 + B_2 b_2).$$

It does also not depend on whether we use the boundary condition or not. It seems, that the problem depends on the subspaces spanned by the coarse and fine scale variables or rather by the corresponding interpolation matrices  $N$  and  $B$ , since it does not occur for the new interpolation function, as can be seen in figure 5.16. However, the problem can also be solved by computing the fully atomistic solution in the atomistic region, like in the bridging scales method, and using the projections only to compute the coarse scale part of the displacement and the boundary condition.

# Chapter 6

## Two dimensional examples

Although all examples in the previous chapters were one dimensional ones, the evolution equations of the orthogonal displacement splitting were derived in chapter 4 for arbitrary dimensions. In section 6.1, we discuss the general aspects of two dimensional simulations like the computation of the boundary condition. The computation of new interpolation functions for various two dimensional atomic interactions is presented in section 6.2. In the last two sections, numerical results for two dimensional examples are given, in section 6.3 for the boundary condition in two dimensions and an approximation of the memory integral, in section 6.4 for the comparison of the different interpolations and a simple model of the sputtering process.

### 6.1 Two dimensional simulations

In two dimensions, we have to decide not only in which distance the coarse scale nodes should be chosen, but also how the regular grid of the nodes should look like. We can think e.g. of a coarse scale discretisation of triangles or squares. The best choice depends in general on the atomistic lattice structure. E.g. for atoms on a lattice like in the left panel of figure 6.1, a coarse scale discretisation using triangles matches the atomistic structure, whereas for atomic equilibrium positions on a quadratic grid, the choice of an also quadratic coarse grid seems more natural (right panel of figure 6.1). In the following, we concentrate on quadratic grids, however, the computation of boundary conditions, interpolation weights, etc. is in general feasible for other coarse scale discretisations.

The computation of the reflectionless boundary condition works in general like for the one dimensional case. If the force is linear in the fine scale variables  $b_2$ , and we write the displacements of the variables in  $x$ - and  $y$ -direction in one vector

$$u = \begin{pmatrix} u_x \\ u_y \end{pmatrix}, \quad b_1 = \begin{pmatrix} b_{1,x} \\ b_{1,y} \end{pmatrix}, \quad b_2 = \begin{pmatrix} b_{2,x} \\ b_{2,y} \end{pmatrix},$$

we obtain for the memory kernel  $\theta(t)$  the same expression as in the one dimensional



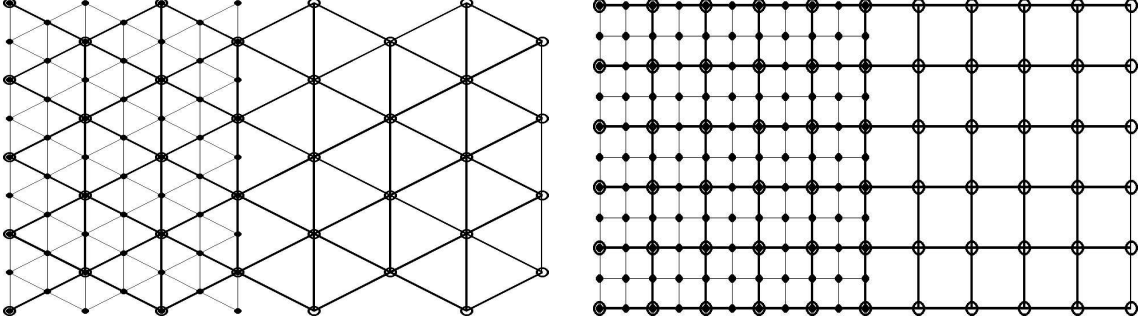


Figure 6.1: different atomistic equilibrium positions with coupling to a coarse scale region

case:

$$\begin{aligned}\theta(t) &= L^{-1} \{ [B_2^T M B_2 s^2 - B_2^T K B_2]^{-1} \} \\ &= \sum_{l=0}^{\infty} \frac{1}{(2l+1)!} [(B_2^T M B_2)^{-1} (B_2^T K B_2)]^l t^{2l+1} (B_2^T M B_2)^{-1}. \quad (6.1)\end{aligned}$$

If the atomistic forces in  $x$ - and  $y$ -direction depend only on the displacements in  $x$ - and  $y$ -direction respectively, the force matrix  $K$  has the following structure

$$K = \begin{bmatrix} K_x & 0 \\ 0 & K_y \end{bmatrix},$$

i.e. the force calculations in both directions are independent from each other. We can compute the memory kernel e.g. from  $K_x$  as

$$\theta_x(t) = \sum_{l=0}^{\infty} \frac{1}{(2l+1)!} [(B_{2,x}^T M B_{2,x})^{-1} (B_{2,x}^T K_x B_{2,x})^{-1}]^l t^{2l+1} (B_{2,x}^T M B_{2,x})^{-1},$$

and use it to compute the forces from the reflectionless boundary condition in  $x$ - and  $y$ -direction, for  $K_x = K_y$ ,

$$\begin{aligned}f_x &= \int_0^t \theta_x(t) B_{2,x}^T K_x (N_x d_x + B_{1,x} b_{1,x})(t - \tau) d\tau, \\ f_y &= \int_0^t \theta_x(t) B_{2,y}^T K_y (N_y d_y + B_{1,y} b_{1,y})(t - \tau) d\tau.\end{aligned}$$

If the force calculations in both directions are not independent from each other, we have to compute the memory kernel from the whole force matrix  $K$  that is now not a block matrix anymore.

If we consider an atomistic region embedded in a coarse scale region, every entry of the memory integral depends on all fine scale displacements  $b_1$  and coarse scale displacements  $d$ . Already for small systems, this can get very time consuming. We can reduce the computational effort significantly, by computing the boundary

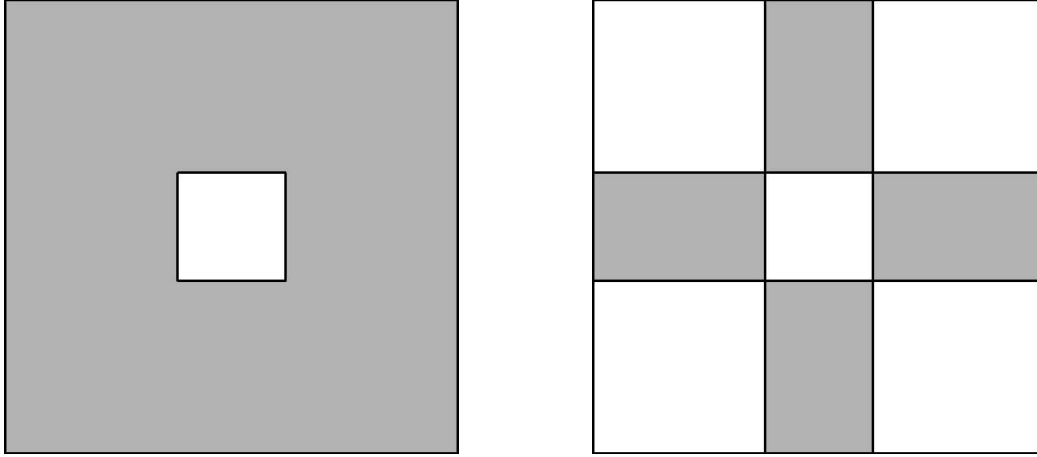


Figure 6.2: computation of boundary condition for the whole boundary (left) and for each side separately (right)

condition separately for each boundary of the atomistic domain. We neglect thereby the influence of the variables on one side of the domain on the memory integral of atoms on the other side of the domain. Instead of taking all fine scale variables  $b_2$  in the coarse scale region into account for the computation of the boundary condition, we consider only those in the stripe neighbouring the boundary. An example is given in figure 6.2. The white square in the middle marks the region of the atoms, the grey regions the support of the fine scale variables  $b_2$ , used for the computation of the boundary condition. Since here the geometry is symmetric, we can use the same matrix  $B_2$  for the computation of all four memory integrals, thereby reducing the number of variables drastically. Numerical results for this approximation are given in section 6.3.

With the interpolation matrix  $N$  from coarse to fine scale, the atomistic interaction, given by the matrix  $K$ , is transferred directly to the interaction of the coarse scale nodes by  $N^T K N$ . If the atomistic forces in  $x$ -direction depend only on the displacements of the neighbours in  $x$ -direction, this holds also for the nodes. Since the interaction of the nodes is the same everywhere in the interior of the domain, the interaction can be computed in a small part of the domain, to avoid the multiplication of large matrices.

## 6.2 New interpolation functions in two dimensions

In this section, we want to discuss, how we can compute interpolation weights in two dimensions with small error in the dispersion relation compared to the atomistic one. Like in the one dimensional case, the dispersion relation depends on the atomic interaction. The interpolation weights depend therefore on the potential energy and in two dimensions also on the atomic lattice structure.

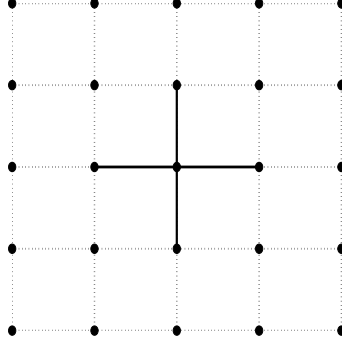


Figure 6.3: harmonic interaction with the four nearest neighbours

For the simplest two dimensional interaction, a harmonic potential with interaction to the four next nearest neighbours (cf. figure 6.3), we show now, how to compute interpolation weights with better dispersion relation than using linear hat functions. They are defined in two dimensions as

$$\begin{aligned}
 f_j(x, y) &= f_{j,x}(x)f_{j,y}(y), \\
 \text{with } f_{j,x}(x) &= \begin{cases} 1 - \frac{\tilde{d}_{j,x}-x}{\Delta X}, & x \in (\tilde{d}_{j,x} - \Delta X, \tilde{d}_{j,x}] \\ 1 + \frac{\tilde{d}_{j,x}-x}{\Delta X}, & x \in (\tilde{d}_{j,x}, \tilde{d}_{j,x} + \Delta X] \end{cases}, \\
 f_{j,y}(y) &= \begin{cases} 1 - \frac{\tilde{d}_{j,y}-y}{\Delta Y}, & y \in (\tilde{d}_{j,y} - \Delta Y, \tilde{d}_{j,y}] \\ 1 + \frac{\tilde{d}_{j,y}-y}{\Delta Y}, & y \in (\tilde{d}_{j,y}, \tilde{d}_{j,y} + \Delta Y] \end{cases},
 \end{aligned} \tag{6.2}$$

where  $\Delta X$  and  $\Delta Y$  denote the distance of the coarse scale nodes in  $x$ - and  $y$ -direction and  $(\tilde{d}_{j,x}, \tilde{d}_{j,y})$  the equilibrium position of node  $j$ .

According to [18], the time continuous harmonic solution for the atomistic system with this interaction is given by

$$u = (u_x, u_y) = A \exp(i(\omega t - \kappa_x \Delta x - \kappa_y \Delta y)), \tag{6.3}$$

with the amplitude  $A = (A_x, A_y)$ , the wave vector  $\kappa = (\kappa_x, \kappa_y)$  and the wave frequency  $\omega$ . For our example, the equilibrium distances of the atoms in  $x$ - and  $y$ -direction are the same,

$$\Delta x = \Delta y = a_0,$$

and we can write the harmonic solution for every atom as

$$u_{k,l} = (u_{x,k,l}, u_{y,k,l}) = A \exp(i(\omega t - \kappa_x k a_0 - \kappa_y l a_0)).$$

If the force in every coordinate direction depends only on the displacements of the atoms in this direction,

$$\begin{aligned}
 m\ddot{u}_{x,k,l} &= k(u_{x,k+1,l} + u_{x,k,l+1} + u_{x,k-1,l} + u_{x,k,l-1} - 4u_{x,k,l}), \\
 m\ddot{u}_{y,k,l} &= k(u_{y,k+1,l} + u_{y,k,l+1} + u_{y,k-1,l} + u_{y,k,l-1} - 4u_{y,k,l}),
 \end{aligned}$$

the dispersion relation for both coordinates is the same,

$$\omega^2 = \frac{4k}{m} \left( \sin^2 \left( \frac{\kappa_x a_0}{2} \right) + \sin^2 \left( \frac{\kappa_y a_0}{2} \right) \right). \tag{6.4}$$

The evolution equations on the coarse scale, and therefore also the corresponding dispersion relations, depend on the number of non-zero entries in the coarse scale mass  $N^T M N$ , and force matrix  $N^T K N$ .

If we have the same distance of the nodes in  $x$ - and  $y$ - direction, i.e.  $\Delta X = \Delta Y = \tilde{n}a_0$ , with linear hat functions (6.2) as interpolation functions, we get non-zero entries in the coarse scale mass and force matrix on the main diagonal and for the entries corresponding to the next nodes in vertical, horizontal and diagonal direction. The evolution equations are given by

$$\begin{aligned} & m_1 \ddot{d}_{k,l} + m_2 \left( \ddot{d}_{k+1,l} + \ddot{d}_{k,l+1} + \ddot{d}_{k-1,l} + \ddot{d}_{k,l-1} \right) \\ & + m_3 \left( \ddot{d}_{k+1,l+1} + \ddot{d}_{k-1,l+1} + \ddot{d}_{k+1,l-1} + \ddot{d}_{k-1,l-1} \right) \\ & = k_1 d_{k,l} + k_2 (d_{k+1,l} + d_{k,l+1} + d_{k-1,l} + d_{k,l-1}) \\ & + k_3 (d_{k-1,l-1} + d_{k-1,l+1} + d_{k+1,l-1} + d_{k+1,l+1}), \end{aligned}$$

with

$$\begin{aligned} m_2 &= -\frac{1}{18} + \frac{\tilde{n}^2}{9} + \frac{1}{9\tilde{n}^2}, \\ m_3 &= \frac{\tilde{n}^2}{36} + \frac{1}{36\tilde{n}^2} - \frac{1}{18}, \\ m_1 &= \tilde{n}^2 - 4m_2 - 4m_3 = \frac{4\tilde{n}^2}{9} + \frac{4}{9} + \frac{1}{9\tilde{n}^2}, \\ k_2 &= \frac{1}{3} - \frac{1}{3\tilde{n}^2}, \\ k_3 &= \frac{1}{3} + \frac{2}{3\tilde{n}^2}, \\ k_1 &= -4k_2 - 4k_3 = -\frac{8}{3} + \frac{4}{3\tilde{n}^2}. \end{aligned}$$

In case of  $\Delta X = \Delta Y = 2a_0$ , we derive the dispersion relation from the harmonic solution  $d_{x,j,k} = \tilde{A} \exp(i(\omega t - \kappa_x j \Delta X - \kappa_y k \Delta Y))$  as

$$\omega^2(\kappa_x, \kappa_y) = \frac{4(3 - \cos(\kappa_x \Delta X) - \cos(\kappa_y \Delta X) - \cos(\kappa_x \Delta X) \cos(\kappa_y \Delta X))}{3 \cos(\kappa_x \Delta X) + 3 \cos(\kappa_y \Delta X) + 9 + \cos(\kappa_y \Delta X) \cos(\kappa_x \Delta X)}.$$

In figure 6.4, we compare this dispersion relation (b) with the atomistic one (a), given by (6.4), for different wave numbers  $(\kappa_x, \kappa_y)$  in  $x$ - and  $y$ - direction. The color indicates the corresponding wave speed. As in the one dimensional case, the limiting wave speed for small wave numbers is the same for both equations, but for large wave numbers the waves are again too fast on the coarse scale. For  $\kappa_x = \kappa_y = \pi/3$  we observe the largest deviation of 9.5%. If we increase the number of non-zero weights and change the interpolation from

$$N_{hat} = \frac{1}{4} \begin{bmatrix} 0 & 0 & 0 & 0 & 0 \\ 0 & 1 & 2 & 1 & 0 \\ 0 & 2 & 4 & 2 & 0 \\ 0 & 1 & 2 & 1 & 0 \\ 0 & 0 & 0 & 0 & 0 \end{bmatrix} \quad \text{to} \quad N_{new} = \frac{1}{64} \begin{bmatrix} 1 & 4 & 6 & 4 & 1 \\ 4 & 16 & 24 & 16 & 4 \\ 6 & 24 & 36 & 24 & 6 \\ 4 & 16 & 24 & 16 & 4 \\ 1 & 4 & 6 & 4 & 1 \end{bmatrix},$$

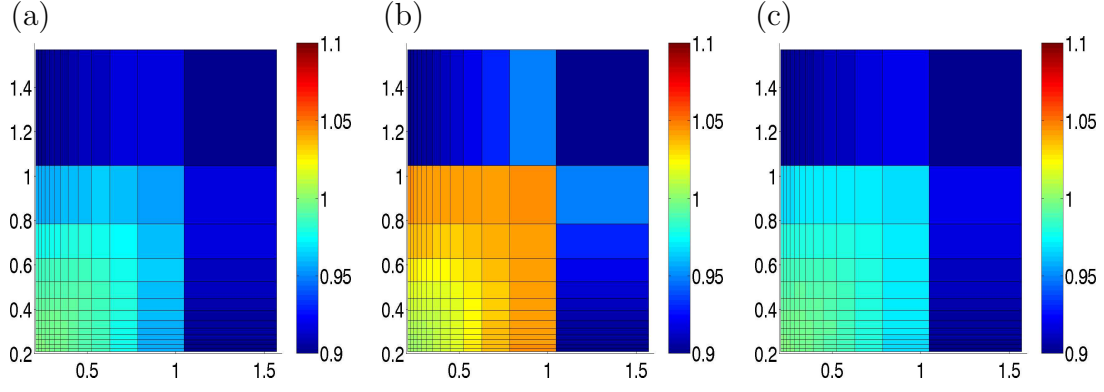


Figure 6.4: two dimensional dispersion relation for fully atomistic system (a), linear interpolation (b) and new interpolation (c)

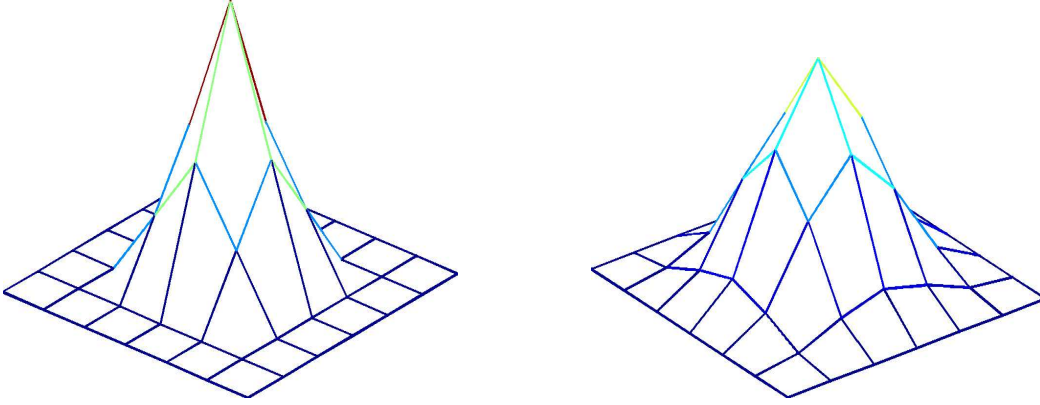
we observe again the largest deviation for  $\kappa_x = \kappa_y = \pi/3$ , but it is now only 1.2% (cf. figure 6.4 (c)).

Like in the one dimensional case, the new weights were computed by choosing first a matrix of  $(2\tilde{n}+1) \times (2\tilde{n}+1)$  arbitrary non-zero weights. With the requirement of symmetry with respect to the maximum weight in the center and the partition of unity, we end up with 3 degrees of freedom,  $w_1$ ,  $w_2$  and  $w_5$ ,

$$\begin{bmatrix} w_5 & w_4 & w_6 & w_4 & w_5 \\ w_4 & w_3 & w_2 & w_3 & w_4 \\ w_6 & w_2 & w_1 & w_2 & w_6 \\ w_4 & w_3 & w_2 & w_3 & w_4 \\ w_5 & w_4 & w_6 & w_4 & w_5 \end{bmatrix}, \quad \begin{aligned} w_3 &= 1/4 \\ w_4 &= 1/4 - w_2/2 \\ w_6 &= 1/4 - w_5 - w_1/4 \end{aligned}.$$

With this degrees of freedom, we compute the entries of the coarse scale mass and force matrix,  $N^T M N$  and  $N^T K N$ , that have now more non-zero entries than for linear hat functions. The coarse scale dispersion relation is calculated from this values as

$$\begin{aligned} \omega^2 = & \frac{-(k_1 + 2k_2(\cos(\kappa_x \Delta X) + \cos(\kappa_y \Delta X)) + 4k_3 \cos(\kappa_x \Delta X) \cos(\kappa_y \Delta X) + \dots}{m_1 + 2m_2(\cos(\kappa_x \Delta X) + \cos(\kappa_y \Delta X)) + 4m_3 \cos(\kappa_x \Delta X) \cos(\kappa_y \Delta X) + \dots} \\ & + 2k_4(\cos(2\kappa_x \Delta X) + \cos(2\kappa_y \Delta X)) + 4k_5 \cos(2\kappa_x \Delta X) \cos(2\kappa_y \Delta X) + \dots \\ & + 2m_4(\cos(2\kappa_x \Delta X) + \cos(2\kappa_y \Delta X)) + 4m_5 \cos(2\kappa_x \Delta X) \cos(2\kappa_y \Delta X) + \dots \\ & + 4k_6(\cos(2\kappa_x \Delta X) \cos(\kappa_y \Delta X) + \cos(\kappa_x \Delta X) \cos(2\kappa_y \Delta X)) \\ & + 4m_6(\cos(2\kappa_x \Delta X) \cos(\kappa_y \Delta X) + \cos(\kappa_x \Delta X) \cos(2\kappa_y \Delta X)), \end{aligned} \quad (6.5)$$

Figure 6.5: interpolation functions  $N_{\hat{}}$  (left) and  $N_{\text{new}}$  (right) for  $\tilde{n} = 2$ 

with  $\Delta X = 2a_0$ ,

$$\begin{aligned}
m_1 &= \frac{5}{4}w_1^2 + 6w_2^2 + 8w_5^2 + 2w_1w_5 - \frac{1}{2}w_1 - 2w_2 - 2w_5 + 1, \\
m_2 &= -\frac{1}{2}w_1^2 - \frac{1}{2}w_2^2 - 4w_5^2 - 3w_1w_5 + \frac{1}{2}w_1 + \frac{1}{2}w_2 + w_5 + \frac{1}{4}, \\
m_3 &= \frac{1}{8}w_1^2 - 2w_2^2 + 2w_5^2 + 3w_1w_5 - \frac{1}{4}w_1 + w_2 - w_5 + \frac{3}{16}, \\
m_4 &= \frac{1}{16}w_1^2 + \frac{1}{2}w_2^2 + 3w_5^2 + \frac{1}{2}w_1w_5 - \frac{1}{8}w_1 - \frac{1}{2}w_2 - \frac{1}{2}w_5 + \frac{3}{16}, \\
m_5 &= w_5^2, \\
m_6 &= \frac{1}{4}w_2^2 - 2w_5^2 - \frac{1}{2}w_1w_5 - \frac{1}{4}w_2 + \frac{1}{2}w_5, \\
k_1 &= -5w_1^2 - 24w_2^2 - 32w_5^2 + 8w_1w_2 - 8w_1w_5 - 8w_2w_5 + w_1 + 10w_2 + 8w_5 + 2, \\
k_2 &= 2w_1^2 + 2w_2^2 + 16w_5^2 - w_1w_2 + 12w_1w_5 - 4w_2w_5 - \frac{3}{2}w_1 - \frac{1}{2}w_2 - 4w_5 + \frac{1}{4}, \\
k_3 &= -\frac{1}{2}w_1^2 + 8w_2^2 - 8w_5^2 - 2w_1w_2 - 12w_1w_5 + 8w_2w_5 + \frac{3}{2}w_1 - 4w_2 + 2w_5 + \frac{1}{4}, \\
k_4 &= -\frac{1}{4}w_1^2 - 2w_2^2 - 12w_5^2 - 2w_1w_5 - 4w_2w_5 + \frac{1}{4}w_1 + \frac{3}{2}w_2 + 3w_5 - \frac{1}{4}, \\
k_5 &= -4w_5^2 - 2w_2w_5 + w_5, \\
k_6 &= -w_2^2 + 8w_5^2 + \frac{1}{2}w_1w_2 + 2w_1w_5 + 2w_2w_5 - \frac{1}{4}w_1 + \frac{1}{4}w_2 - 2w_5 + \frac{1}{8}.
\end{aligned}$$

We expand the dispersion relation (6.5) around  $\kappa_x = \kappa_y = 0$  and require that the terms up to power three match that of the expansion of the atomistic dispersion relation (6.4), to obtain the new interpolation weights. A comparison of the two interpolation functions is shown in figure 6.5.

At the boundary elements of the coarse scale region, we have to change the weights in such a way that the partition of unity is still fulfilled. The interpolation weights from the neighbouring elements are no longer zero, and therefore, some weights are missing at the boundary.

Like in the one dimensional case, the interpolation matrix  $B$  from the fine scale

variables  $b$  to the atoms should be chosen in such a way that the support of the interpolation for each fine scale variable is as small as possible. This depends on the distance of the coarse scale nodes and the support of the interpolation from the nodes.

If the force in  $x$ -direction depends not only on the displacement in  $x$ -direction of the neighbouring atoms, the dispersion relation gets more complicated. We can now have longitudinal and shear waves, with different wave speed. I.e. we get two equations for the dispersion relation [18]. If the atomistic interaction is for example

$$\begin{aligned} m\ddot{u}_{x,k,l} = & k \left( u_{x,k+1,l} + u_{x,k-1,l} + u_{x,k,l+1} + u_{x,k,l-1} + \frac{1}{2}u_{x,k+1,l+1} + \frac{1}{2}u_{x,k-1,l+1} \right. \\ & + \frac{1}{2}u_{x,k+1,l-1} + \frac{1}{2}u_{x,k-1,l-1} + \frac{1}{2}u_{y,k+1,l+1} + \frac{1}{2}u_{y,k-1,l+1} + \frac{1}{2}u_{y,k+1,l-1} \\ & \left. + \frac{1}{2}u_{y,k-1,l-1} - 6u_{x,k,l} - 2u_{y,k,l} \right), \end{aligned}$$

we derive again the dispersion relation from (6.3). It depends now on  $A_x$  and  $A_y$ ,

$$\begin{aligned} -\omega^2 m A_x &= k A_x (2 \cos(\kappa_x a_0) + 2 \cos(\kappa_y a_0) + \cos(\kappa_x a_0 + \kappa_y a_0) + \cos(\kappa_x a_0 - \kappa_y a_0)) \\ &+ k A_y (\cos(\kappa_x a_0 + \kappa_y a_0) + \cos(\kappa_x a_0 - \kappa_y a_0)) - 6k A_x - 2k A_y \\ &=: A_x a + A_y b. \end{aligned} \tag{6.6}$$

The same holds for the dispersion relation computed from the evolution equation in  $y$ -direction, only  $A_x$  and  $A_y$  are changed,

$$-\omega^2 m A_y = A_x b + A_y a. \tag{6.7}$$

If we determine  $\omega$  in such a way that the system of equations (6.6) and (6.7) has a unique solution, we obtain two different equations that correspond to the longitudinal and shear waves,

$$\begin{aligned} \omega_L^2 &= -\frac{2k}{m} (-2 + \cos(\kappa_y a_0) + \cos(\kappa_x a_0)), \\ \omega_S^2 &= -\frac{2k}{m} (-4 + \cos(\kappa_y a_0) + \cos(\kappa_x a_0) + 2 \cos(\kappa_x a_0) \cos(\kappa_y a_0)). \end{aligned}$$

On the coarse scale, we get also two different dispersion relations, and we have to choose now the interpolation weights in such a way that the error in both terms is reduced.

### 6.3 Reflectionless boundary condition in two dimensions

To test the boundary condition in two dimensions and the approximation of computing the boundary condition on each boundary separately (cf. section 6.1), we consider the test case given in [42]. We take a quadratic lattice of  $\hat{N} \times \hat{N}$  atoms,

with each atom interacting with its four nearest neighbours (cf. figure 6.3), and forces depending linearly on the atomic displacements in  $x$ - and  $y$ -direction, with spring constant  $k = 1$  and mass  $m = 1$ . In section 6.3.1, we consider this square embedded in a larger atomistic region, in section 6.3.2 in a coarse scale region. All velocities are initially zero and the initial displacements are taken according to a Gaussian pulse of maximum one in the center of the lattice with width  $\sigma = 1.25$  times the atomic equilibrium distance. To measure the wave reflection at the boundary of the square, we compute the relative error in the energy,

$$\epsilon_r := \frac{E_T - E_T^{bm}}{E_0},$$

with  $E_T$  the energy in the system after time  $T$ ,  $E_T^{bm}$  a benchmark value computed from a larger atomistic simulation and  $E_0$  the initial energy.

### 6.3.1 Small atomistic system

First, we consider only an atomistic region together with the reflectionless boundary condition but without the coupling to a coarse scale. I.e. we do not split the displacements into fine and coarse scale part but only in two parts, the displacements of the atoms in the small atomistic region and the surrounding atoms, which are only necessary to compute the boundary condition. Such a splitting was explained at the end of section 4.3. In this case, the bridging scales approximation and the orthogonal displacement splitting are the same.

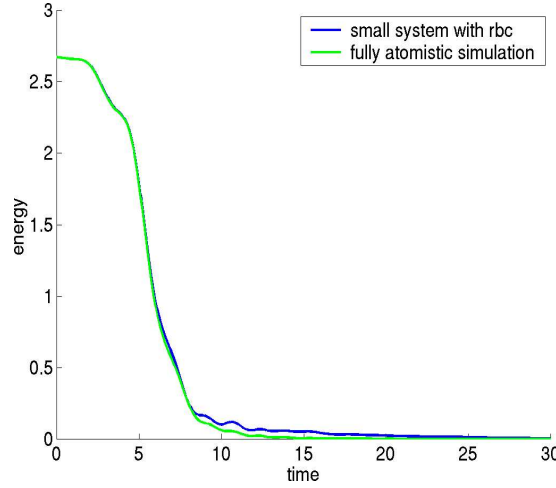
The boundary condition is computed from a layer of  $\hat{N} - 1$  atoms around the atomistic region of  $\hat{N} \times \hat{N}$  atoms, using an integration time of  $t_I = 3$  for the values  $E_1$  and  $t_I = 3.5$  for the values of  $E_2$  in the table 6.1. The time step for the integration is  $\Delta t = 0.1$ . To avoid the computation of the projection matrix  $\hat{P}$ , necessary for the computation of the memory kernel function  $\theta(t)$  according to (4.16), we compute the memory kernel function  $\theta(t)$  from the first 20 terms of the expansion of the sine function (6.1) for the integration time  $t_I = 3$  and from the first 30 terms for the integration time  $t_I = 3.5$ . According to the approximation in section 6.1, the boundary condition is applied separately on each boundary. The energy is computed once directly after the pulse passes the boundary of the  $\hat{N} \times \hat{N}$  atoms and once for  $T = 50$  for all different system sizes. The results are shown in table 6.1 for the relative error in the energy, which depends on the integration time of the memory integral, i.e. on the accuracy of the boundary condition and on the point in time where we compare the energies.



$\hat{N}$	T	$E_{1,T}$	$E_{2,T}$	$E_T^{bm}$	$\epsilon_{r,1}$	$\epsilon_{r,2}$
8	14	6.19 e-02	5.77e-02	1.28e-02	1.84%	1.68%
8	50	2.10e-02	3.13e-04	4.43e-05	0.78%	0.01%
16	20	1.02e-01	9.27e-02	6.35e-02	1.45%	1.09%
16	50	1.32e-02	9.2e-03	8.00e-04	0.46%	0.31%
24	30	9.82e-02	8.68e-02	6.37e-02	1.20%	0.86%
24	50	2.76e-02	2.49e-02	4.3e-03	0.87%	0.77%
32	40	9.15e-02	8.28e-02	6.06e-02	1.16%	0.83%
32	50	4.33e-02	3.84e-02	3.90e-02	0.16%	-0.02%

Table 6.1: wave reflection with reflectionless boundary condition

The reason for this can be seen in figure 6.6, where we compare the small system with reflectionless boundary condition for  $\hat{N} = 8$  with a fully atomistic simulation. For the small system with boundary condition, the energy leaves the system a little bit slower. If we compute the relative error after a long simulation time, it is therefore smaller than directly after the pulse passes the boundary. However, it is always smaller than 2%, which shows that the approximation is quite good.

Figure 6.6: energy of the inner  $8 \times 8$  atoms for fully atomistic simulation (green) and for small system of  $8 \times 8$  atoms with reflectionless boundary condition (blue)

### 6.3.2 Coupling of atomistic and coarse scale

Next, we study the reflectionless boundary condition for a coupled system of atoms and nodes and the difference between the bridging scales approximation and the orthogonal displacement splitting for such a coupling in two dimensions. We consider an initial setting similar to that in the previous subsection. All velocities are initially zero. The initial displacements are taken from a Gaussian pulse of maximum one in the center of the lattice and width  $\sigma = 1.25$ . We choose 11 atoms in each coordinate direction for the atomistic region. The center of the lattice is located now at the

equilibrium position of the atom in the middle. The equilibrium position of every fifth atom in each direction is chosen as a coarse scale node, i.e.  $\tilde{n} = 5$ , and the matrix  $B_2$  is taken into account for the layer of elements next to the atomistic region. For a fully atomistic simulation, to compare the results with, we used 41 atoms in each coordinate direction.

Again, the memory kernel is computed as an approximation of the sine function. First, we analyse the influence of the integration time of the memory integral on the error in the approximation. For the orthogonal displacement splitting with linear hat functions and the bridging scales approximation, we compare in figure 6.7 the decay of the energy in the system for different numbers of time steps for this integration. The system with the orthogonal displacement splitting was run twice, once with the boundary condition computed for each boundary separately (left), like for the bridging scales method (right), and once with reflectionless boundary condition for all four boundaries together (middle). We compare the integration of the memory integral over 15 (blue), 25 (green) and 35 (red) atomistic time steps  $\Delta t = 0.1$ .

For the orthogonal displacement splitting with boundary condition computed for all four boundaries together (panel in the middle of figure 6.7), the behaviour is the same as in one dimension. A longer integration time, i.e. a more exact computation of the memory integral, reduces the reflection at the interface. But, if the memory integral is computed only from a few fine scale variables  $b_2$ , integrating too long leads to reflections at the end of the support of this fine scale variables. Therefore, the red line decreases faster after the pulse passes the interface, but, at the end of the simulation, we get the least energy for the green line, i.e. for  $t_I = 2.5$ .

If we approximate the boundary condition by computing it separately for each boundary, we get the best result at the end of the simulation already for the shortest integration time.

For the bridging scales approximation, a longer integration reduces the energy in the atomistic region at the end of the simulation, however, the difference between the red and the green line is quite small. The boundary condition is here also computed separately for each boundary.

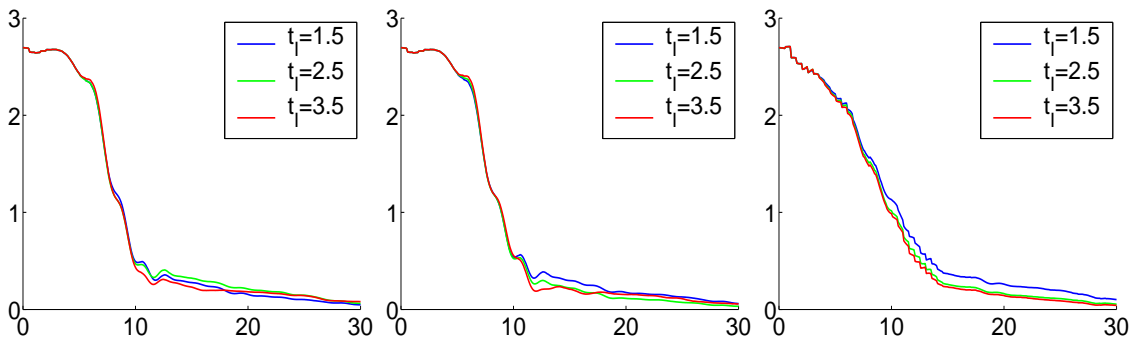


Figure 6.7: energy for different integration times in the memory integral for orthogonal displacement splitting with (left) and without (middle) approximation in the boundary condition and for bridging scales approximation (right)

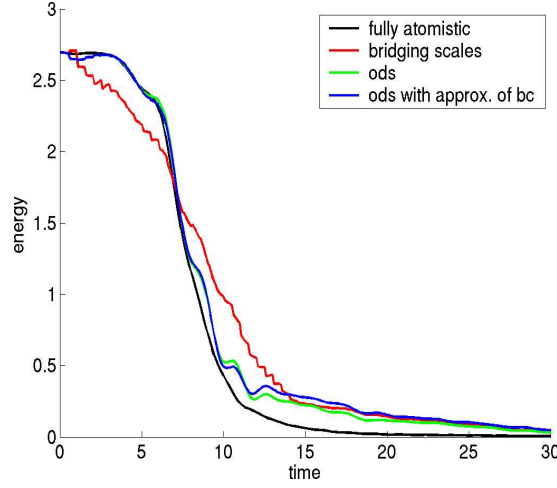


Figure 6.8: energy for fully atomistic simulation (black), bridging scales approximation (red) and orthogonal displacement splitting without (blue) and with (green) approximation in the boundary condition

Next, we compare the best result of all three simulations with the result of a fully atomistic simulation (figure 6.8). There is no visible difference in the error at the end of the simulation for the different approximations, but the deviation of the energy during the simulation is quite large with the bridging scales approximation. In the following tabular, we compare the resulting relative error of the three simulations above and that of the same simulation for a small system with boundary condition without coupling to a coarse scale region, according to section 6.3.1. The initial energy is  $E_0 = 2.6955$  and the reference energy after 300 time steps of a fully atomistic simulation  $E_{\text{ref}} = 6.1\text{e} - 03$ .

$t_I$	orth. splitting coupled sys. approx. b.c.	orth. splitting coupled sys.	bridging scales coupled sys. approx. b.c.	atomistic approx. b.c.	atomistic
1.5	1.57%	2.06%	3.55%	1.53%	1.84%
2.5	2.12%	1.00%	1.81%	2.16%	0.77%
3.5	2.79%	1.88%	1.34%	2.57%	1.64%

The error with coupling to a coarse scale region is nearly the same as for the computation of atomistic boundary condition, the latter giving slightly better results. The reason is that, for the simulations in this chapter, linear interpolation from the coarse scale to the atoms is used. This leads to an error in the coarse scale dispersion relation compared to the atomistic dispersion relation. We cannot avoid the resulting reflections at the interface if we use only few variables to compute the reflectionless boundary condition.

The computation of the reflectionless boundary condition on each boundary separately is much cheaper than the computation for the whole boundary. However, the resulting error is small, compared to the computation on the whole boundary, and the result is even better for small integration time.

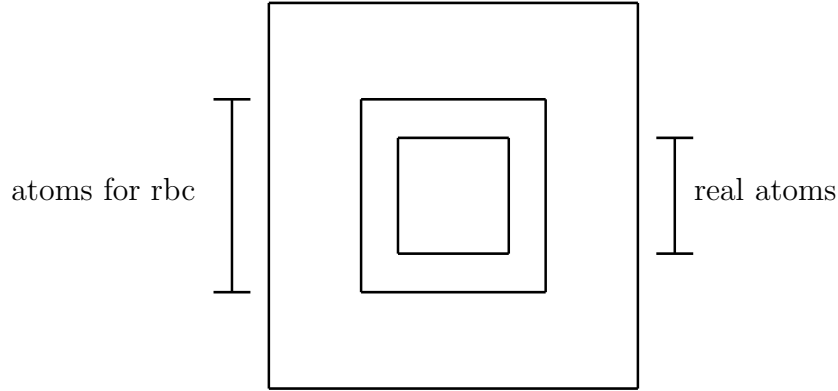


Figure 6.9: geometry for test case 1

## 6.4 Test cases, comparison of interpolation functions

In the following, we consider now several test cases to compare the orthogonal displacement splitting for different interpolations and the bridging scales approximation in two dimensions. For this examples, we consider once more the simplest two dimensional interaction to the four next nearest neighbours (cf. figure 6.3). The distance of the coarse scale nodes is for all examples twice the atomic equilibrium distance,  $\Delta X = \Delta Y = 2a_0$ .

**Test case 1** The first example is a symmetric domain with an atomistic region in the middle, to test the reflectionless boundary condition. The atomistic region consists of 21 atoms in each direction, and the atom in the middle gets an initial displacement in  $x$ - and  $y$ - direction ( $u_x(0) = u_y(0) = 0.8$ ). The atomistic parameters are  $k = m = 1$ ,  $\Delta t = 0.1$ , and we keep the fine scale degrees of freedom  $b_2$  till the second node after the interface in each direction. The simulation was run for the bridging scales approximation and the orthogonal displacement splitting, once using interpolation with linear hat functions and once using the interpolation weights computed in section 6.2. We compare the energy of the inner  $15 \times 15$  atoms. The reason why the energy is computed only for the inner atoms is a technical one. Due to the small overlap of the support of the variables  $b_1$  and  $b_2$  in the orthogonal displacement splitting, we need also the variables  $b_2$  and  $\dot{b}_2$  to compute the total displacements and velocities at the boundary, whereas this is not necessary for the inner atoms.

The results are shown in figure 6.10. For all three approximations, the reflectionless boundary condition gives good results. Only for the bridging scales approximation, there is a little bit more energy left in the system after a simulation of 600 time steps.

Because of the small distance of the nodes ( $\tilde{n} = 2$ ), there is nearly no difference between the energy in the bridging scales approximation and the orthogonal dis-

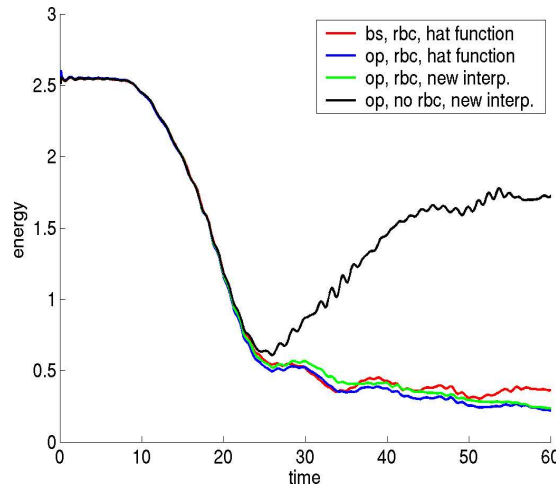


Figure 6.10: comparison of energies for different simulations using an initial displacement of the atom in the center,  $u_x = u_y = 0.8$

placement splitting when the perturbation reaches the interface. Since the fine scale part is smaller for a small distance of the coarse scale nodes, also the error due to the approximations in the derivation of the boundary condition is smaller.

The memory kernel was computed from the first 20 terms of the series expansion of the sine function, and the memory integral was integrated over 25 time steps. Without reflectionless boundary condition, the energy is also decreasing first, since we are computing only the energy of the inner atoms. The fine scale part of the perturbation is then reflected at the interface, and the energy is increasing again. Only the coarse scale part of the perturbation can leave the atomistic region completely.

The simulation without boundary condition was carried out with orthogonal displacement splitting and the new interpolation weights. However, for the other two approximations results are similar. For the energy in the atomistic region there is thus no big difference which interpolation we use, especially if the number of degrees of freedom for the computation of the boundary condition is small and the integration time is short. In the third example, we show that the situation is different if we consider the perturbation not only in the atomistic but also in the coarse scale region.

In figure 6.11, we compare the displacements of the inner atoms at the end of the simulation, using orthogonal displacement splitting with (left) and without (right) reflectionless boundary condition. The values are scaled with a factor 3. A large difference between the simulations with and without boundary condition can be observed, although we have an initial displacement only for one of the atoms, which is distributed over the  $21 \times 21$  atoms in the atomistic region during the simulation.

As another comparison, we show in figure 6.12 the two dimensional stress tensor for both simulations in different time steps. The panels on the left show the simulation with, that on the right panel the simulation without boundary condition. The figures visualize the eigenvectors of the stress tensor, and the color indicates the corresponding eigenvalues. Red colors mark positive values, blue colors negative ones, and the opacity of the vectors scales with the absolute value. The plots

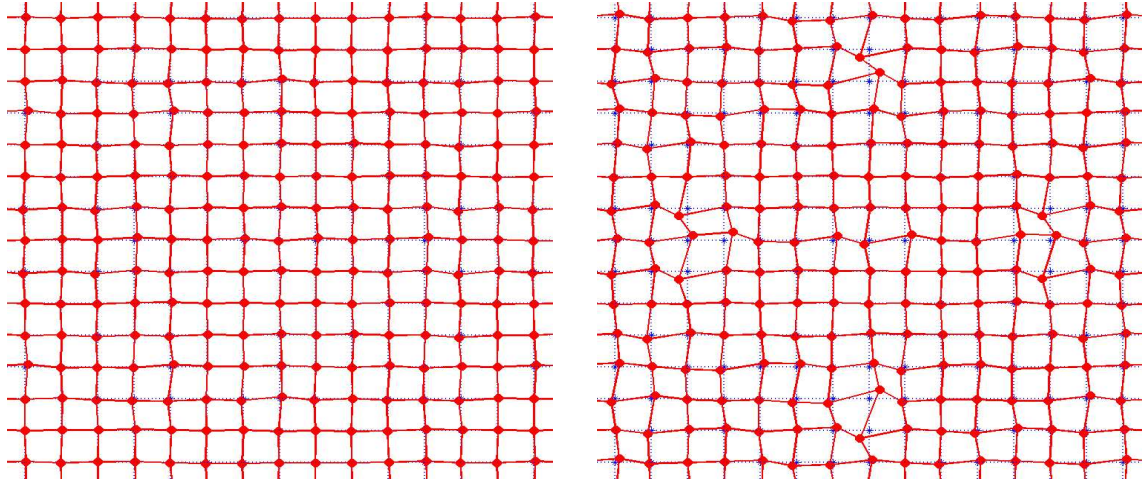


Figure 6.11: displacement of the inner atoms after 600 time steps with (left) and without (right) reflectionless boundary condition

were made with Data Explorer Version -4.2.0. Since the absolute values are high at the beginning and decrease during the simulation, due to the distribution of the initial displacement, we used a piecewise linear colormap between the values  $[-0.25, -0.056, 0.056, 0.25]$ . The figures in the first row are for the initial setting, which is of course the same for both simulations. The second row shows the stress after 100 time steps, i.e.  $T = 10$ . There is still no difference between both simulations. Also for the energy, we can observe no difference at  $T = 10$  in figure 6.10. For the stress after 490 time steps ( $T = 49$ ) we see, like in the energy plots, a difference between the simulation with and without boundary condition. The difference is better visible in the energy plots, although a piecewise linear colormap is used for the stress plots, since the energy scales quadratically with the displacements and velocities of the atoms, whereas the stress is only linear with respect to these values.

**Test case 2, simple model of the sputtering** The second example is a simplified model of the sputtering process, discussed in section 1.1. The interaction is again harmonic to the four nearest neighbours, but the geometry (cf. figure 6.13) is chosen according to the sputtering process. We have an atomistic region of  $11 \times 21$  atoms with one free boundary, surrounded by a coarse scale region on the three other sides. The atom in the middle of the left boundary of the atomistic region gets an initial displacement in  $x$ -direction, all other initial values are zero. Like in the previous example, the fine scale degrees of freedom till the first two nodes after the interface are used for the computation of the boundary condition. The computation was performed with orthogonal displacement splitting with the new interpolation weights computed in section 6.2. Figure 6.14 shows the energy of the inner  $9 \times 17$  atoms for the simulation with (green) and without (blue) boundary condition. Again, the use of a few extra variables for the computation of the memory integral leads to an evident improvement in the simulation. We compare in



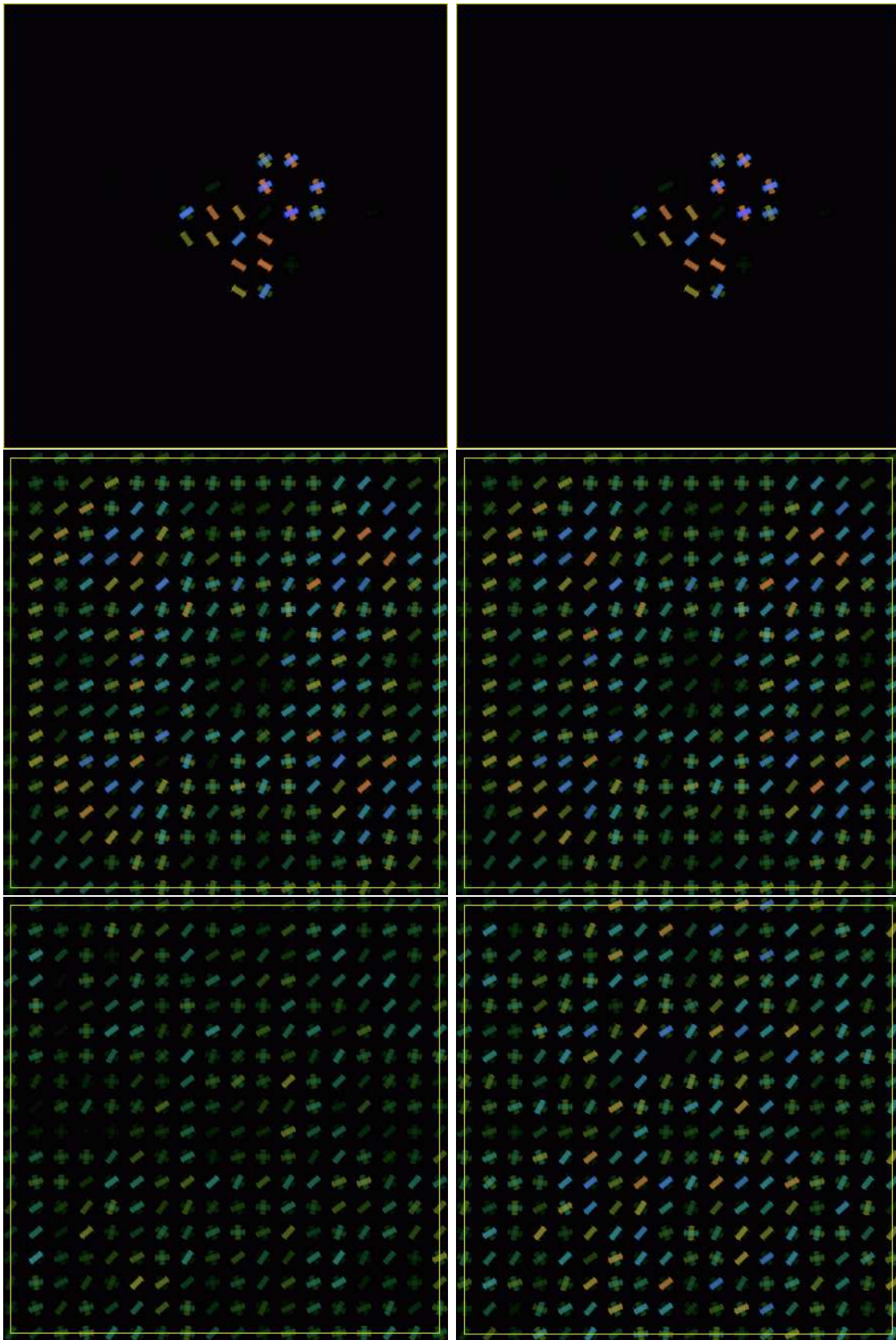


Figure 6.12: stress for test case 2 for  $T = 0, 10$  and  $49$  for a simulation with (left column) and without (right column) boundary condition

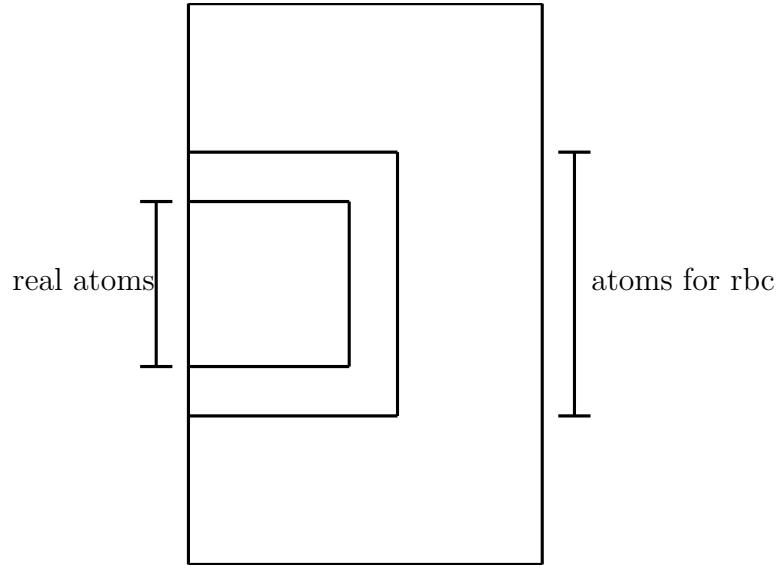


Figure 6.13: geometry for test case 2

figure 6.15 the initial displacements of the inner atoms with the displacements after 600 time steps. The difference between a simulation with and without boundary condition is again obvious. The values of the panels on the right and in the middle were scaled with the factor 3.

**Test case 3, coarse scale initial displacement** As a last example, we consider a geometry similar to that of the sputtering example, but using now more atoms in  $x$ - than in  $y$ -direction. This time, the initial displacement is given in the coarse scale nodes. To all nodes on the left side an initial displacement of 0.8 in  $y$ -direction is applied. We run the simulation with the orthogonal displacement splitting, once with interpolation with linear hat functions and once with the new interpolation weights. The displacements of atoms and nodes for  $T = 0, 40, 60$  and  $72$  are shown in figure 6.17 for interpolation with the new interpolation weights and in figure 6.18 for interpolation with linear hat functions. Large red dots mark the positions of the nodes, small red dots the positions of the atoms and blue stars the corresponding equilibrium positions. All displacements are scaled by a factor of 2. Whereas with the new interpolation, the velocity of the perturbation is nearly the same for the parts of the perturbation travelling through the atomistic and the coarse scale region, in case of the linear interpolation the difference is clearly visible. In figure 6.19, we compare the region of the last nodes in  $x$ -direction for both interpolations. Whereas in the left panel all nodes in the last column have nearly the same displacements, the difference in the right panel is obvious. Due to the different dispersion relations in the atomistic and the coarse scale region, the perturbation is travelling faster in the coarse scale region. This results in different displacements of the nodes on top and on the bottom of the column compared to the nodes in the middle.

If we consider non-zero initial conditions in the coarse scale region, we get in principle the same problem as for non-zero temperature simulations, discussed in



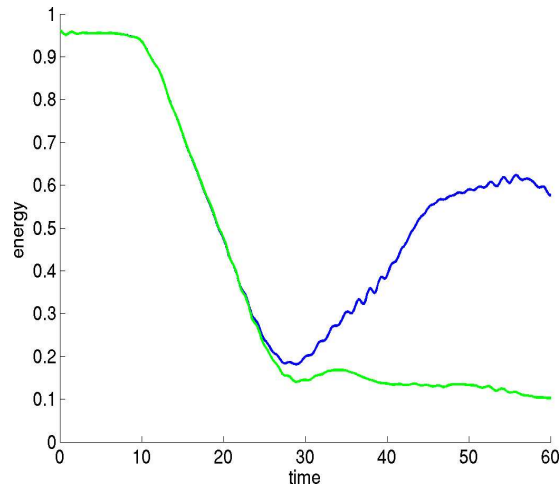


Figure 6.14: energy for sputtering example (test case 2) with (green) and without (blue) reflectionless boundary condition

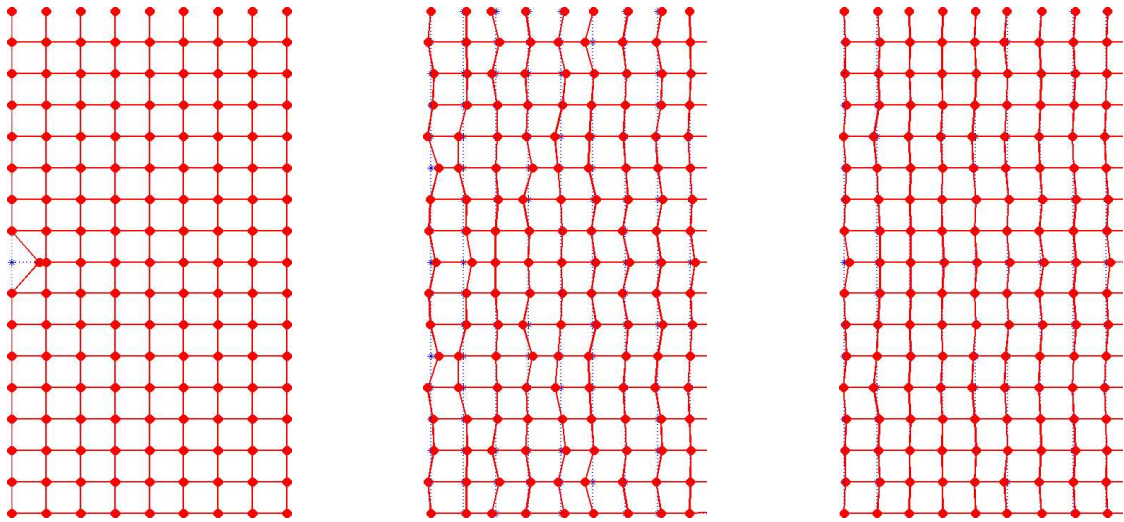


Figure 6.15: initial displacement for the sputtering example (left), displacements after 600 time steps without (middle) and with (right) reflectionless boundary condition, values of middle and right panel three times magnified

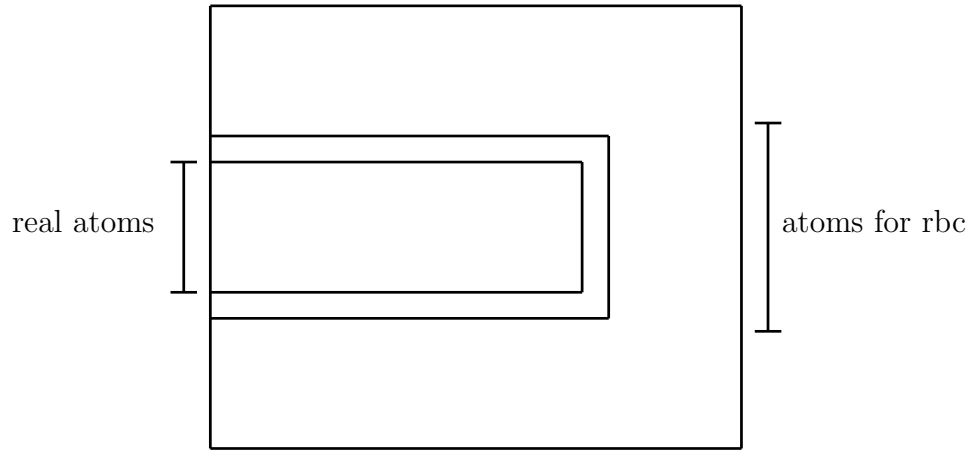


Figure 6.16: geometry for test case 3

section 4.4. The damping character of the boundary condition can be changed by cutting the memory kernel. Since we do not have a periodic excitation of every normal mode, like in the non-zero temperature simulations, the problem is not that serious here. But it should be taken into account, especially if the perturbation passes the interface several times.

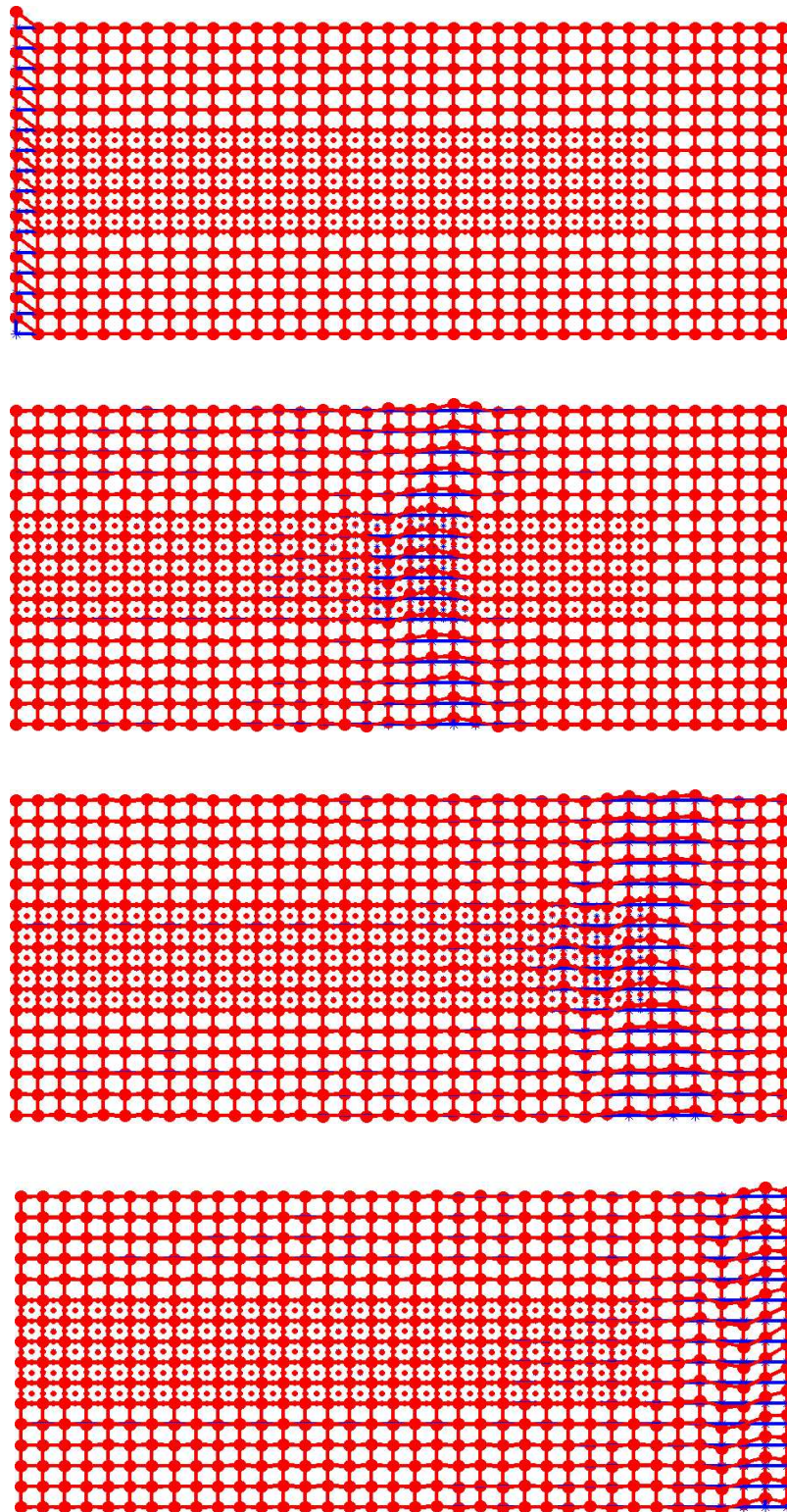


Figure 6.17: test case 3 with linear hat functions for  $T = 0, 40, 60, 72$ .



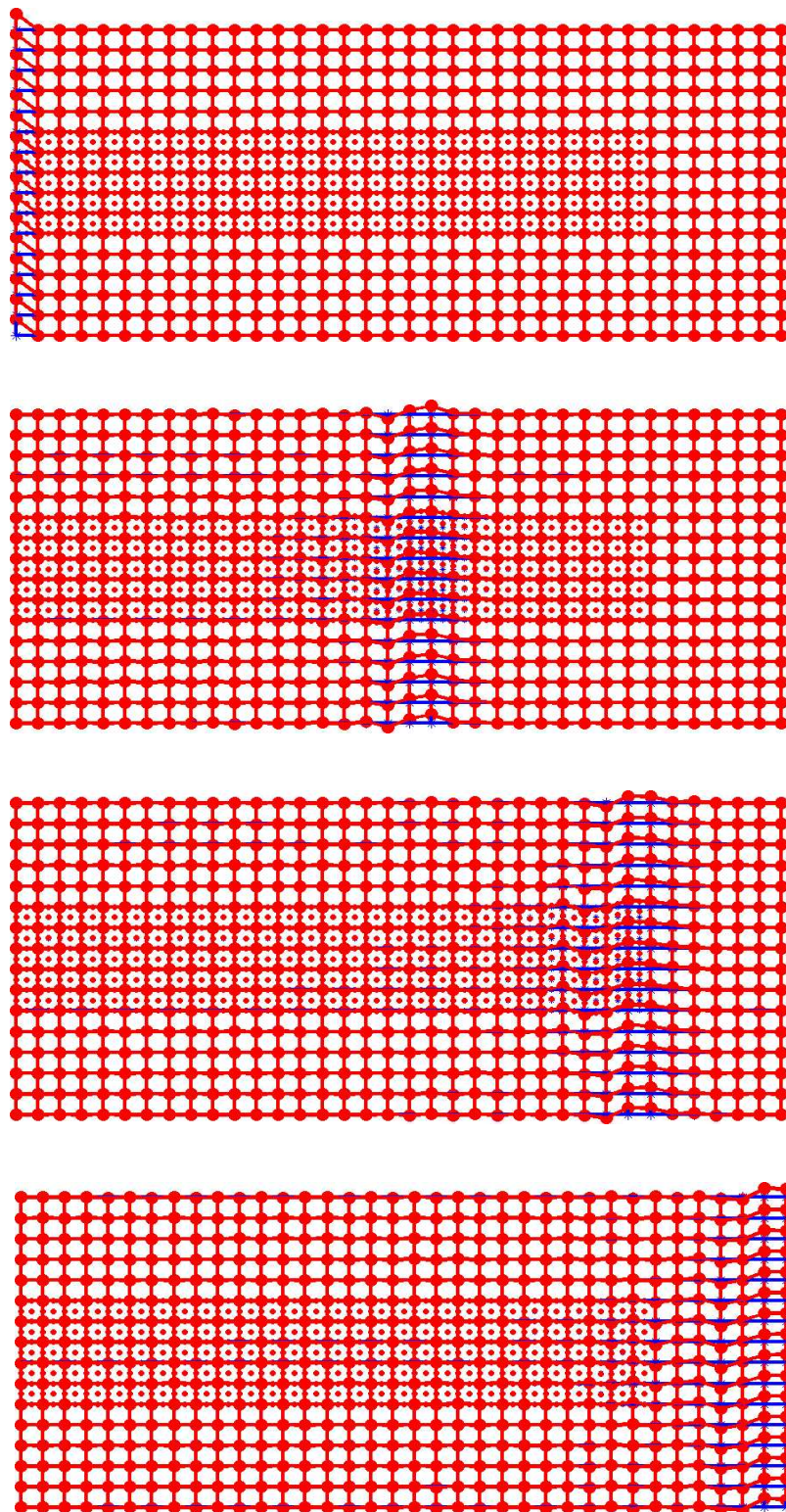


Figure 6.18: test case 3 with new interpolation for  $T = 0, 40, 60, 72$

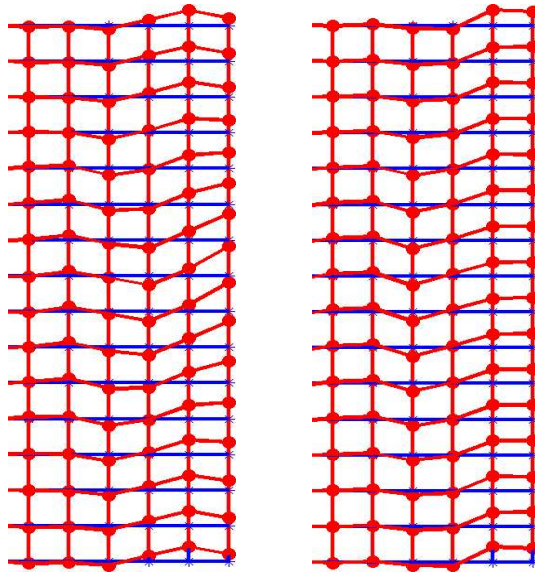


Figure 6.19: displacement of the last nodes for  $T = 72$  for linear hat functions (left) and new interpolation (right)

# Summary

An investigation of concurrent coupling methods in molecular dynamics simulations for the coupling of an atomistic with a coarse scale region in the special setting for the simulation of a surface coating process by sputtering was presented. It was shown, that the concurrent coupling of length scales method leads to an energy conserving system but also to reflections of fine scale waves at the interface between atomistic and coarse scale region. In the bridging scales method this reflections are suppressed by a reflectionless boundary condition, but the resulting approximated system is not energy conserving. Therefore, a method was presented to derive the coupling of an atomistic and a coarse scale region together with a reflectionless boundary condition directly from the atomistic Lagrangian. The only necessary assumption to derive the boundary condition is, that the forces are linear in the fine scale degrees of freedom in the coarse scale region. Especially, there is no need for harmonic interaction of the coarse scale variables. The method can therefore be used for non-harmonic potentials as long as the linearization in the fine scale variables provides a sufficiently good approximation for the force calculation in the coarse scale region. For harmonic interaction, the force calculation is not very time consuming. But for realistic potentials it is the bottleneck in molecular dynamics simulations. The advantage of an approximation by coupling an atomistic and a coarse scale region in this case is even larger.

A method to determine interpolation functions with the correct dispersion relation on the coarse scale without the fine scale variables was given that allows to solve only the coarse scale equations in the coarse scale region, thereby keeping the correct dispersion.

Extensions of the method are possible in several directions. It can be easily extended to the case of atoms or particles with different masses, however the behaviour of the memory kernel and possible approximations in the memory integral need a careful investigation.

Another possibility is the use of more than one coarse scale. Since the computation of new interpolation functions is straightforward if the coarse scale node distance is small (i.e.  $\tilde{n} < 10$ ), it leads to a quadratic system with many unknowns that requires under certain conditions a numerical optimization for larger values. The use of more than one coarse scale with increasing node distances can therefore be helpful. Next to the atomistic region we can use a region in which we neglect only the degrees of freedom of the finest scale till a region where only the variables of the coarsest scale are kept, with a reflectionless boundary condition everywhere in between. If the ratio of two succeeding grids is constant, the same interpolation

and projection and therefore also the same memory kernel can be used for every transition between two scales. Such a multigrid simulation seems also more natural, since the appropriate grid size is not changed abruptly but step by step. Additionally, the size of the domain, which can be covered by such a multigrid simulation, can be much larger than for a simulation using only two different scales.

For the simulation of non-zero temperature systems, the simulation of constant temperature outside of the atomistic region by sampling the normal mode coordinates gets more complicated if several different scales are used. One can think therefore of other methods for sampling the random force in a multigrid simulation. However, it is not enough to sample the random force with the correct distribution. Also the autocorrelation has to be correct to guarantee a constant temperature in simulations with the orthogonal displacement splitting.

The method can also be extended in the direction of the interpretation of the resulting coarse scale equations as discretization of continuum equations and finding faster methods to solve this equations on the coarse grid.

Since the interpolation weights are constant, the method is so far basically suited for the simulation of solids. To extend it for the simulation of liquids, the interpolation weights should not depend on the equilibrium positions, but on the actual positions of the atoms, like in the definition of the local stress tensor, and have to be updated in every time step for the numerical solution.

For the examples considered in this thesis, we used always small systems to focus on the behaviour of the system at the interface between atomistic and coarse scale region and in the coarse scale region. However, it is clear that the advantage of such a coupling pays off only for large systems and for long simulation times.

As shown in the second test case in the last chapter, the method of the orthogonal displacement splitting seems promising in the simulation of surface coating by sputtering. If the forces are not linear, the use of a splitting of the variables into the contributions on different scales seems even more reasonable. If we assume, that the excitation of every normal mode is approximately the same when an atoms hits the surface of the crystal, the amplitudes of the small wave length will decay and that of the long wave length will increase during the simulation. This is due to the equipartition theorem, which states, that in equilibrium the energy of every normal mode is the same and the fact that the energy is proportional to the squared wave frequency.

# Bibliography

- [1] F. F. Abraham, J. Q. Broughton, N. Bernstein, and E. Kaxiras. Spanning the continuum to quantum length scales in a dynamic simulation of brittle fracture. *Europhys. Lett.*, 44(6):783–787, 1998.
- [2] R. Abraham and J. E. Marsden. *Foundation of Mechanics*. The Benjamin/Cumming Publishing Company, 1978.
- [3] S. A. Adelman and J. D. Doll. Generalized Langevin equation approach for atom/solid-surface scattering: Collinear atom/harmonic chain model. *J. Chem. Phys.*, 61(10):4242–4245, 1974.
- [4] S. A. Adelman and J. D. Doll. Generalized Langevin equation approach for atom/solid-surface scattering: General formulation for classical scattering off harmonic solids. *J. Chem. Phys.*, 64(6):2375–2388, 1976.
- [5] M. P. Allen and D. J. Tildesley. *Computer Simulation of Liquids*. Oxford University Press, New York, 1992.
- [6] M. Arndt and M. Griebel. Derivation of higher order gradient continuum models from atomistic models for crystalline solids. *Multiscale Model. Sim.*, 4(2):531–562, 2005.
- [7] M. E. Bachlechner, A. Omeltchenko, A. Nakano, R. K. Kalia, and P. Vashishta. Dislocation emission at the silicon/silicon nitride interface: A million atom molecular dynamics simulation on parallel computers. *Phys. Rev. Lett.*, 84(2):322–325, 2000.
- [8] R. Barauskas. Optimum mass matrices for short wave pulse propagation finite element models. *Nonlinear Anal., Model. Control*, 8(2):3–25, 2003.
- [9] K.-J. Bathe. *Finite Element Procedures*. Prentice Hall, 1996.
- [10] T. Belytschko and S. P. Xiao. Coupling methods for continuum model with molecular model. *J. Mult. Comput. Engrg.*, 1(1):115–126, 2003.
- [11] H. J. C. Berendsen, J. P. M. Postma, W. F. van Gunsteren, A. DiNola, and J. R. Haak. Molecular dynamics with coupling to an external heat bath. *J. Chem. Phys.*, 81(8):3684–3690, 1984.



- [12] D. Braess. *Finite Elements*. Cambridge University Press, 2001.
- [13] A. Brandt. Multigrid methods in lattice field computations. *Nucl. Phys. B (Proc. Suppl.)*, 24:137–180, 1992.
- [14] A. Brandt and M. Galun. Optimal multigrid algorithms for variable-coupling isotropic Gaussian models. *J. Stat. Phys.*, 88(3-4):637–664, 1997.
- [15] A. Brandt, M. Galun, and D. Ron. Optimal multigrid algorithms for calculating thermodynamic limits. *J. Stat. Phys.*, 74(1-2):313–348, 1994.
- [16] J. Q. Broughton, F. F. Abraham, N. Bernstein, and E. Kaxiras. Concurrent coupling of length scales: Methodology and application. *Phys. Rev. B*, 60(4):2391–2403, 1999.
- [17] W. Cai, M. de Koning, V. V. Bulatov, and S. Yip. Minimizing boundary reflections in coupled-domain simulations. *Phys. Rev. Lett.*, 85(15):3213–3216, 2000.
- [18] H. P. Cherukuri. Dispersion analysis of numerical approximations to plane wave motions in an isotropic elastic solid. *Computational Mechanics*, 25(4):317–328, 2000.
- [19] A. J. Chorin, O. H. Hald, and R. Kupferman. Optimal prediction and the Mori-Zwanzig representation of irreversible processes. *Proc. Natl. Acad. Sci. USA*, 97(7):2968–2973, 2000.
- [20] M. A. Christon. The influence of the mass matrix on the dispersive nature of the semi-discrete, second-order wave equation. *Comput. Methods Appl. Mech. Engrg.*, 173(1):147–166, 1999.
- [21] S. Curtarolo and G. Ceder. Dynamics of an inhomogeneously coarse grained multiscale system. *Phys. Rev. Lett.*, 88(25):255504, 2002.
- [22] W. A. Curtin and R. E. Miller. Atomistic/continuum coupling in computational materials science. *Modelling Simul. Mater. Sci. Eng.*, 11(R33-R68), 2003.
- [23] D. J. Diestler. Coarse-grained descriptions of multiple scale processes in solid systems. *Phys. Rev. B*, 66:184104, 2002.
- [24] W. Dreyer and M. Kunik. Cold, thermal and oscillator closure of the atomic chain. *J. Phys. A*, 33:2097–2129, 2000.
- [25] W. E and B. Engquist. The heterogeneous multiscale method. *Comm. Math. Sci.*, 1(1):87–132, 2003.
- [26] W. E and B. Engquist. Multiscale modeling and computation. *Notices Am. Math. Soc.*, 50(9):1062–1070, 2003.

- [27] W. E and Z. Huang. Matching conditions in atomistic-continuum modeling of materials. *Phys. Rev. Lett.*, 87(13):135501, 2001.
- [28] W. E and Z. Huang. A dynamic atomistic-continuum method for the simulation of crystalline materials. *J. Comput. Phys.*, 182(1):234–261, 2002.
- [29] B. Engquist and A. Majda. Absorbing boundary conditions for the numerical simulation of waves. *Math. Comput.*, 31(139):629–651, 1977.
- [30] B. Engquist and A. Majda. Radiation boundary conditions for acoustic and elastic wave calculations. *Commun. Pure Appl. Math.*, 32:313–357, 1979.
- [31] E. Fick and G. Sauermann. *The Quantum Statistics of Dynamic Processes*. Springer, 1990.
- [32] J. Fish and W. Chen. Discrete-to-continuum bridging based on multigrid principles. *Comput. Methods Appl. Mech. Engrg.*, 193(17-20):1693–1711, 2004.
- [33] D. Fraenkel and B. Smit. *Understanding molecular simulation*. Academic Press, 2002.
- [34] G. Gallavotti. *The elements of mechanics*. Springer, 1983.
- [35] G. Gallavotti. *Statistical mechanics*. Springer, 1999.
- [36] I. Goldhirsch and C. Goldenberg. On the microscopic foundations of elasticity. *Eur. Phys. J. E*, 9(3):245–251, 2002.
- [37] M. Griebel, S. Knapek, G. Zumbusch, and A. Caglar. *Numerische Simulation in der Moleküldynamik*. Springer, 2004.
- [38] R. Haberlandt, S. Fritzsche, G. Peinel, and K. Heinzinger. *Molekulardynamik*. Vieweg, 1995.
- [39] I. Harari. Reducing spurious dispersion, anisotropy and reflection in finite element analysis of time-harmonic acoustics. *Comput. Methods Appl. Mech. Engrg.*, 140(1-2):39–58, 1997.
- [40] K. Huang. *Statistical Mechanics*. John Wiley and Sons, 1963.
- [41] M. Junk and Z. Yang. Asymptotic analysis of finite difference methods. *Appl. Math. and Comput.*, 158(1):267–301, 2004.
- [42] E. G. Karpov, G. J. Wagner, and W. K. Liu. A green’s function approach to deriving non-reflecting boundary conditions in molecular dynamics simulations. *Int. J. Numer. Meth. Engrg.*, 62(9):1250–1262, 2005.
- [43] P. Klein. *Klassische und Tight-Binding Molekulardynamik für niederenergetische Prozesse in Materialien*. PhD thesis, Universität Kaiserslautern, Fachbereich Physik, 1998.

- [44] P. Klein. Pressure and temperature control in molecular dynamics simulation: a unitary approach in discrete time. *Modelling Simul. Mater. Sci. Eng.*, 6(4):405–421, 1998.
- [45] P. Klein and P. Baumann. On the definition of local stress tensors in molecular dynamics. unpublished.
- [46] J. Knap and M. Ortiz. An analysis of the quasicontinuum method. *J. Mech. Phys. Solids*, 49(9):1899–1923, 2001.
- [47] S. Kohlhoff, P. Gumbsch, and H. F. Fischmeister. Crack propagation in b.c.c. crystals studied with a combined finite-element and atomistic model. *Philos. Mag. A*, 64(4):851–878, 1991.
- [48] E. Lidorikis, M. E. Bachlechner, R. K. Kalia, A. Nakano, P. Vashishta, and G. Z. Voyiadjis. Coupling length scales for multiscale atomistics-continuum simulations: Atomistically induced stress distributions in Si/Si<sub>3</sub>N<sub>4</sub> nanopixels. *Phys. Rev. Lett.*, 87(8):086104, 2001.
- [49] W. K. Liu, E. G. Karpov, S. Zhang, and H. S. Park. An introduction to computational nanomechanics and materials. *Comput. Methods Appl. Mech. Engrg.*, 193(17-20):1529–1578, 2004.
- [50] M. Moseler, J. Nordiek, and H. Haberland. Reduction of the reflected pressure wave in the molecular-dynamics simulation of energetic particle-solid collisions. *Phys. Rev. B*, 56(23):15439–15445, 1997.
- [51] R. Mullen and T. Belytschko. Dispersion analysis of the finite element semidiscretizations of the two-dimensional wave equation. *Int. J. Numer. Meth. Engrg.*, 18(1):11–29, 1982.
- [52] A. Nakano, M. E. Bachlechner, R. K. Kalia, E. Lidorikis, P. Vashishta, G. Z. Voyiadjis, T. J. Campbell, S. Ogata, and F. Shimojo. Multiscale simulation of nanosystems. *Comput. Sci. Engrg.*, 3(4):56–66, 2001.
- [53] H. S. Park, E. G. Karpov, P. A. Klein, and W. K. Liu. Three-dimensional bridging scale analysis of dynamic fracture. *J. Comput. Phys.*, 207(2):588–609, 2005.
- [54] H. S. Park, E. G. Karpov, and W. K. Liu. A temperature equation for coupled atomistic/continuum simulations. *Comput. Methods Appl. Mech. Engrg.*, 193(17-20):1713–1732, 2004.
- [55] H. S. Park, E. G. Karpov, W. K. Liu, and P. A. Klein. The bridging scale for two-dimensional atomistic/continuum coupling. *Philos. Mag.*, 85(1):79–113, 2005.
- [56] H. S. Park and W. K. Liu. An introduction and tutorial on multiple-scale analysis in solids. *Comput. Methods Appl. Mech. Engrg.*, 193(17-20):1733–1772, 2004.

- [57] A. V. Plyukhin and J. Schofield. Stochastic dynamics with a mesoscopic bath. *Phys. Rev. E*, 64(4):041103, 2001.
- [58] R. E. Rudd and J. Q. Broughton. Coarse-grained molecular dynamics and the atomic limit of finite elements. *Phys. Rev. B*, 58(10):R5893–5896, 1998.
- [59] R. E. Rudd and J. Q. Broughton. Concurrent coupling of length scales in solid state systems. *Phys. Stat. Sol. B*, 217(1):251–291, 2000.
- [60] R. E. Rudd and J. Q. Broughton. Coarse-grained molecular dynamics: Nonlinear finite elements and finite temperature. *Phys. Rev. B*, 72(14):144104, 2005.
- [61] L. A. Segel and G. H. Handelman. *Mathematics applied to continuum mechanics*. Dover Publ., 1987.
- [62] B. Seibold. Optimal prediction in molecular dynamics. Master’s thesis, Universität Kaiserslautern, Mathematisches Institut, 2003.
- [63] B. Seibold. Optimal prediction in molecular dynamics. *Monte Carlo Methods Appl.*, 10(1):25–50, 2004.
- [64] V. B. Shenoy, R. Miller, E. B. Tadmor, R. Phillips, and M. Ortiz. Quasi-continuum models of interfacial structure and deformation. *Phys. Rev. Lett.*, 80(4):742–745, 1998.
- [65] V. B. Shenoy, R. Miller, E. B. Tadmor, D. Rodney, R. Phillips, and M. Ortiz. An adaptive finite element approach to atomic-scale mechanics-the quasicontinuum method. *J. Mech. Phys. Solids*, 47(3):611–642, 1999.
- [66] A. Streit and P. Klein. Coupling the continuum with molecular dynamics using a projection operator approach. *submitted to J. Comput. Phys.*, 2006.
- [67] A. Streit, R. E. Zillich, P. Baumann, and P. Klein. Differentiable mesoscopic fields in molecular dynamics simulation: construction, dynamics, and coupling of length scales. In *Multiscale Materials Modeling 2006, Conference Proceedings*. to appear 2006.
- [68] E. B. Tadmor, M. Ortiz, and R. Phillips. Quasicontinuum analysis of defects in solids. *Philos. Mag. A*, 73(6):1529–1563, 1996.
- [69] E. B. Tadmor, G. S. Smith, N. Bernstein, and E. Kaxiras. Mixed finite element and atomistic formulation for complex crystals. *Phys. Rev. B*, 59(1):235–245, 1999.
- [70] M. Toda, R. Kubo, and N. Saitô. *Statistical Physics I: Equilibrium Statistical Mechanics*. Springer-Verlag, 1992.
- [71] G. J. Wagner and W. K. Liu. Coupling of atomistic and continuum simulations using a bridging scale decomposition. *J. Comput. Phys.*, 190(1):249–274, 2003.

- [72] Z.-B. Wu, D. J. Diestler, R. Feng, and X. C. Zeng. Coarse-graining description of solid systems at nonzero temperature. *J. Chem. Phys.*, 119(15):8013–8023, 2003.
- [73] S. P. Xiao and T. Belytschko. A bridging domain method for coupling continua with molecular dynamics. *Comput. Methods in Appl. Mech. Engrg.*, 193:1645–1669, 2004.
- [74] O. C. Zienkiewicz and R. L. Taylor. *The Finite Element Method, Vol. 1: The Basis*. Butterworth-Heinemann, 2000.
- [75] R. E. Zillich. Non-reflecting boundary conditions for finite temperature molecular dynamics. *submitted to Comp. Phys. Comm.*, 2006.

## CURRICULUM VITAE

21.06.1977	geboren in Stuttgart
1983 – 1987	Besuch der Weilerhau-Grundschule in Filderstadt
1987 – 1996	Besuch des Eduard-Spranger-Gymnasiums in Filderstadt
10/1996 – 07/2002	Studium im Fach Mathematik an der Universität Stuttgart
07/2002	Diplom in Mathematik an der Universität Stuttgart
10/2002 – 02/2003	wissenschaftliche Mitarbeiterin an der Universität Stuttgart, Institut für Mathematische Methoden in den Ingenieurwissenschaften, Numerik und geometrische Modellierung
03/2003 – 09/2006	Promotionsstipendium am Fraunhofer Institut für Techno- und Wirtschaftsmathematik
03/2003 – 12/2006	Doktorand am Fachbereich Mathematik der TU Kaiserslautern

## CURRICULUM VITAE

21.06.1977	born in Stuttgart
1983 – 1987	Weilerhau-Grundschule in Filderstadt
1987 – 1996	Eduard-Spranger-Gymnasium in Filderstadt
10/1996 – 07/2002	studies in mathematics at the university of Stuttgart
07/2002	diploma in mathematics at the university of Stuttgart
10/2002 – 02/2003	research associate in the department of mathematics at the university of Stuttgart
03/2003 – 09/2006	PhD scholarship at Fraunhofer institute for industrial mathematics (ITWM)
03/2003 – 12/2006	PhD student in the department of mathematics at the university of Kaiserslautern